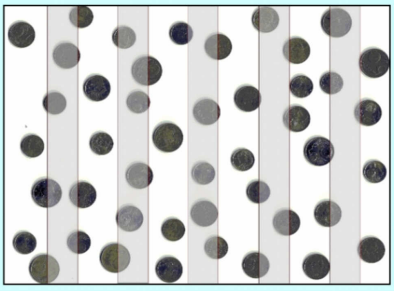
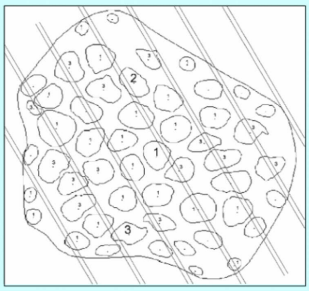

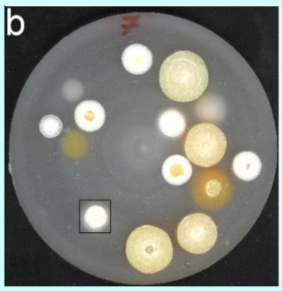

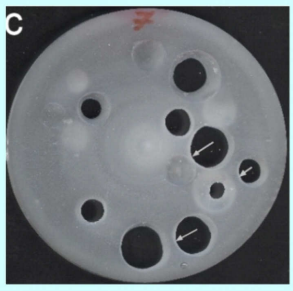

Estimating the Numbers and Sizes of Perfectly or Approximately Circular or Spherical Objects from Slices

P. Bussières

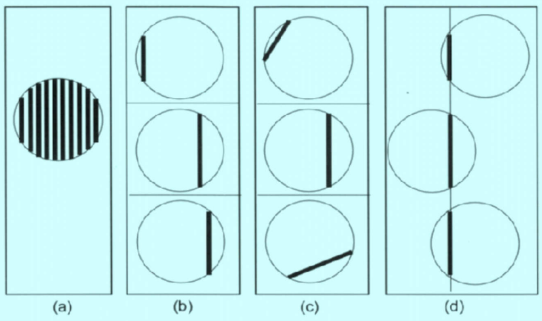

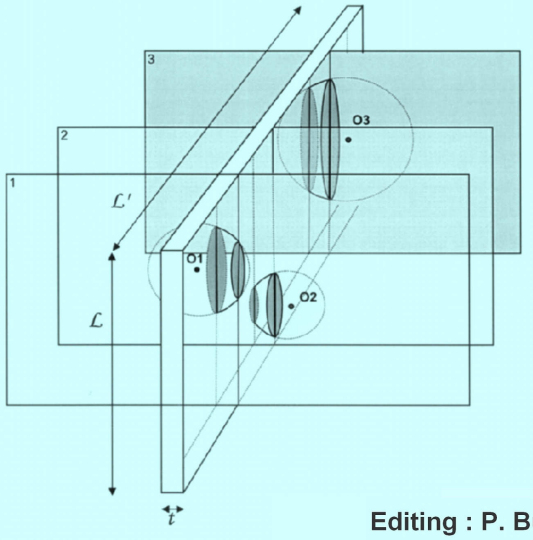

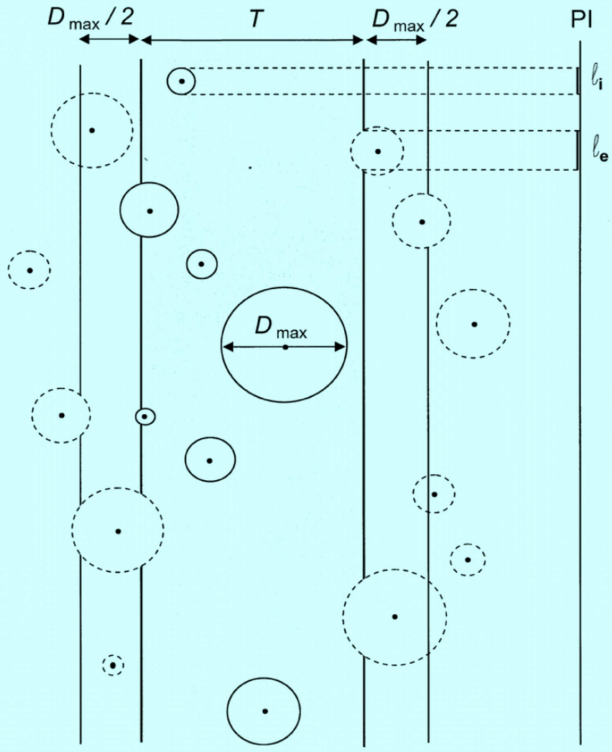

Editing : P. Bussières - 2013 (Second edition)

Second edition (October 2013)

List of corrections made to the initial edition (February 2013)

P. Bussières.

(Note that possible future corrections would be indicated on the website http://www.diameters-slices.org).

p. 13. In Table 1.2, in Eqn. T2-10: the second sign minus has been replaced by ±.

p. 22. In the third sentence of the last paragraph, "the predicted values of cv_D and D_m were higer than…", higer was replaced by "higher".

p. 46. In the line after Eqn. 6, "decreasing" has been replaced by "increasing".

p. 53 - 54. In Eqns . 3 and 4, the sign minus has been deleted.

p. 54. In Fig.3.3, in the line at the figure middle, "$l_{i, F,}$" has been replaced by $l_{i, F, 0}$ and, "$l_{m,}$" has been replaced by $l_{m, 0}$

p. 55. In Table 3.1:

the values of cv_{length} for P1, P2 and P3 (0.355, 0.338 and 0.344) have been replaced by 0.396, 0.385 and 0.366,

the values of D_m for P1, P2 and P3 (0.391, 0.420 and 0.436) have been replaced by 0.373, 0.401 and 0.419,

the values of cv_D for P1, P2 and P3 (0.259, 0.222 and 0.184) have been replaced by 0.345, 0.315 and 0.273.

p. 60. In the first paragraph of the paragraph 3.2., the values 0.416, 0.222, 0.412 and 0.231 have been replaced by the values 0.398, 0.310, 0.394 and 0.314, respectively.

p. 64. In Fig. 3.7, the values 0.416 and 0.222 have been replaced by 0.394 and 0.314. The dotted fine line has been replaced by a fine curve slightly above the heavy line in its left part and slightly below in its right part.

p. 65. In the first line, 0.412 and 0.231 have been replaced by 0.394 and 0.314. In the second and third lines, "Although was slightly underestimated," Has been deleted.

Estimating the Numbers and Sizes of Perfectly or Approximately Circular or Spherical Objects from Slices

Philippe BUSSIÈRES

-

From the same author

Around the soil

Bussières P. Loi de variation du pH d'un sol acide après apport de particules calcaires de caractéristiques différentes. *Annales Agronomiques*, 1978, 29: 559-581.

Bussières P. Influence des caractéristiques de particules d'amendements calcaires sur leur solubilité carbonique. *Annales Agronomiques*, 1979, 30: 121-138.

Bussières P, **Girou A**, **Callot G**, **André L**. Dissolution de particules d'amendement calcaire. *Science du sol*, 1982, 4: 263-273.

Bussières P, **Hostalery J**, **Battilani A**. Simple device for estimating soil water content at permanent wilting point. *Acta Horticulturae*, 2003, 613: 163–168.

Around the fruit

Bussières P. Potential dry matter and water import rates in the tomato fruit in relationship to fruit size. *Annals of Botany*, 1993, 72: 63-72.

Bussières P. Water import rate in tomato fruit: a resistance model. *Annals of Botany*, 1994, 73: 75-82.

Bussières P. Dry matter and water import rates in the tomato fruit: a model incorporating the changes in sap viscosity and osmotic potential with temperature. *Annals of Botany*, 1995, 75: 469-476.

Bussières P. Water import in the young tomato fruit limited by pedicel resistance and calyx transpiration. *Functional Plant Biology*, 2002, 29: 631-641.

Bussières P. Effect of tomato fruit pedicel temperature on fruit expansion predicted by a model based on pedicel conductivity. *Acta Horticulturae*, 2003, 613: 33–37.

Bussières P, **Bertin N**, **Morris CE**., **Vigne C**, **Orlando P**, **Glaux C**, **Floret H**, **Bernadac J**, **Sévénier V**, **Korownikoff S**. High external sucrose concentration inhibits the expansion of detached tomato fruits grown in a novel semi-open device. *In Vitro Cellular and Development Biology – Plant*, 2011, 47: 743–751.

Around the field

Bussières P. Canevas de modèle d'une ligne de plantes de tomate semées explicitant sa variabilité spatiale. *Acta Horticulturae*, 1990, 277: 221-227.

Bussières P, **Dumas Y**. An analysis scheme for modelling the functioning of a tomato canopy. *Acta Horticulturae*, 1992, 376: 171-176.

Bussières P, **Battilani A**, **Combres P**, **Dumas Y**. Irrigere: a generalized version of an irrigation scheduling model for a large range of crops. *Acta Horticulturae*, 2000, 537: 527- 534.

Machado RMA, **Bussières P**, **Koutsos TV**, **Prieto MH**, **Ho LC**. Prediction of optimal harvest date for processing tomato based on the accumulation of daily heat units over the fruit ripening period. *Journal of Horticultural Science and Biotechnology*, 2004, 79: 452-457.

Around crop tools

Bussières P. Method and apparatus for regulating the sowing depth of seeds in a seed drill, and products for this regulation. *European Patent Office*, 1990, EP 0 206 848.

Estimating the Numbers and Sizes of Perfectly or Approximately Circular or Spherical Objects from Slices

Where the Wicksell's problem and the problems of the tomato salad and Swiss cheese are re-considered

Philippe BUSSIÈRES

Ingénieur Agronome
Docteur Ingénieur

Chargé de Recherche à l'Institut National de la Recherche Agronomique
Unité Plantes et Systèmes de Culture Horticoles, Avignon, France

philippe.bussieres@avignon.inra.fr

Editing: Philippe BUSSIÈRES

2013
(Second edition: October 2013)

Estimating the numbers and sizes of perfectly or approximately circular or spherical objects from slices

Author: Philippe Bussières. Editor: Philippe Bussières

ISBN 978 – 2 – 9544261 – 0 – 5

February 2013

(Second edition: October 2013)

CONTENTS

INTRODUCTION AND PRESENTATION

It is often important to estimate the number and size distribution of objects which are dispersed in a matrix. However, in many cases these objects can be observed only partially from slices made through the matrix. These slices produce object sections from which images are obtained when they are lighted. Here we consider approximately or perfectly spherical objects and approximately or perfectly circular surfaces. An example of such surfaces - which will be better illustrated later - is obtained on a plane which cuts perpendicularly a bundle of parallel cylinders. When a slice perpendicular to such surfaces is made through the matrix, sections of these objects are circle sections between two parallel planes. It is the case when an ultra-thin slice of plant phloem tissue is made in parallel to the sieve tubes which are shaped like cylinders. Estimation of components of this tissue which limit likely the tomato fruit expansion (Bussières, 2002) initiated the researches presented in this book. Another example is that of an observer who moves along a straight line in a landscape and comes across circular surfaces, characterized for example by the same type of plants, without he is able to see the limits of these surfaces. He can only see short distances and record the section length travelled in each surface. If these surfaces, with possibly different sizes, are distributed randomly in the landscape (that is his path is at random distances of their centres), he can want to estimate the number of surfaces per unit area of the landscape and the distribution of their diameter from the recorded section lengths.

The size of a section obtained from perfectly circular or spherical objects depends on the object diameter and on the position of the slice into the object. When all the objects are entirely cut into small sections by a sufficient number of slices having a same thickness, the section size distribution is completely determinate by the object diameter distribution. Therefore it is possible to suspect that the object diameter distribution may be assessed from the section size distribution. However, generally there is only a small number of slices; they section only a small proportion of the objects and there is only one section per object. Moreover, as a slice cuts an object according to a probability increasing with its diameter, this has to be considered to obtain unbiased estimations. In addition, when a given slice is placed under light, the object sections are often only partially observed (for example, the light crosses a gas bubble section at the narrowest sectioned point), so that only images of these sections are obtained.

Therefore, it is expected that the estimation of the number and diameter distribution of such objects would involve several factors:

- the thickness of the slice, which can be smaller than the smallest diameter or greater than the largest diameter or to be intermediate. In the extreme case where it is zero, the matrix is in fact divided into two parts,

- the transparency and opacity of the objects and matrix. For examples, gas bubbles in volcanic rocks are transparent objects in an opaque matrix. On the contrary, many cell components are seen under light microscopy to be opaque within a thin slice of transparent cytosol. Note that the atmosphere can be considered as a transparent matrix,

- the limit of detection of the smaller images,

- the diameter distribution (possibly symmetrical, normal, or asymmetrical, with one or several peaks).

However, many planar surfaces or volumes of interest which are observed, in particular by microscopy and imaging techniques, and in particular in materials science, geology, biology, histology, anatomy, are only approximately circular or spherical. Also in this case, the size of a given section obtained from a given object depends on the object size and on the position of the slice into the object. As the diameter - named equivalent diameter - of the circle or sphere with the same area or volume as that of these objects can be calculated, it is expected that the estimation of their numbers and sizes would involve also the previous factors, but with a greater complexity.

Many studies were made to estimate the size distribution of spheres. Wicksell (1925) proposed a method valuable when the slice thickness is nil. Methods were proposed in the cases where the slice thickness is not zero for opaque spheres in a transparent matrix or transparent spheres in an opaque matrix. However, as these methods are not perfect, the Wicksell's method is still often used even if the slice thickness is not quite zero and if the objects are not perfectly spherical.

Here a new approach is proposed for the case where the slice thickness is less than the smallest diameter and perfectly circular or spherical objects whose diameter distribution is symmetrical. It is valid for both opaque objects in a transparent matrix and transparent objects in an opaque matrix and even with a detection limit of images. This new approach was found to be very fruitful for dealing with any distributions or only approximately circular shapes or the case of slices thicker than the largest diameter.

However, this new approach was not published, although Reviewers of respected journals were very favourable to its publication, presumably mainly because this approach deals with perfectly circular or spherical objects and a normal diameter distribution - which are rare in nature - what is not in line with the present "modern stereology" largely focussed on new unbiased sampling methods for natural object shapes (Baddeley and Jensen, 2005). However, it was difficult to show at the same time his interest for any distributions, for only approximately circular shapes and for slices thicker than the diameters.

Hence this book meets several manuscripts and presents, in the first three chapters, the case of slices thinner than the smallest diameter. The first two deal with the case of perfectly circular or spherical objects, the first with the case of a symmetrical and even normal diameter distribution, the second with the case of any distribution. The third chapter is for shapes only approximately circular. The fourth chapter deals with the case of slices thicker than the largest diameter. Finally, the fifth chapter indicate very briefly the case of objects in an opaque matrix visible only on section planes.

I thank here anonymous Reviewers and Translators for their very helpful comments for these findings. Also, I thank Brigitte Delécolle for her help in electron microscopy and image interpretation and the Station of Pathology of INRA in Avignon, C. Vigne for his very competent contribution in making the bonbon slices, and Nadia Bertin for a number of advices.

References

Baddeley, A., Jensen, E. 2005. Stereology for Statisticians. Boca Raton, USA: Chapman and Hall-CRC.

Bussières, P. 2002. Water import in the young tomato fruit limited by pedicel resistance and calyx transpiration. *Funct. Plant Biol*. 29, 631–641.

Wicksell, S.D. 1925. The corpuscle problem: a mathematical study of a biometric problem. *Biometrika* 17, 84–99.

CHAPTER 1

Estimating the numbers and diameters of objects from their images in slices: an equation and a method for symmetrical diameter distributions

Abstract

Estimation of the numbers and diameters of circular, cylindrical, or spherical objects from their images obtained in slices through the embedding medium is investigated. Cases of limited image-detection, of slices which are thick but smaller than the diameters, and of opaque or transparent objects are taken into account. From the general relations proposed here for these cases, an approximate equation was found for symmetrical or roughly symmetrical diameter distributions. It involves only the coefficients of variation of diameters and image lengths. Based on this equation, a very simple estimation method is proposed for such distributions. Valuable predictions were obtained in simulated or real examples when the slice was not too thick and the lower image-detection limit was not too high, and with at least a few dozen images. This method is expected to provide a basis for future methods for any diameter distributions, for only approximately circular objects or for very thick slices.

1. Introduction

Estimation of the numbers and diameter distributions of circular, cylindrical, or spherical objects from their images obtained in slices through the material in which they are included is often difficult, whereas these parameters are involved in important issues. An example is the case of plant phloem pores (Bussières, 2002), which are very short thin tubes of a few tenths of a micrometer in diameter. The sap flow is suspected largely to depend on their number and size. However they are difficult to estimate because the pores are visible almost solely in longitudinal slices. Other examples are related to roughly spherical components such as gas bubbles in volcanic magma (Sahagian and Proussevitch, 1998), neural vesicles (Feuerverger et al., 2000), and focal tissue lesions (Kopp-Schneider, 2003).

Modern stereology methods (see the review by Cruz-Orive, 1997; Howard and Reed, 1998; Baddeley and Jensen, 2005) should be used for estimating the numbers and sizes of objects which are only approximately cylindrical or spherical, because these methods are based on sampling designs rather than on the object shape. However, use of these methods presents difficulties in certain cases. The dissector method may be difficult to use for extremely rare structures in tissue (Jastrow et al., 1997). With a large number of particles, perfect registration of the positions of the images in successive section planes is laborious (Davtian et al., 2000). When thick slices are used or when the image-detection limit is high, the larger parts of transparent objects included in opaque material or the smaller parts of opaque objects included in transparent material cannot be observed, as noted by the latter authors and by Hedreen (1998).

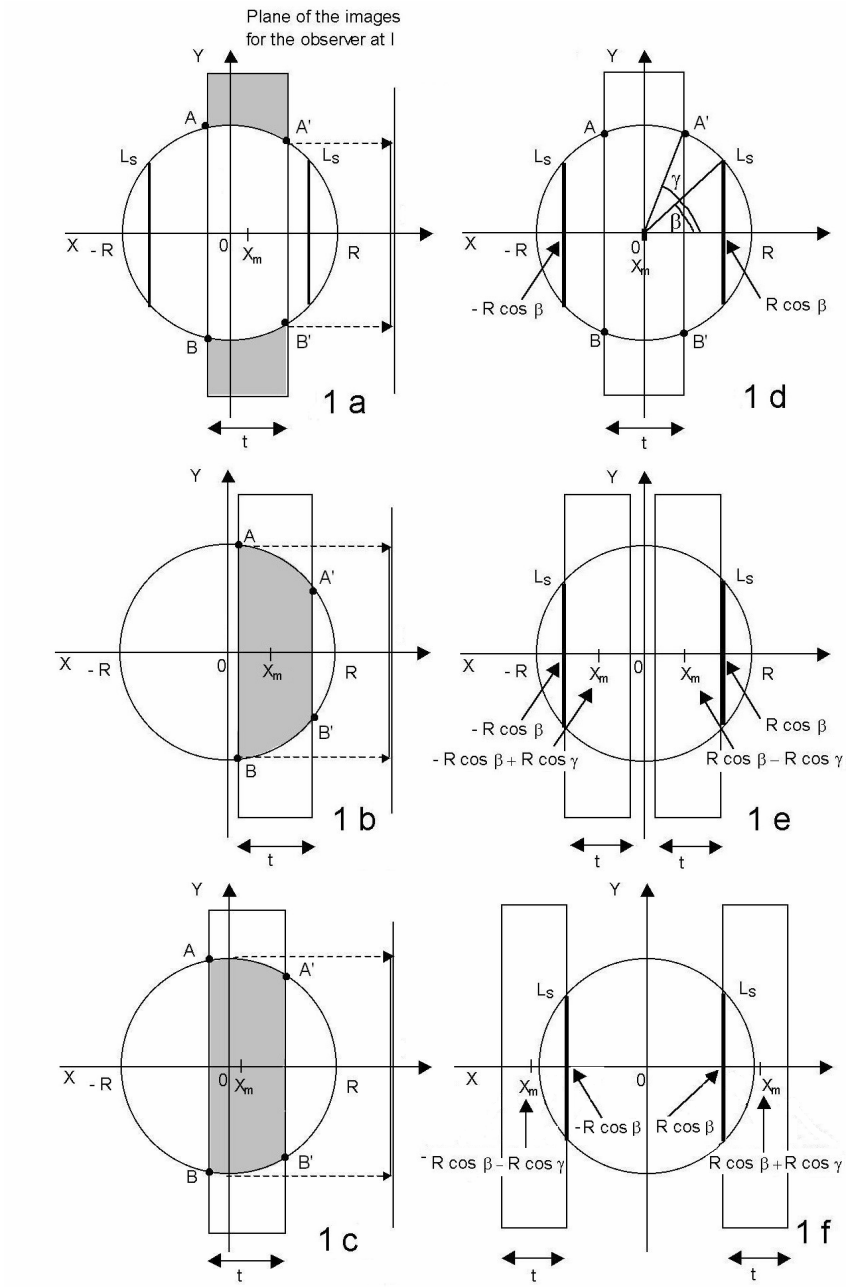

Fig. 1.1. Images of a circle of diameter D observable in a slice having a thickness t smaller than D and with image-detection limit L_S. Cases of a transparent circle in an opaque slice (case E) and of an opaque circle in a transparent slice (case F).

When the distance x_m of the slice midpoint from the circle center varies, the images seen by the observer on the plane at I are projections of circle chords. (**a**) shows a transparent circle which generates an image with length equal to that of the smaller of the two chords which delimit the slice. An opaque circle generates an image with length equal to that of the longer of the two chords which delimit the slice when the circle center is exterior to the slice (**b**) or to the diameter when it is interior to the slice (**c**). (**d**) shows the angles β and γ. (**e**) and (**f**) show the slice midpoint abscissa at the most extreme positions which can generate an image in cases E and F. For clarity, L_S is not drawn on (**b**) and (**c**).

Moreover, controversies remain with regard to the particle-counting approach used in these methods (Baddeley and Jensen, 2005). These methods are also time-consuming, whereas in a number of cases, approximate estimates could provide useful information. Finally, in some cases, the aim is precisely to compare the objects to perfect shapes, for example, to compare plant phloem pores to tubes to be able to apply fluid flow laws.

For these reasons, it can still be useful to research methods which compare the previously mentioned objects with circles, cylinders, or spheres and therefore to research firstly methods in the case of perfect circles, cylinders or spheres. Many studies have been performed to estimate sphere diameter distributions from the diameters of a number of their circular sections viewed in slices or sections. Several reviews are available in the literature (Weibel, 1980; Cruz-Orive, 1983; Cau, 1990; Kok, 1990; Stoyan et al., 1995; Howard and Reed, 1998; Baddeley and Jensen, 2005). Important references in recent years include Coleman (1983), Cruz-Orive (1983), Wilson (1989), Silverman et al. (1990), Fleischer (1994), Mase (1995), Feuerverger and Hall (2000), Antoniadis et al. (2001), and Xu and Pitot (2002).

The problem differs according to whether the sphere images are obtained by intersection with planes or with thicker slices. In the latter case, it differs further for opaque objects included in transparent material and for transparent objects in opaque material (a case called the “Swiss cheese problem” by Coleman, 1983). It also differs according to whether the images are obtained with or without an image-detection limit. Initially, the problem was studied by Wicksell (1925), who called it the “corpuscle problem” in the case of intersection with planes, i.e. slices of the thickness equal to zero. The case of transparent objects has been studied mainly by Coleman (1983), who proposed a solution which was valid only in the case of very thin slices. The various approaches taken to this problem have been classified by Cruz-Orive (1983) and more recently by Stoyan et al. (1995). Most of them use mathematical developments and equations (Abel’s integral, for example) which are difficult, and the methods are rather cumbersome for use by nonspecialists, including many biologists. Moreover, these methods, which work with a number of image size classes, need a rather large sample of images (some hundreds or thousands are generally used in the description of these methods).

Here the cases considered involve slices which are thick, but less thick than the circle diameters, possibly of zero thickness, possibly with an image-detection limit, and of either opaque or transparent objects. Moreover, the case of circles cut by slices perpendicular to the circle plane, which yields images which are line segments rather than planar sections, is considered initially and constitutes the basis for the treatment of the cylinder and the sphere. After proposing some general relations, the author found that one of these relations is an approximate equation involving the two first moments of the circle diameter and the two first moments of the image length when the diameter distribution is symmetrical or approximately symmetrical. Therefore, the problem can be greatly simplified, and a simple method is described to estimate the mean and the coefficient of variation of the diameter for such distributions. The validity of these relations and methods has been studied with simulated or real examples, including fairly small samples. Valuable predictions have been obtained from these examples when the slice thickness was not too great and the image-detection limit not too high, and with at least several dozen images.

2. Materials and methods

2.1. Development of the model and relations

The cases of circular, cylindrical, and spherical objects are considered here. However, as will be shown later in this paper, the cases of cylindrical and spherical objects flow from the case of the circle. Therefore, first the developments for circular objects will be presented, and then they will be extended to cylinders and spheres.

Consider a circle in (x, y, z) space, on a plane perpendicular to the z-axis, having its center at (0, 0), with diameter D and radius R (**Fig. 1.1a**). Consider a slice of thickness t, perpendicular to the x-axis, with its midpoint having abscissa x_m. The possible forms of the intersection between the circle and the slice are a circular cap or a circle segment delimited by two chords, AB and A'B'. Consider the image of this intersection obtained by its projection without magnification onto a plane perpendicular to the x-axis at a point I external to the circle and to the slice. There are two cases: the circle is either more transparent (the case denoted by E, for "empty") or more opaque (the case denoted by F, for "full") than the slice matrix. In case E, an image can be obtained only if the circle is cut by the two faces of the slice, or in other words, if $t < D$ and if $|x_m| < R - t / 2$. The image length is that of the shortest chord (A'B' in **Fig. 1.1a**). In case F, an image can be obtained only if the circle is partly or entirely in the slice. If $t < D$, this occurs if $|x_m| < R + t / 2$. The image length is that of the longest chord (AB in **Fig. 1.1b**) when the circle center is outside the slice, or is equal to D when the circle center is inside the slice (**Fig. 1.1c**). The case where $t > D$ is not considered here.

However, images are obtained only if they are longer than the shortest detectable image length, L_S (**Fig. 1.1a**). The diameter of the smallest circle which can generate at least one image is equal to $(L_S^2 + t^2)^{0.5}$ in case E and to L_S in case F.

When several circles of the plane are cut by the slice, images composed of overlapping circle images can be obtained in case F, but not in case E. Here, the case of such images is excluded.

Consider now, at least virtually, a set of parallel slices having their abscissa values x_m equally spaced by a very small value dx—relative to the smallest diameter—which cut one or several circles on the plane or on parallel planes. This is possible even if t is thicker than dx, if the slices are cut successively and replaced after recording the circle images. When only one circle or circles having the same diameter D are considered, or when the diameter distribution is symmetrical or roughly symmetrical, relations can be obtained between various parameters relative to the circles and their images, as shown later in this paper.

Tabèle 1.1. *Relations between the diameter (*D*) of a circle cut by a set of slices of thickness* t *equally spaced by 1 /* q*, the number (*M*) of images, and the mean (*L_m*) and the coefficient of variation (*cv_L*) of the image length when the image-detection limit is* L_S

The angles β *and* γ *are equal to asin (*L_S / D*) and acos (*t / D*) respectively. Some relations differ in case E (transparent circle sectioned by opaque slices) and in case F (opaque circle sectioned by transparent slices).*

	Case E	**Case F**	**Eqs.**
$c_1 =$	$\cos\beta - \cos\gamma$	$\cos\beta + \cos\gamma$	T1-1
$c_2 =$	$2\gamma - 2\beta - \sin 2\gamma + \sin 2\beta$	$\pi - 2\beta + 4\cos\gamma + \sin 2\beta$	T1-2
$c_3 =$	$(3 - \cos^2\beta)\cos\beta - (3 - \cos^2\gamma)\cos\gamma$	$(3 - \cos^2\beta)\cos\beta + 3\cos\gamma$	T1-3
$M / D =$	$q\, c_1$		T1-4
$L_m / D =$	$c_2 / 4\, c_1$		T1-5
$(L^2)_m / D^2 =$	$c_3 / 3\, c_1$		T1-6
$cv_L^2 =$	$16\, c_1\, c_3 / 3\, c_2^2 - 1$		T1-7

Approximately similar relations can also be obtained when one single, almost infinitely long slice cuts a sufficiently large number of circles which centers are at random distances from the middle of the slice. This is also true when this almost infinitely long slice is constructed from an equivalent set of slice portions such that each circle is cut by at most one slice portion.

2.1.1. Case of one or several circles of diameter D

Consider all the images generated by the previous circle of diameter D when it is cut, at least virtually, by a set of parallel slices such that x_m varies by a small value dx, between $-R + t / 2$ and $R - t / 2$ in case E or between $-R - t / 2$ and $R + t / 2$ in case F. Let q be the number of slices per unit length along the x-axis, which is equal to one unit length divided by dx. Let β, which is equal to asin (L_S / D), be the half-angle at the center of the circle which supports a chord of length L_S (**Fig. 1.1d**). Let γ be the angle at the center of the circle equal to acos (t / D) such that $R \cos \gamma = t / 2$. Moreover, let c_1 be the difference $\cos \beta - \cos \gamma$ in case E or the sum $\cos \beta + \cos \gamma$ in case F (Eq. 1 in **Table 1.1**).

In case E, if an image is observed, $R \cos \gamma$ is shorter than or equal to $R \cos \beta$. Thus, the abscissa x_m of a slice which generates an image varies between $-R\, c_1$ and $R\, c_1$ (**Fig. 1.1e**). When x_m varies from $-R\, c_1$ to 0, the abscissa x of the chord which generates an image varies from $-R \cos \beta$ to $-R \cos \gamma$. When x_m varies from zero to $R\, c_1$, the abscissa x varies from $R \cos \gamma$ to $R \cos \beta$ (**Fig. 1.1e**). No image of a chord with an abscissa between $-t / 2$ and $t / 2$ can be observed. The number of images is:

$$M = \int_{-R \cos \beta}^{R \cos \beta} q \, dx - \int_{-R \cos \gamma}^{R \cos \gamma} q \, dx \qquad (1)$$

Because the length of each chord is:

$$L = 2 (R^2 - x^2)^{0.5} \qquad (2)$$

the sum of the image lengths obtained when x varies from $-R \cos \beta$ to $-R \cos \gamma$ is:

$$S_{E1} = \int_{-R \cos \beta}^{-R \cos \gamma} 2 (R^2 - x^2)^{0.5} \, q \, dx \qquad (3)$$

and the sum S_{E2} of the image lengths obtained when x varies from $R \cos \gamma$ to $R \cos \beta$ is given by an equation similar to Eq. (3), in which the limits are $R \cos \gamma$ and $R \cos \beta$. The sum of the image lengths is equal to $S_{E1} + S_{E2}$.

In case F, the abscissa x_m of a slice which generates an image varies between $-R\, c_1$ and $R\, c_1$ (**Fig. 1.1f**). When x_m varies from $-R\, c_1$ to $-R \cos \gamma$, the abscissa x of the chord which generates an image varies from $-R \cos \beta$ to 0. When x_m varies from $-R \cos \gamma$ to $R \cos \gamma$, the abscissa x is equal to zero (**Fig. 1.1c**). When x_m varies from $R \cos \gamma$ to $R\, c_1$, the abscissa x varies from zero to $R \cos \beta$ (**Fig. 1.1d**). The total number of images is given by Eq. (1), but with the minus sign between the two sums replaced by the plus sign. The sum of the lengths of the images is equal to $S_{F1} + S_{F2} + S_{F3}$, these sums being given by equations similar to Eq. (3), in which the limits are $-R \cos \beta$ and 0, $-R \cos \gamma$ and $R \cos \gamma$, and 0 and $R \cos \beta$ respectively, and in which x is equal to zero in the case of S_{F2}.

After integration, the ratio M / D is given by Eq. 4 in **Table 1.1**. The ratio of the first moment of the image length, which is the mean image length, L_m, to D is given by Eq. -5 in **Table 1.1**, in which c_2 is given by Eq. 2 in **Table 1.1**. This ratio L_m / D depends only on L_S / D and t / D. **Fig. 1.2** shows values of L_m / D calculated by these equations with given values of L_S / D and t / D with respect to L_S / L_m and t / L_m (which are equal to L_S / D and t / D divided by L_m / D respectively).

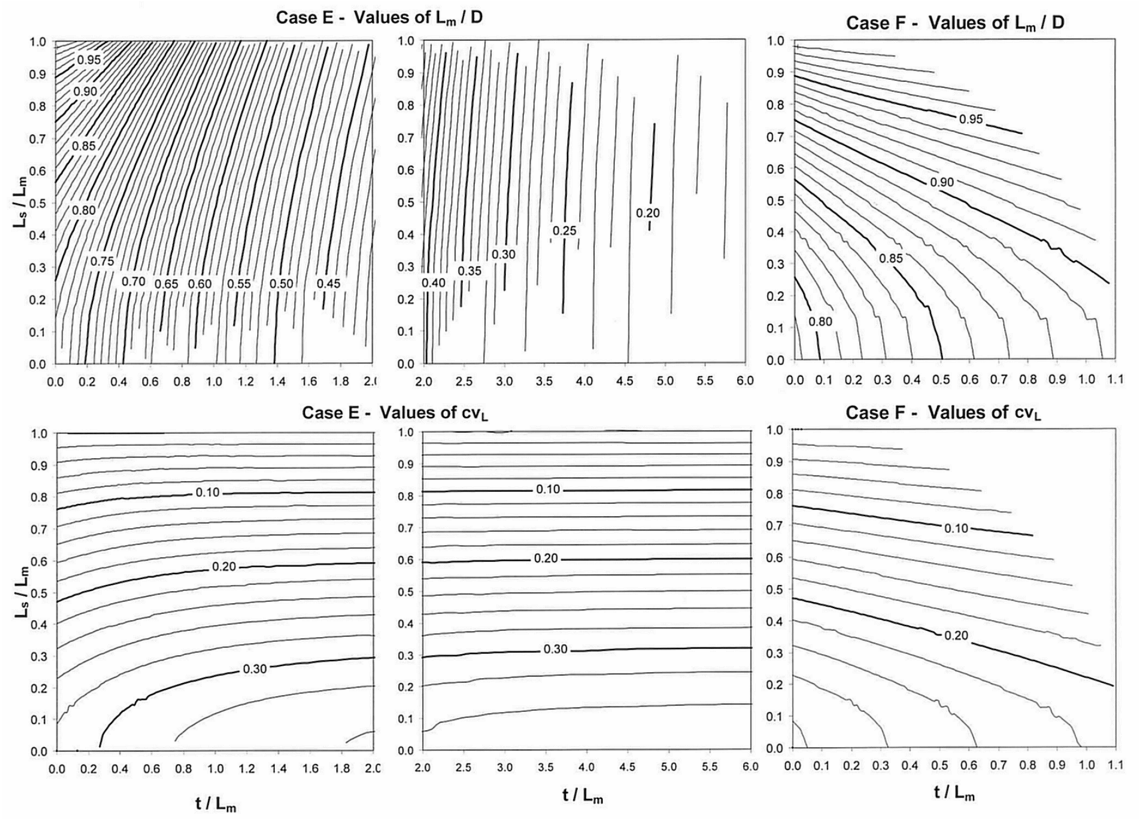

Fig. 1.2. Variations of L_m / D or of cv_L with respect to t / L_m and L_s / L_m according to Eqs. 2 in **Table 1.1** in cases E and F.

Each line meets points for which the value of L_m / D is the same (indicated only for the heavy lines). In case E, two figures for which the abscissa scale is different are given for L_m / D or cv_L. All points were obtained from values of t / D spaced 0.01 apart between 0 and 0.99 and values of L_s / L_m which were predicted by successive approximations made using Eqs. 2 and 4 in **Table 1.1**, with the values of L_m / D spaced 0.01 apart between 0.15 and 0.99 and the values of cv_L spaced 0.02 apart between 0.02 and 0.34. In case F, L_m / D is always greater than 0.784 and cv_L is always less than 0.284.

Based on Eq. (2), the second moment of the image length, $(L^2)_m$, which is the mean squared image length, is:

$$(L^2)_m = \frac{1}{M} \{ \int_{-R\cos\beta}^{R\cos\beta} 4\,(R^2 - x^2)\,q\,dx \pm \int_{-R\cos\gamma}^{R\cos\gamma} 4\,(R^2 - x^2)\,q\,dx \} \qquad (4)$$

with a minus sign in case E and a plus sign in case F, and with x^2 being equal to zero in the second term in case F. After integration, $(L^2)_m$ / D^2 is given by Eq. 6 in **Table 1.1**.

The squared coefficient of variation, cv_L^2, of the image length, which is equal to the ratio of the second moment to the squared first moment minus one, is given by Eq. 7 in **Table 1.1**. **Fig. 1.2** shows the values of cv_L calculated by this equation for given values of L_S / D and t / D with respect to L_S / L_m and to t / L_m.

The previous relations are also obtained when the images are generated from a sufficiently large number n of circles of diameter D, each circle being cut by at most one slice of which the midpoint is at a distance $|x_m|$ from the circle center, which distance varies by a small value dx between zero and $R - t$ / 2 in case E or zero and $R + t$ / 2 in case F (**Fig. 1.3b**). On account of the symmetry of a circle around its center,

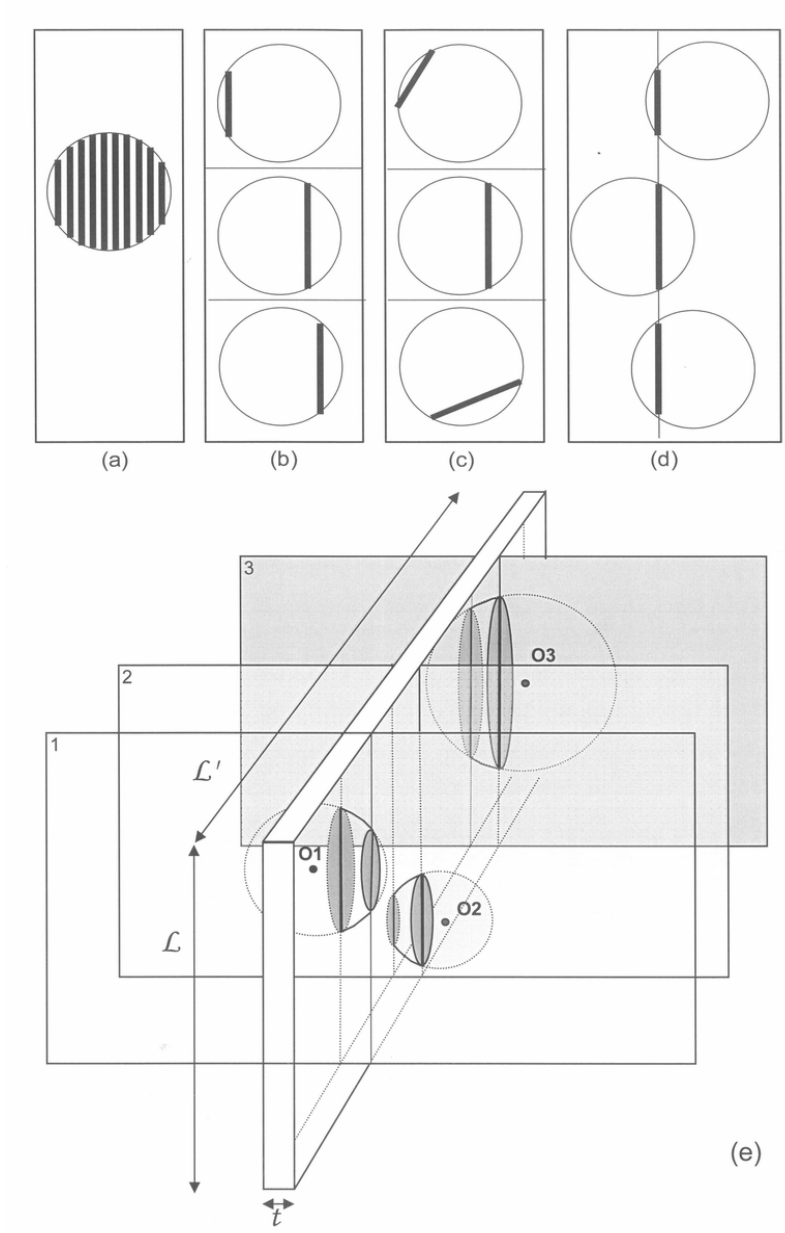

Fig. 1.3. Various cases of circles which generate similar sets of images:

(**a**) a circle is cut by equally spaced parallel slices; (**b**) the three slices in the left part of (**a**) are obtained from three different circles; (**c**) the three slices of case (**b**) are obtained from slices made through the volume in various directions; (**d**) the three slices of case (**b**) are obtained from a common slice made through the volume (here it is more evident than in the two previous cases to say that the distance of the circle centers to the slice varies, but in all three cases, the distance between the slices and the circle centers in fact varies); (**e**) case of three circles (possibly equatorial circles of spheres) in three different planes, 1, 2, and 3, cut perpendicularly by a slice of thickness t, with a section S_A equal to $\mathcal{L}\,\mathcal{L}'$. The images of these circles are the chords indicated by heavy lines in case F (in the case in which the circles are equatorial circles of spheres, circular sections are shown in the slice).

the same images can also be obtained from slices which are not parallel (**Fig. 1.3c**). They can also be obtained from a single slice which cuts the n circles of which the centers are at distances from the slice midpoint which differ by a small value dx (**Fig. 1.3d**). These relations can also be expected, with a probable deviation due to sampling, when the distances between the slice(s) and the centers of the n circles vary randomly between zero and $R - t / 2$ in case E or zero and $R + t / 2$ in case F. Finally, they can also be expected when the circles are in different parallel planes. In all these cases, a number of circles do not generate an image, and the number of images is:

$$M = \frac{n\, c_1\, D}{D \pm t} \qquad \text{(minus sign: case E; plus sign: case F)} \tag{5}$$

This equation is similar to Eq. 4 in **Table 1.1** with q equal to $1 / \mathrm{d}x$ and $(D \pm t) / n$ equivalent to $\mathrm{d}x$.

2.1.2. Case of a population of circles having possibly different diameters

Consider a population of n circles on a plane which have possibly different diameters. Let g be the function by which the fraction $g(D)$ of the population of circles having diameters between D and $D + \mathrm{d}D$ is related to D. This function g, which could be evaluated if the diameter distribution was known, will be eliminated in the cases considered following. Evidently:

$$\int_{D=0}^{\infty} g(D)\, \mathrm{d}D = 1 \tag{6}$$

Consider a set of parallel slices spaced by small $\mathrm{d}x$ and perpendicular to the plane. Assume the circles to be positioned so that their images obtained from the slices do not overlap. Because the number M of images of a circle of diameter D is equal to $q\, c_1\, D$ (Eq. 4 in **Table 1.1**), the total number, m, of images of the n circles is:

$$m = \int_{D=0}^{\infty} q\, c_1\, D\, n\, g(D)\, \mathrm{d}D \tag{7}$$

Denoting by L_m and $(L^2)_\mathrm{m}$ the first and second moments of the image length of a circle of diameter D, the first moment, l_m, and the second moment, $(l^2)_\mathrm{m}$, of the length of the m images are:

$$l_\mathrm{m} = \frac{1}{m} \int_{D=0}^{\infty} L_\mathrm{m}\, M\, n\, g(D)\, \mathrm{d}D \tag{8}$$

$$(l^2)_\mathrm{m} = \frac{1}{m} \int_{D=0}^{\infty} (L^2)_\mathrm{m}\, M\, n\, g(D)\, \mathrm{d}D \tag{9}$$

in which M, L_m, and $(L^2)_\mathrm{m}$ vary with D. From Eqs. 5 and 7 in **Table 1.1**, Eqs. (8) and (9) give:

$$l_\mathrm{m} = \frac{\mathrm{A}}{\mathrm{B}} \quad \text{with } \mathrm{A} = \int_{D=0}^{\infty} c_2\, D^2\, g(D)\, \mathrm{d}D \quad \text{and } \mathrm{B} = 4 \int_{D=0}^{\infty} c_1\, D\, g(D)\, \mathrm{d}D \tag{10}$$

$$(l^2)_\mathrm{m} = \frac{\mathrm{A}}{\mathrm{B}} \quad \text{with } \mathrm{A} = \int_{D=0}^{\infty} c_3\, D^3\, g(D)\, \mathrm{d}D \quad \text{and } \mathrm{B} = 3 \int_{D=0}^{\infty} c_1\, D\, g(D)\, \mathrm{d}D \tag{11}$$

The squared coefficient of variation ($cv_{\mathrm{length}}{}^2$) of the image length can be obtained from Eqs. (10) and (11) as:

$$cv_{\text{lengths}}{}^2 = \frac{\left(l^2\right)_{\text{m}}}{\left(l_{\text{m}}\right)^2} - 1 \tag{12}$$

2.1.3. Approximations in the case of a sample and especially of an almost infinitely long slice

Consider a part of a plane with area $\mathcal{A}$ where the number n of circles is large. Consider a set of slices $\mathcal{L}$ long, parallel, and spaced by a small dx along a distance $D_{\max} \pm t$ (with a minus sign in case E and a plus sign in case F), $D_{\max}$ being the diameter of one rather large circle of the population such that the plane region, $D_{\max} \pm t$ wide and $\mathcal{L}$ long, cut by these slices contains a sample of the circle population. This occurs if the number of circles is sufficiently large, and thus if $\mathcal{L}$ is sufficiently long (the case described as an "almost infinitely long slice"). Evidently, like any sample, this one probably does not contain the largest or the smallest circles in the population. The number of circles having centers falling in this region is:

$$n_{D\max} = \frac{n\,\mathcal{L}\left(D_{\max} \pm t\right)}{\mathcal{A}} \qquad \text{(minus sign: case E; plus sign: case F)} \tag{13}$$

The number of slices is $q\,(D_{\max} \pm t)$. The number $m_{D\max}$ of images of the $n_{D\max}$ circles is given by Eq. (7), with n equal to $n_{D\max}$.

If, in this region, the distances between the circle centers and the slices are random, and if the number of circles cut by each slice is sufficiently large, then each slice cuts a sample of circles having almost the same diameter at various distances from its center. Note that this is independent of the circle density, which can vary along $\mathcal{L}$. Therefore, because the slices are roughly similar, the number $m_{D\max,\,\text{one}}$ of images of circles obtained from only one almost infinitely long slice is, based on Eq. 7:

$$m_{D\max,\,\text{one}} = \frac{n_{D\max}}{D_{\max} \pm t} \int_{D=0}^{\infty} c_1\, D\, g(D)\, \mathrm{d}D \quad \text{(minus sign: case E; plus sign: case F)} \tag{14}$$

and Eqs. (10) to (12) are approximately valid for the images obtained by this slice.

Evidently, a sufficiently large set of slice portions, each taken from sampled regions like the previous plane region, $D_{\max} \pm t$ wide, of the surface $\mathcal{A}$, is equivalent to an almost infinitely long slice. The circle density and diameter distributions in the various regions can be different; it is sufficient only that the distances between the midpoints of the slice portions are greater than $D_{\max} \pm t$, so that each circle is cut by at most one slice portion.

2.1.4. Approximations for the case in which c_1, c_2, *and* c_3 *vary only slightly*

Fig. 1.4 shows that c_1, c_2, and c_3 vary only slightly when the ratios D / t or D / L_{S} are high.

Therefore, in this case, if t and L_{S} are given, c_1, c_2, and c_3 vary only slightly relative to D, and *a fortiori* to D^2 or D^3. Therefore, in Eqs. (10) and (11), they can be factored. Evidently, they can also be factored if D varies only slightly and if D / t, D / L_{S}, or both are smaller. In particular, their mean values are approximately equal to that which would occur if all the circles had the same diameter, this diameter being equal to that of a circle generating images of mean length equal to l_{m}. Let $D_{l\text{m}}$ be this diameter, $\beta_{Dl\text{m}}$ and $\gamma_{Dl\text{m}}$ the angles, equal to acos ($t / D_{l\text{m}}$) and to asin ($L_{\text{S}} / D_{l\text{m}}$), indicated in Eqs. 3 and 4 in **Table 1.2**,

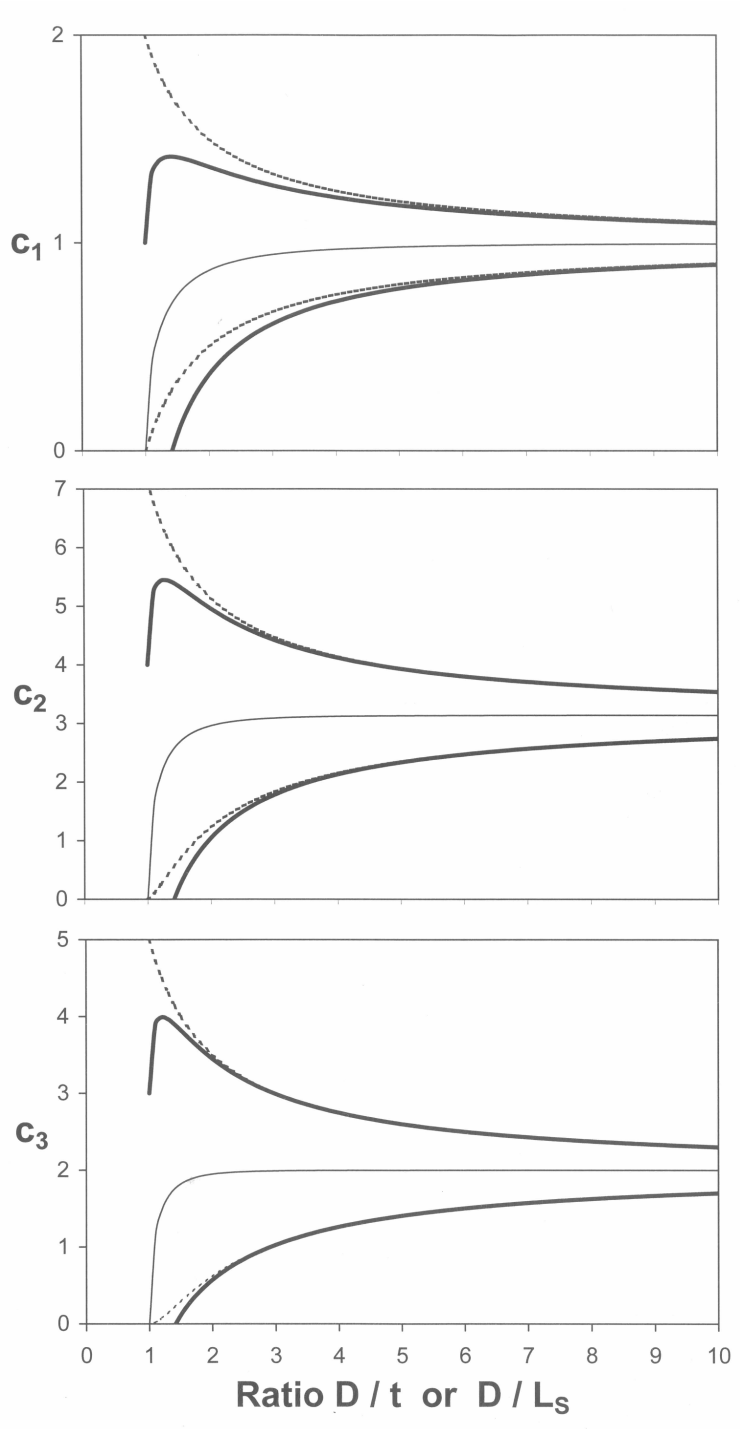

Fig. 1.4. Variation of c_1, c_2, or c_3 with respect to the ratios D / t and D / L_S in cases E and F.

Fine lines: variations when $t = 0$ in cases E and F. Heavy lines: variations when $L_S = t$ in cases E (lower heavy line) and F (higher heavy line). Dotted lines: variations when $L_S = 0$ in cases E (lower dotted line) and F (higher dotted line). Note that in case E, the values of D / t and D / L_S are greater than 1.414 (the square root of 2) if t and L_S are equal, because t and L_S are constrained by the relation $D^2 > t^2 + L_S^2$.

Table 1.2. *Equations to estimate the number of circles and the mean and coefficient of variation of their diameters when the diameter distribution is symmetrical or roughly symmetrical.*

Some relations differ in case E (transparent circle sectioned by opaque slices) and in case F (opaque circle sectioned by transparent slices).

	Case E	Case F	Eqs.
$l_m / D_{lm} =$	relations with (L_S / l_m) and (t / l_m) shown in **Fig. 2**		
$L_S / D_{lm} =$	$(L_S / l_m)\ (l_m / D_{lm})$		T2-1
$t / D_{lm} =$	$(t / l_m)\ (l_m / D_{lm})$		T2-2
$\beta_{Dlm} =$	$\text{asin}\ (L_S / D_{lm})$		T2-3
$\gamma_{Dlm} =$	$\text{acos}\ (t / D_{lm})$		T2-4
$c_{1,\,Dlm} =$	$\cos \beta_{Dlm} - \cos \gamma_{Dlm}$	$\cos \beta_{Dlm} + \cos \gamma_{Dlm}$	T2-5
$c_{2,\,Dlm} =$	$2\gamma_{Dlm} - 2\beta_{Dlm} - \sin 2\gamma_{Dlm} + \sin 2\beta_{Dlm}$	$\pi - 2\beta_{Dlm} + 4 \cos \gamma_{Dlm} + \sin 2\beta_{Dlm}$	T2-6
$c_{3,\,Dlm} =$	$(3 - \cos^2 \beta_{Dlm}) \cos \beta_{Dlm} - (3 - \cos^2 \gamma_{Dlm}) \cos \gamma_{Dlm}$	$(3 - \cos^2 \beta_{Dlm}) \cos \beta_{Dlm} + 3 \cos \gamma_{Dlm}$	T2-7
$cv_{L,\,Dlm}{}^2 =$	$16\ c_{1,\,Dlm}\ c_{3,\,Dlm} / 3\ c_{2,\,Dlm}{}^2 - 1$		T2-8
$\Delta =$	$(cv_{L,\,Dlm}{}^2 + 1)\ (9\ cv_{L,\,Dlm}{}^2 - 8\ cv_{\text{lengths}}{}^2 + 1)$		T2-9
$cv_D{}^2 =$	$(3\ cv_{L,\,Dlm}{}^2 - 2\ cv_{\text{lengths}}{}^2 + 1 \pm \Delta^{0.5}) / 2\ (cv_{\text{lengths}}{}^2 + 1)$		T2-10
$D_m =$	$4\ l_m\ c_{1,\,Dlm} / \{c_{2,\,Dlm}\ (cv_D{}^2 + 1)\}$		T2-11
$\beta_{Dm} =$	$\text{asin}\ (L_S / D_m)$		T2-12
$\gamma_{Dm} =$	$\text{acos}\ (t / D_m)$		T2-13
$c_{1,\,Dm} =$	$\cos \beta_{Dm} - \cos \gamma_{Dm}$	$\cos \beta_{Dm} + \cos \gamma_{Dm}$	T2-14
Case of slices equally spaced by small d*x*			
$n =$	$m / (q\ c_{1,\,Dm}\ D_m)$		T2-15
Case of an almost infinitely long slice			
$n =$	case of a surface: $m_{Dmax,\,one}\ \mathcal{A} / (\mathcal{L}\ c_{1,\,Dm}\ D_m)$ case of a volume: $m_{Dmax,\,one}\ \mathcal{V} / (S_A\ c_{1,\,Dm}\ D_m)$		T2-16

and $c_{1,\,Dlm}$, $c_{2,\,Dlm}$, and $c_{3,\,Dlm}$ the values of c_1, c_2, and c_3 indicated in Eqs. 5 to 7 in **Table 1.2**. Let D_m, $(D^2)_m$, and $(D^3)_m$ be the first, second, and third moments of the diameter distribution of the circles. Eqs. (10) to (12) provide the following approximations:

$$l_m \approx \frac{c_{2,\,Dlm} \left(D^2\right)_m}{4\, c_{1,\,Dlm}\, D_m} \tag{15}$$

$$(l^2)_m \approx \frac{c_{3,\,Dlm} \left(D^3\right)_m}{3\, c_{1,\,Dlm}\, D_m} \tag{16}$$

$$cv_{\text{lengths}}{}^2 \approx \frac{16\, c_{1,\,Dlm}\, c_{3,\,Dlm}\, D_m \left(D^3\right)_m}{3\, c_{2,\,Dlm}{}^2 \left(D^2\right)_m{}^2} - 1 \tag{17}$$

Because the ratio $16\ c_{1,\,Dlm}\ c_{3,\,Dlm} / 3\ c_{2,\,Dlm}{}^2$ is obtained from Eq. 7 in **Table 1.1**, Eq. 17 becomes:

$$cv_{\text{lengths}}{}^2 + 1 \approx (cv_{L,\,Dlm}{}^2 + 1)\ \frac{D_m \left(D^3\right)_m}{\left(D^2\right)_m{}^2} \tag{18}$$

representing by $cv_{L,\,Dlm}$ the coefficient of variation (cv_L in Eq. 7 in **Table 1.1**) of the length of images as given by the circle of diameter D_{lm}.

Moreover, in Eq. (7), c_1 can be factored. Assuming here that D_m is known and representing by β_{Dm} and γ_{Dm} the angles given by Eqs. 12 and 13 in **Table 1.2**, the value of c_1, now called $c_{1,\,Dm}$, is given by Eq. 14 in **Table 1.2**. It follows that:

$$m = n\, q\, c_{1,\,Dm} D_m \tag{19}$$

In the case of one almost infinitely long slice, Eqs. (13) and (14) give:

$$m_{D\max,\,one} = \frac{n\, \mathcal{L}\, c_{1,Dm}\, D_m}{\mathcal{A}} \tag{20}$$

2.1.5. Approximation of the case in which c_1, c_2, *and* c_3 *vary only slightly and in which the distribution is symmetrical*

If the diameter distribution is symmetrical, Eq. (18) gives, after the calculations indicated in Annex, the quadratic equation in $(cv_D^2 + 1)$:

$$(cv_{lengths}^2 + 1)\,(cv_D^2 + 1)^2 - 3\,(cv_{L,\,Dlm}^2 + 1)\,(cv_D^2 + 1) + 2\,(cv_{L,\,Dlm}^2 + 1) \approx 0 \tag{21}$$

where cv_D is the coefficient of variation of the diameter.

2.1.6. Case of circles on different parallel planes

Consider (**Fig. 1.3e**) a population of n circles randomly dispersed on different parallel planes spaced along a distance $\mathcal{L}'$ in a large volume $\mathcal{V}$, each circle being cut perpendicularly by one slice at most, of which the largest surface area is denoted by S_A (equal to $\mathcal{L}'\ \mathcal{L}$). If the diameter of a rather large circle is D_{max}, a region $D_{max} \pm t$ wide and of sectional area S_A is an unbiased sample of the volume. All the previous equations are valid for these circles and their images obtained from an almost infinitely long slice in this region if $\mathcal{L}$ and $\mathcal{A}$ are replaced by S_A and $\mathcal{V}$ respectively. Eq. (20) then becomes:

$$m_{D\max,\,one} = \frac{n\, S_A\, c_{1,Dm}\, D_m}{\mathcal{V}} \tag{22}$$

2.1.7. Application to sphere or cylinder images

Because an image of a sphere cut by a slice is a circle (**Fig. 1.3e**), whereas a diameter of this circle is equal to a chord of the equatorial circle of the sphere in a perpendicular plane, images of spheres dispersed in a medium are also chords of their equatorial circles. Because a cross-section of a cylinder is a circle, images of cylinders dispersed in a medium, which are generated by slices parallel to the cylinder axis, are chords of their circular sections. Thus the relations previously developed for circles are also applicable to spheres and cylinders.

2.2. Proposed method

Consider a set of images of circles possibly obtained from spheres or cylinders and generated either from a set of slices of thickness t which are equally spaced by a very small distance dx, or from a single random, almost infinitely long slice of thickness t. When this latter case consists of a set of slice portions, each must be selected at random from each sampled region of surface $\mathcal{A}$, and the slice portions must be distant from each other by more than $D_{max} \pm t$. Therefore, D_{max} has to be evaluated before sampling, for

example by the dissector method, or else it is necessary to verify *a posteriori* that $(L_{max}^2 + t^2)^{0.5} - t$ in case E or $L_{max} + t$ in case F, L_{max} being the greatest image length, is shorter than the distance between the midpoints of the slices.

Suppose that i) only images longer than L_S can be measured, ii) the images of two or several circles obtained by a slice do not overlap in case F (this is not possible in case E), and iii) the circles are not smaller than t in case F. To satisfy this last condition when the smallest circle size is unknown, only images longer than t are considered, and L_S is increased to be equal to t. In case E, where no image of any circle smaller than t can be obtained, the estimates will be made relative to circles larger than the greater of t or L_S; in case F, they will be made relative to circles larger than L_S.

Based on the relations presented previously, a method is proposed below to estimate the number of circles and the mean and coefficient of variation of the diameter when its distribution is symmetrical or roughly symmetrical. The special but simple case of a single circle or several circles known to have the same diameter value which has to be estimated is first presented. These methods vary slightly according to whether the images are obtained from a set of slices of thickness t equally spaced by a very small distance dx or from only one randomly chosen, almost infinitely long slice of thickness t.

2.2.1. Case of a circle or circles having the same diameter

Let D, L_m, and cv_L represent the circle diameter, mean, and coefficient of variation respectively of the M image lengths.

D is estimated from L_m, t, and L_S by successive approximations, substituting values of D into the equation for L_m derived from Eq. 5 in **Table 1.1** until the calculated value of L_m is sufficiently close to its measured value. Rough estimates can be obtained from **Fig. 1.2**, with D obtained by dividing L_m by L_m / D. If t or L_S is poorly known, t / L_m or L_S / L_m can be estimated from cv_L and L_S / L_m or t / L_m using **Fig. 1.2**.

The number of circles is estimated as $M / q\ c_1\ D$, based on Eq. 4 in **Table 1.1**, when the images are obtained from slices equally spaced by small dx, or as $M\ (D \pm t) / c_1\ D$, based on Eq. (5), when they are obtained from a single, almost infinitely long slice.

2.2.2. Case of circles of which the diameter distribution is symmetrical or roughly symmetrical

Let D_m, cv_D, l_m, and $cv_{lengths}$ represent the means and coefficients of variation of the n circle diameters and of the m image lengths.

From l_m, t, and L_S, D_{lm} is estimated as previously described for the case of a circle, with L_m and D set equal to l_m and D_m respectively. Then the values of L_S / D_{lm}, t / D_{lm}, β_{Dlm}, γ_{Dlm}, $c_{1,\,Dlm}$, $c_{2,\,Dlm}$, $c_{3,\,Dlm}$, and $cv_{L,\,Dlm}$ are calculated using Eqs. 1 to 8 in **Table 1.2**.

There are one or two values of cv_D^2 which are calculated using Eq. (21), for which the general form is: $a\ (cv_D^2 + 1)^2 + b\ (cv_D^2 + 1) + c = 0$. If the quantity $b^2 - 4\ a\ c$, denoted by Δ and calculated using Eq. 9 in **Table 1.2**, is positive, in other words, if $9\ cv_{L,\,Dlm}^2 - 8\ cv_{lengths}^2 + 1 > 0$, then the two values of cv_D^2 are given by Eq. 10 in **Table 1.2**. These values are symmetrical relative to the value of cv_D^2, which is equal to $(3\ cv_{L,\,Dlm}^2 - 2\ cv_{lengths}^2 + 1) / 2\ (cv_{lengths}^2 + 1)$, which verifies Eq. (21) when Δ is nil. Because of approximations in the measurements, a small sample size, or both, Δ may be slightly negative, especially

if its true value is very small. In this case, Δ is set equal to zero. When Δ is positive, one value of cv_D^2 may also be negative for the reasons previously stated, especially if the true value of cv_D is very small. In this case, cv_D^2 is set equal to zero.

Based on the values of cv_D^2, there are one or two groups of values of D_m and n which are obtained using Eqs. 11 to 16 in **Table 1.2**, Eq. 11 in **Table 1.2** being obtained from Eq. (15) in which $(D^2)_m$, the second moment of D, is:

$$(D^2)_m = (cv_D^2 + 1)\,(D_m)^2 \tag{23}$$

and Eqs. 15 and 16 in **Table 1.2** being derived from Eqs. (19), (20), and (22).

When there are two groups, one of them must be selected. This choice can be made in a number of cases and in a number of ways as shown below, especially if the symmetrical distribution is simple, for example normal or roughly normal.

First, when in a particular group, n is very small and not close to a whole number, this group is eliminated. Second, a group may be eliminated if its cv_D is too high, because the probability that a random variable is distant from its mean value by more than k times its standard deviation is less than $1 / k^2$ (Bienaymé-Tchebycheff's inequality). For example, in the case of a normal or roughly normal distribution, a group is eliminated if its shortest or longest diameter or both, as predicted by cv_D and D_m, is negative or very different from L_{max} in case F or from $(L_{max}^2 + t^2)^{0.5}$ in case E. These diameters are equal to $D_m\,(1 \pm \tau\, cv_D)$, τ being the value of the unit normal probability density function for the probability $1 - 1 / 2n$. Therefore, the predicted shortest diameter is estimated to be negative if $\tau\, cv_D$ is greater than one, or in other words, if cv_D is greater than, for example, 0.78, 0.39, or 0.30 when n is greater than or equal to 5, 100, or 1000 respectively. Thus, in the case of an almost infinitely long slice in which the number of images is less than n, the shortest diameter will be negative if cv_D is greater than the limit given by the number of images. Therefore, generally, the smallest value of cv_D is selected (see Results).

Moreover, a group is selected if the distribution of the image lengths calculated for a sample of circles with the values of cv_D^2 and D_m of this group is very close to the observed image-length distribution. Determining this consists of calculating the length of the image of each circle possibly generated by a slice of which the midpoint is at a distance $|x_m|$ from the circle center, with the distance varying by a small value between zero and the radius of the largest circle minus $t / 2$ in case E or plus $t / 2$ in case F. For a given circle of radius R and a given slice, the length of the image obtained is calculated as follows. In case E, if $|x_m| > R - t / 2$, no image is considered. Otherwise, the circle image length is equal to $2\,[R^2 - (|x_m| + t / 2)^2]^{0.5}$. In case F, if $|x_m| > R + t / 2$, no image is considered. Otherwise, if $|x_m| < t / 2$, then the image length is equal to D, else it is equal to $2\,[R^2 - (|x_m| - t / 2)^2]^{0.5}$. However, in both cases, E and F, if the image length is shorter than L_S, no image is considered.

If neither of the two groups of values can be selected, the diameter distribution may not be a simple symmetrical distribution or may not be symmetrical at all. Perspectives on such cases are given at the end of this paper.

3. Results

A number of examples were considered to validate the previously proposed relations and method.

3.1. Case of perfectly symmetrical distributions and of slices equally spaced by small d**x**, *with* **t / D** *and*

L_S / D ***equal to zero: set of three circles***

Two sets of three circles 2, 10, and 18 mm in diameter (set s_1, $cv_D = 0.653$, $D_m = 10$) and 10, 12, and 14 mm in diameter (set s_2, $cv_D = 0.136$, $D_m = 12$) were considered to examine a simple case and especially the selection of the value of cv_D. The image lengths were calculated as the lengths of all parallel chords equally spaced by one-thousandth of the diameter of the largest circle, with t and L_S equal to zero. Thus there were 1665 and 2571 images in s_1 and s_2 respectively. These lengths were then assumed to be measured lengths, and the diameters were assumed to be unknown. The values of l_m were 11.216 and 9.601 mm for s_1 and s_2 respectively, those of $cv_{lengths}$ were 0.458 and 0.315, and those of the longest images were 18.000 and 14.000 mm.

The relations shown in **Table 1.2** predict two possible groups (a and b) of values of cv_D, D_m, and n for each set: 0.494, 11.484 mm, and 2.61 (a) or 0.661, 9.937 mm, and 3.01 (b) for s_1, and 0.136, 12.004 mm, and 2.99 (a) or 0.965, 6.332 mm, and 5.68 (b) for s_2. Group (b) for s_1 and group (a) for s_2 were selected because in these groups, the predicted number of circles, which is small, is close to a whole number. Moreover, for s_2, the longest diameter (15.638 mm) predicted for group (b), assuming a normal distribution, is longer than the longest image (an obvious prediction because the value of cv_D is larger than the expected largest value (0.78) previously indicated for $n = 5$ in a normal distribution). These estimates are close to the real values.

With smaller numbers of equally spaced chords, the estimates were still close to the true values. For examples, with chords spaced by one-hundredth of the largest diameter (there were 165 and 255 images in s_1 and s_2 respectively), cv_D, D_m, and n were calculated as 0.707, 9.59 mm, and 3.10 for s_1 and 0.104, 12.18 mm, and 2.93 for s_2.

With very small numbers of chords spaced by a tenth of the greatest diameter, cv_D^2 was negative in some cases, for example in group (a) of s_2 with only 25 images. By setting cv_D equal to zero, D_m and n were calculated to be 12.49 mm and 2.80, values which are only slightly different from the true values. In group (b), cv_D was very much larger. In s_1, with only 15 images (1, 5, and 9 images from the three circles 2, 10, and 18 mm in diameter respectively), the estimated values of cv_D, D_m, and n were 0.280, 14.3 mm, and 1.9 for group (a) and 0.864, 8.8 mm, and 3.07 for group (b). Therefore, neither of the two groups could be selected based on their estimated numbers of circles (both close to whole numbers) or on the estimated longest diameters (18.18 and 17.78 mm) (both close to those of the longest images). This means that for s_1, the number of images (15) was too low to select one of the two groups.

Even with a greater number of chords, for example chords spaced by one-thousandth of the largest diameter, there were cases of sets of three circles, for example with diameters equal to 3, 10, and 17, for which Δ was found to be negative, with 8 $cv_{lengths}^2$ being slightly larger than $1 + 9\ cv_{L,\,Dlm}^2$. Therefore, cv_D, D_m, and n were estimated with $\Delta = 0$. The estimates were very close to the real values (0.577, 9.95, and 3.02 vs. 0.572, 10, and 3).

3.2. Case of slices equally spaced by small **d**x*: effects of the distribution and of* **t / D** *and* **L_S / D**

Five populations of one hundred circles were constructed to have symmetrical or approximately symmetrical diameter distributions (**Fig. 1.5** and **Table 1.3a**). Various values of t and L_S were considered, with $(L_S^2 + t^2)^{0.5}$ and t being smaller than the diameter of the smallest circle in cases E and F respectively.

To assess only the effect of the distribution type, without any deviation due to random sampling, the circle images were obtained from slices equally spaced by one-hundredth of the radius of the largest circle in the population minus t / 2 in case E or plus t / 2 in case F. The number of images ranged from approximately 1000 to 8000 depending on the distribution and the values of t and L_S. The image lengths were calculated as in the previously described test and considered as measured values. Then l_m and $cv_{lengths}$ were calculated. The values of cv_D, D_m, and n were estimated by the proposed method. In all cases, cv_D was estimated by the smaller root of Eq. (21) and was less than 0.40, because the value of cv_D estimated by the larger root was greater than 0.76, which is much greater than the highest value expected, as previously indicated, for a sample with one hundred circles from a normal population (0.39).

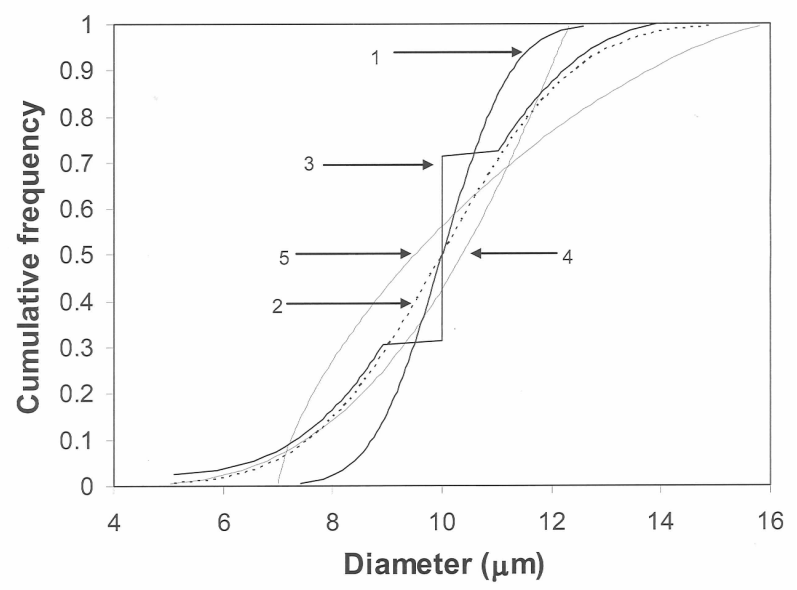

Fig. 1.5. Diameter distributions for five populations of circles.

Populations 1 and 2 (D_m = 10.0; cv_D = 0.099 and D_m = 10.0; cv_D = 0.189 respectively) are taken from normal distributions (D_m = 10.0; cv_D = 0.1 and D_m = 10.0; cv_D = 0.2 respectively). Distribution 3 is derived from population 2, the diameter being equal to 10 in all the classes between 30% and 70% (D_m = 10.0; cv_D = 0.185). Populations 4 and 5 (D_m = 10.0; cv_D = 0.171 and D_m = 10.0; cv_D = 0.243 respectively) are taken from beta distributions with parameters (p = 2.9; q = 1.09; min = 3.6; max = 12.35) or (p = 0.7; q = 1.4; min = 7; max = 16.1) respectively, p and q being the standard parameters of the beta distribution of the variable (D – min) / (max – min). Population 3 is slightly displaced upward to fit onto the figure. Fisher's coefficients of asymmetry (g_1) and skewness (g_2) are, for the five populations respectively: (0; -0.17), (0; -0.17), (-0.02; -0.06), (-0.77; -0.11), (0.61; -0.74).

In the three symmetrical distributions (1, 2, and 3), cv_D was very close to the real values when t and L_S were small (**Table 1.3a**). When t and L_S were larger, cv_D was slightly underestimated in case F. In case E, these parameters were underestimated when L_S was high and overestimated when t was high. In distribution 4, cv_D was almost always underestimated (estimated values between 0.128 and 0.182 vs. the true value of 0.171). In distribution 5, cv_D was highly variable with respect to t and L_S in case E, whereas it was close to the real values in case F except when L_S alone was very large. D_m and n were very close to the real values (estimated values between 9.8 and 10.3 vs. a true value of 10.0 for D_m; estimated values between 94 and 102 vs. a true value of 100 for n), except for distribution 5 when L_S alone was very large

Table 1.3a. *Coefficients of variation of the diameter (cv_D), mean diameter (D_m), and number of circles (n) estimated by the proposed method from the images generated by slices equally spaced by small dx, compared with the real values.*

Cases of five populations of 100 circles of which the diameter distributions are shown in Fig. 5. *The two cases, E (transparent circles) and F (opaque circles), are considered with various arbitrary values of* t *and* L_S. *The diameters of the smallest circles of populations 1 to 5 are 7.4, 5.1, 5.1, 5.0, and 7.0 respectively. Because only circles larger than* $(t^2 + L_S^2)^{0.5}$ *in case E or* L_S *in case F can generate images, only arbitrary values of* t *and* L_S *for which the smallest circle can generate at least one image were examined (except for distribution 5 in case E with* t *and* L_S *equal to 5, for which only four circles were too small). As predicted, the values are approximately equal in both cases E and F when* t = 0, *small differences being due to approximations in* L_m / D.

			Distribution 1			**Distribution 2**			**Distribution 3**			**Distribution 4**			**Distribution 5**		
			cv_D	D_m	n	cv_D	D_m	n	cv_D	D_m	n	cv_D	D_m	n	cv_D	D_m	n
		Real values:	0.10	10.0	100	0.19	10.0	100	0.19	100	100	0.17	10.0	100	0.24	10.0	100
t	L_S	$(t^2 + L_S^2)^{0.5}$															
Case E																	
0	0	0000	0.10	10.0	101	0.19	10.0	101	0.19	10.0	101	0.16	10.1	100	0.26	9.9	102
3	0	3.000	0.11	10.0	100	0.21	10.1	99	0.20	10.1	98	0.17	10.2	99	0.30	10.0	102
5	0	5.000	0.13	10.2	96	0.24	10.2	98	0.24	10.1	99	0.18	10.3	96	0.36	9.9	103
7	0	7.000	0.19	10.2	94										0.40	10.3	94
0	3	3.000	0.09	10.0	100	0.18	10.1	100	0.18	10.1	100	0.14	10.2	99	0.25	10.1	100
0	5	5.000	0.08	10.1	99	0.16	10.3	96	0.16	10.2	97	0.13	10.3	96	0.23	10.3	96
0	7	7.000	0.08	10.2	97										0.19	11.0	80
3	3	4.243	0.11	10.1	100	0.19	10.2	97	0.18	10.3	96	0.15	10.3	96	0.27	10.2	98
5	5	7.071	0.11	10.2	94										0.22	11.4	69
Case F																	
0	0		0.10	10.0	101	0.19	10.0	101	0.18	10.0	101	0.16	10.1	100	0.26	10.0	102
3	0		0.09	10.0	101	0.18	10.0	101	0.17	10.0	100	0.16	10.0	101	0.25	9.9	102
5	0		0.09	10.0	101	0.18	9.9	101	0.18	9.9	101	0.16	10.0	101	0.25	9.8	102
7	0		0.09	10.0	101										0.25	9.8	102
0	3		0.09	10.0	100	0.18	10.1	99	0.17	10.1	100	0.15	10.1	99	0.25	10.1	100
0	5		0.08	10.1	99	0.16	10.3	96	0.16	10.3	97	0.13	10.3	96	0.23	10.3	96
0	7		0.08	10.2	97										0.19	11.0	79
3	3		0.09	10.0	100	0.18	10.0	101	0.17	10.0	101	0.15	10.1	100	0.25	9.9	101
5	5		0.08	10.0	100	0.17	10.1	100	0.16	10.1	99	0.14	10.1	99	0.24	10.0	100
7	7		0.09	10.0	100										0.23	10.1	96

or when, in case E, both t and L_S were large.

It was verified (**Table 1.3b**) for distribution 2 (the only one examined to investigate this point) that the values of l_m and $cv_{lengths}$ calculated using Eqs. (15) to (17), in which the terms c_1, c_2, and c_3 are factored, were very close to the values calculated using Eqs. (10) to (12), in which the terms c_1, c_2, and c_3 are calculated for each circle using Eqs. 1 to 3 in **Table 1.1**.

Table 1.3b. *Values of* l_m *and* $cv_{lengths}$ *calculated either with the values of* c_1, c_2, *and* c_3 *specific to each circle in Eqs. (10) – (12), or with* $c_{1, Dlm}$, $c_{2, Dlm}$, *and* $c_{3, Dlm}$ *in Eqs. (15) – (17).*

The case of distribution 2 is shown. For case F, only some values of t *and* L_S *are shown.*

		Case E					Case F				
	t	0	3	0	3	5	0	3	3	5	5
	L_S	0	0	3	3	0	5	0	3	0	5
l_m	from Eq. (10)	8.13	7.40	8.44	7.80	6.73	8.93	8.57	8.82	8.76	9.32
l_m	from Eq. (15)	8.13	7.30	8.41	7.64	6.49	8.79	8.64	8.86	8.87	9.35
$cv_{lengths}$	from Eq. (12)	0.34	0.37	0.29	0.31	0.40	0.23	0.32	0.28	0.30	0.22
$cv_{lengths}$	from Eq. (17)	0.34	0.36	0.30	0.31	0.37	0.25	0.32	0.28	0.31	0.24

3.3. Case of an almost infinitely long slice: effects of the number of circles and of t / D *and* L_S / D

The previous calculations for the five circle populations were repeated with either one hundred circles or one thousand circles, taking only the image of each circle possibly generated by a slice at a random distance from the circle center according to a Monte Carlo method. The distance was less than or equal to the radius of the largest circle minus t / 2 in case E or plus t / 2 in case F. The calculations were replicated ten times. The number of images varied between 28 and 92 (for one hundred circles) or between 89 and 880 (for thousand circles), depending on the distribution, the values of L_S and t, and the effects of replication.

With one thousand circles, the values of cv_D (obtained as the smaller root of Eq. (21)) and of D_m were very close to those previously calculated with slices equally spaced by small dx (**Table 1.4** shows the data only for distribution 2). In only two simulations, which were performed using distribution 1 in case F, cv_D was set equal to zero because Δ was found to be negative. With only one hundred circles, for many of the simulations (23 of 90 in case E and 20 of 100 in case F with various values of t and L_S), cv_D was set to 0 because Δ was found to be negative, especially for distribution 1 which has the lowest coefficient of variation. For distributions 2, 3, 4, and 5, the numbers of such simulations were much smaller (6, 3, 9, and 8 respectively of approximately 130 simulations performed for each distribution). The variability between replications was greater than that observed with one thousand circles.

The number of circles n_{Dmax} as given by Eq. (13), with $n \mathcal{L} / \mathcal{A}$ estimated from Eq. (20), was most often slightly underestimated when D_{max} was estimated using L_{max} (**Table 1.4**), but was close to 100 or 1000 on average (data not shown) when D_{max} was equal to its true value.

3.4. Case of an almost infinitely long slice constituted by a set of slice portions: examples with real data and small numbers of images

Table 1.4. *Values of* cv_D, D_m, *and* n_{Dmax} *estimated by the proposed method from the simulated image lengths obtained according to a Monte Carlo method, drawing at random the distances of the bonbons to the slices, from an almost infinitely long slice.*

The case of distribution 2 (real values: $cv_D = 0.20$; $D_m = 10.0$*) which is shown in* Fig. 5. *Two circle sample sizes (100 and 1000 circles) and various arbitrary values of* t *and* L_S *were considered. Each result is shown as the average and, between parentheses, the lowest and highest values of each variable obtained in ten replications. With 100 circles, there are one or two replications (one or two asterisks marked in the third column) where* cv_D *was set equal to zero because it was estimated as negative.*

t	L_S		Number of images, m		Estimated cv_D		Estimated D_m		Estimated n_{Dmax}	
			100 circles	1000 circles	100 circles	1000 circles	100 circles	1000 circles	100 circles	1000 circles
Case E										
0	0	*	68 (60–76)	600 (582–621)	0.21 (0.06–0.29)	0.21 (0.15–0.23)	9.8 (9.1–10.7)	9.9 (9.8–10.4)	99 (87–115)	931 (881–1002)
3	0		57 (52–66)	533 (511–567)	0.17 (0.00–0.42)	0.23 (0.18–0.29)	10.3 (8.3–11.2)	10.0 (9.6–10.3)	83 (60–104)	928 (856–999)
5	0		52 (43–64)	440 (421–456)	0.24 (0.16–0.33)	0.24 (0.19–0.29)	10.2 (9.1–11.0)	10.2 (9.8–10.8)	94 (62–133)	836 (694–990)
0	3	*	62 (58–68)	585 (549–609)	0.17 (0.11–0.25)	0.18 (0.15–0.20)	10.1 (9.7–10.6)	10.2 (10.1–10.4)	88 (74–107)	930 (864–979)
0	5		56 (50–64)	534 (517–554)	0.17 (0.09–0.21)	0.17 (0.16–0.18)	10.3 (9.7–11.2)	10.3 (10.0–10.5)	88 (75–102)	913 (870–959)
3	3	**	54 (46–61)	494 (475–518)	0.18 (0.04–0.28)	0.19 (0.17–0.21)	10.3 (9.3–11.3)	10.3 (10.1–10.7)	84 (69–102)	877 (783–971)
Case F										
0	0	*	66 (59–74)	604 (575–632)	0.22 (0.09–0.33)	0.19 (0.15–0.22)	9.8 (9.5–10.5)	10.0 (9.7–10.3)	93 (78–101)	915 (873–1012)
3	0		71 (66–78)	677 (657–700)	0.20 (0.00–0.33)	0.20 (0.18–0.22)	9.9 (8.5–10.7)	9.9 (9.7–10.1)	96 (83–109)	988 (943–1048)
5	0	*	77 (69–82)	701 (671–739)	0.19 (0.07–0.29)	0.20 (0.18–0.23)	9.8 (8.6–10.6)	9.8 (9.6–10.0)	100 (83–112)	981 (955–1038)
0	3		63 (58–68)	598 (567–624)	0.19 (0.13–0.24)	0.19 (0.16–0.21)	10.1 (9.6–10.7)	10.1 (9.9–10.2)	95 (84–102)	973 (943–1069)
0	5		58 (54–64)	524 (487–546)	0.16 (0.11–0.19)	0.17 (0.16–0.18)	10.3 (9.8–10.8)	10.3 (10.2–10.4)	91 (77–100)	908 (840–991)
3	3		67 (57–81)	657 (640–678)	0.20 (0.14–0.25)	0.19 (0.17–0.21)	9.9 (9.2–10.6)	9.9 (9.7–10.0)	97 (78–124)	982 (887–1019)
5	5		66 (56–75)	639 (616–651)	0.16 (0.13–0.18)	0.18 (0.16–0.19)	10.1 (9.8–10.6)	10.1 (10.0–10.3)	94 (79–106)	962 (940–984)

Two populations of approximately spherical bonbons, white (WB) or yellow-orange (YB) (100 and 150 bonbons respectively, measured with a caliper (**Table 1.5**)) were mixed, included in a semi-transparent resin (Soloplast, GTS Pro type, France), and placed into a transparent tube of 52 mm internal diameter and 195 mm in length (**Fig. 1.6**). The smallest diameters of WB and YB were equal to 4.83 and 7.44 mm respectively, and the largest were equal to 6.75 and 9.95 mm respectively (**Fig. 1.7**). Fischer's coefficients of asymmetry (g_1) of WB and YB (-0.43 and 0.31 respectively) were in the range of those of the five previously studied populations (as indicated in **Fig. 1.5**). It was suspected that the density of the bonbons was highly heterogeneous, varying both along and perpendicular to the cylinder axis.

Evidently, because here D_{max} was known, there was no need to estimate it by the dissector method. Logically, this would have given, for example in case F, no more than six successive slices 2 mm thick with an image of the same bonbon, and therefore the largest diameter would have been estimated to be smaller than 10 mm. Because the slices were made by sawing and thinned by turning, the distance between slices was constant, for convenience. Therefore, ten slices, 3.00 ± 0.01 mm thick and spaced 15 mm apart, were made perpendicularly to the cylinder axis to enable systematic sampling along the cylinder axis, taking variability perpendicular to the cylinder axis into account and minimizing the edge surfaces which are poorly sampled (the two cylinder ends). The slices were then scanned (**Fig. 1.6**). The bonbon image diameters (case F) were obtained using the *Image J* software as the mean of the sides of a rectangle circumscribing the image. Then the slices were left in water until the bonbons dissolved, leaving spherical holes. The slices were then re-scanned (**Fig. 1.6**) and the hole image diameters (case E) were obtained as previously. The smallest image diameters of WB and YB were 1.36 and 1.98 mm respectively in case E and 2.13 and 1.91 mm in case F. The absence of smaller images was probably attributable to removal of small bonbon lumps by sawing and turning. The largest image diameters were 5.01 and 7.87 mm in case E and 6.89 and 9.83 mm in case F for WB and YB respectively. As a result, $(L_{max}^2 + t^2)^{0.5} - t$ and $L_{max} + t$ were smaller than the distance between the slice portions. Note that the slices were semi-transparent and small enough to see whether bonbons were entirely overlapping; only two such cases among 118 images were observed. Because the distance of the bonbon centers from the cylinder wall was at least equal to their radius, the volume $\mathcal{V}$ in Eq. T2-16 was calculated as $\pi\,(R - D_m / 2)^2\,(195 - D_m)$, R and 195 being the radius and length respectively of the resin cylinder, and S_A was calculated as $10\,\pi\,(R - D_m / 2)^2$, ten being the number of slices.

Although the numbers of bonbon images were very small, especially in case E (**Table 1.5**), the proposed method was applied to the diameters of the bonbon images (case F) and the hole images (case E) of WB or YB with t equal to 3 mm and L_S equal to the smallest image diameter. **Table 1.5** shows the estimated values of cv_D, D_m, and n. In case E for WB and in case F for WB and YB, the predicted values of cv_D and D_m were higher than the observed values. **Fig. 1.7** shows that the distributions predicted for WB and YB in case F from the estimated values of cv_D and D_m, assuming normal distributions were larger. To examine whether the discrepancies between the estimated and real values could be due to random sampling variability of the circle diameters and of the distance of their centers to the slice portions, one hundred simulations were performed with a number n_{Dmax} of bonbons having their centers in an almost infinitely long region, $D_{max} \pm t$ large, with surface area S_A. The number n_{Dmax} was estimated (**Table 1.5**) using Eq. 13, with n equal to 150 and 100 for WB and YB respectively and $\mathcal{L}$ and $\mathcal{A}$ being replaced by S_A and $\mathcal{V}$ respectively. The diameter of each bonbon was given by random sampling from the theoretical normal distribution defined by the real values of cv_D and D_m, thus distinguishing n_{Dmax} classes.

D_{max} was the diameter of the largest class. The distances of the bonbon centers to the slice midpoint were also obtained by random sampling between zero and $D_{max} / 2 \pm t / 2$. The mean values and the standard deviations of cv_D and D_m calculated for the one hundred simulations (**Table 1.5**) indicated, at confidence levels higher than 95%, that the discrepancies could be due to random variability, because they were smaller than twice the standard deviation. The same was also observed for the predicted number of bonbons, except in case F for WB. In this case, the predicted numbers of bonbons and of images were less than the expected numbers by approximately five times the standard deviation.

Simulations were also performed, according to a Monte Carlo method, drawing at random the distances of the bonbons to the slice, with various arbitrary values of n_{Dmax}, assuming cv_D and D_m known, to determine the variability of the estimates of YB in cases E and F with respect to the number of images (**Fig. 1.8**). Such simulations can indicate the number of images which must be observed to estimate cv_D and D_m with a given confidence level. For example, if only 33 images were observed in case F (**Fig. 1.8**), D_m would be estimated, at confidence level 95%, to be between 8.54 – 2 (0.49) = 7.56 and 8.54 + 2 (0.49) = 9.52, and similarly, cv_D would be estimated, at this same confidence level, to be between 0.057 – 2 (0.076) (effectively zero) and 0.057 + 2 (0.076) = 0.209.

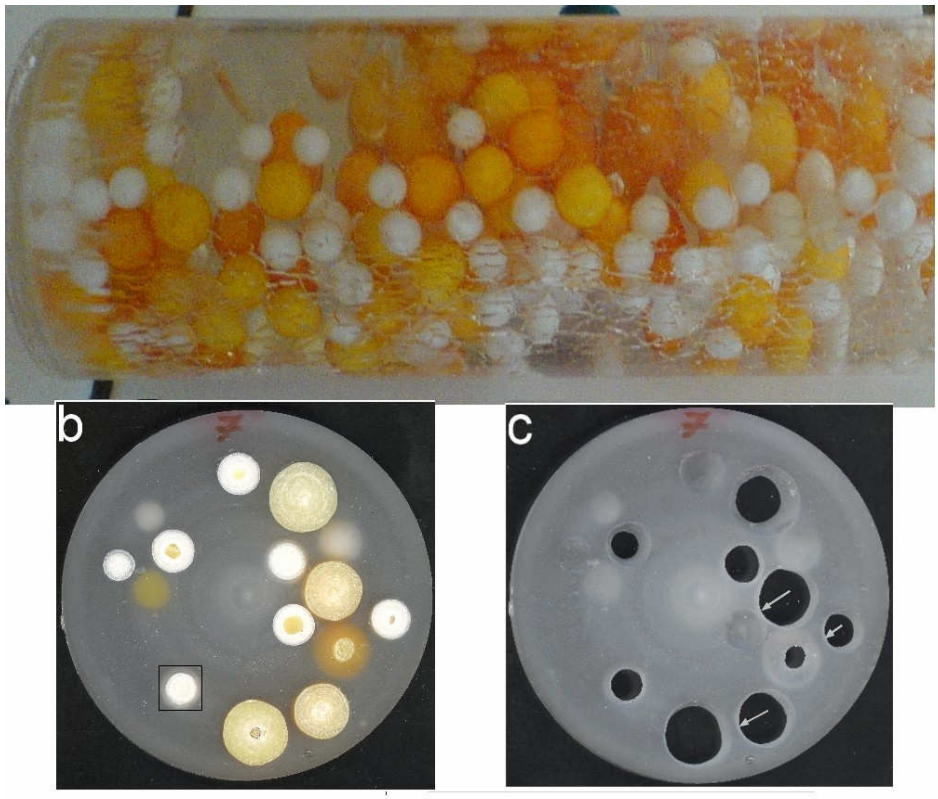

Fig. 1.6. Photos of bonbons from two mixed populations: WB (white with a small yellow stone visible in some cases) or YB (yellow-orange) included in a semi-transparent resin inside a tube (diameter = 52 mm; length = 195 mm); (**a**). Slices 3 mm thick were made, generating images belonging to case F (**b**) or, after dissolution of the bonbons, to case E (**c**).

In case F, a rectangle drawn to estimate the diameter is shown. In case E, it seems that the lighting of some holes, such as those indicated by arrows, was not exactly perpendicular to the slice.

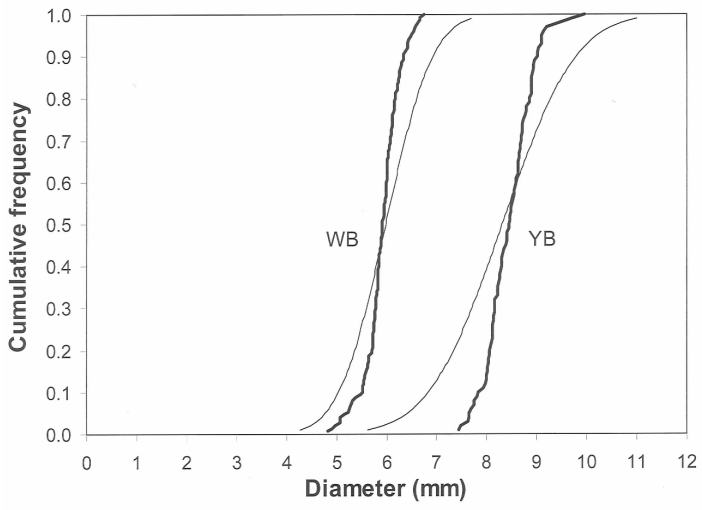

Fig. 1.7. Observed diameter distributions (heavy lines) of the two bonbon populations (WB and YB) and their predicted distributions based on the mean diameter and the coefficient of variation of the diameter as estimated by the proposed method from images obtained in case F using slices 3 mm thick, assuming normal distributions (fine lines). Fisher's coefficients of asymmetry (g_1) and skewness (g_2) are (-0.43; 0.72) and (0.31; -0.33) for WB and YB respectively.

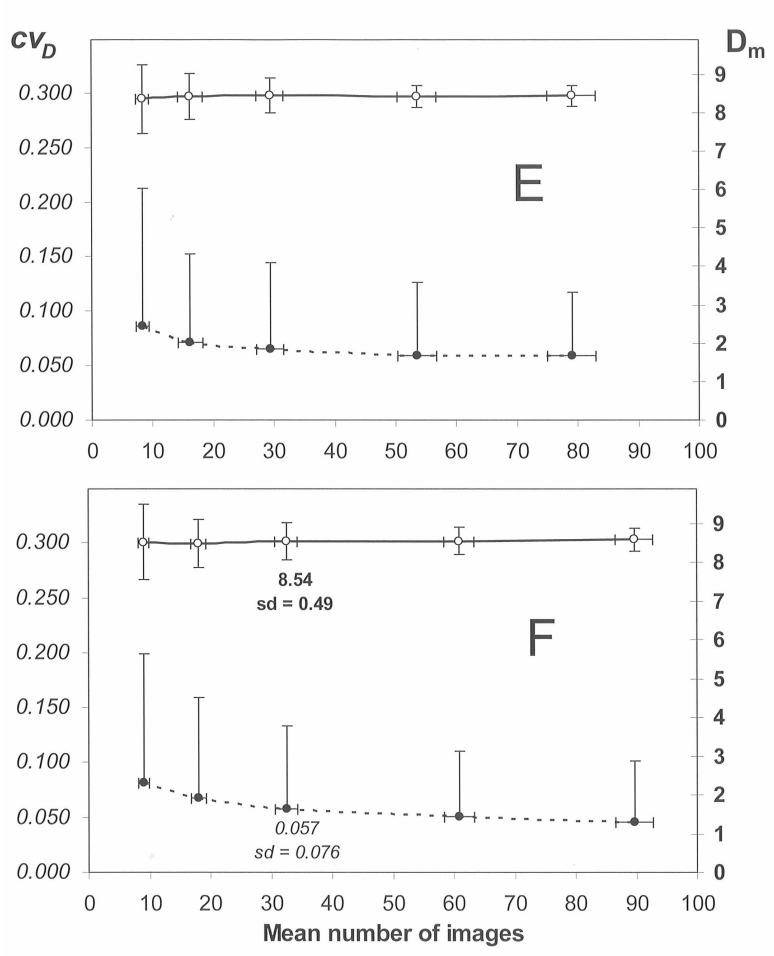

Fig. 1.8. Means of D_m (heavy line) and cv_D (dotted line) with respect to the mean number of images obtained in one hundred simulations performed with the number n_{Dmax} of bonbons equal to 10, 20, 36, 68, and 100. The delimiting vertical and horizontal lines show the observed standard deviations. The case of bonbon population YB in cases E and F is shown.

Table 1.5. *Application of the method to images of two populations of yellow-orange (YB) or white (WB) bonbons from slices 3 mm thick.*

Additional parameters are indicated for YB to show the sequence of calculations. The values of the mean and standard deviation (between parentheses) were calculated from one hundred simulations according to a Monte Carlo method, drawing at random the distances of the bonbons to the slices, with the real values of cv_D *and* D_m *and with* n_{Dmax} *equal to 36 and 68 for YB for cases E and F respectively, and to 31 and 78 for WB in cases E and F respectively.*

	Real values		Estimated values		Values from 100 simulations	
	case E	**case F**	**case E**	**case F**	**case E**	**case F**
YB						
$m_{D\max,\,one}$	32	64			29.0 (2.4)	60.9 (2.5)
l_m (mm)	6.30	7.24				
$cv_{lengths}$	0.211	0.264				
L_S (mm)	1.983	1.908				
$l_m / D_{l\mathrm{m}}$			0.710	0.860		
$cv_{L,\,Dl\mathrm{m}}$			0.267	0.225		
cv_D	0.055		0.001*	0.139	0.064 (0.075)	0.050 (0.060)
D_m (mm)	8.45		8.91	8.31	8.42 (0.46)	8.56 (0.35)
β_{Dm}			0.224	0.232		
γ_{Dm}			1.227	1.201		
n	100		105	108	101.4 (12)	98.1 (6.2)
WB						
$m_{D\max,\,one}$	22	54			23.3 (2.4)	68.7 (2.7)
cv_D	0.060		0.233	0.114	0.075 (0.081)	0.040 (0.049)
D_m (mm)	5.91		5.32	5.98	5.86 (0.33)	5.98 (0.17)
n	150		194	119	155.2 (26.6)	150.7 (6.9)

* Value assigned to assess D_m because cv_D^2 was calculated as negative.

4. Discussion

The method proposed here is based largely on Eq. (21), which assumes that the diameter distribution is perfectly or roughly symmetrical. It links the coefficients of variation of the circle diameters, of the image lengths, and of the lengths of the images of a virtual circle having as its mean image length the same value as the mean length of the images of the circles. This equation assumes that the parameters c_1, c_2, and c_3 can be factored in Eqs. (10) and (12) without significant error. This was found to be an acceptable approach when D / t and D / L_S are large enough (**Table 1.3b**) because these parameters are almost constant in these cases (**Fig. 1.4**). Moreover, because for symmetrical diameter distributions, the number of circles smaller than D_m is equal to the number of circles larger than D_m, compensations occur between the deviations introduced for each of the circles smaller than D_m by factoring $c_{1,Dl\mathrm{m}}$ or $c_{1,Dm}$, $c_{2,Dl\mathrm{m}}$, and $c_{3,Dl\mathrm{m}}$ and those introduced for the circles larger than D_m. In case E, these compensations are likely smaller when D / t and D / L_S are small because they vary rapidly (**Fig. 1.4**). The proposed method requires selection of one of the two roots of Eq. (21). In most of the examples previously described, the smaller root was selected. In the set s_1 of only three circles, the larger root was selected. This case is likely to occur only when the variability of the diameter is very large relatively to that of the image

length. The selection can be made based on the predicted longest image or on the number of circles. In cases where Δ and cv_D are negative, they can be set equal to zero, although this entails lower accuracy. In cases where neither the smaller nor the larger root can be selected, for example in set s_1 with a very small number of chords (15), the number of images must be increased.

The method was found to be applicable even to fairly small image samples (several dozen images) in the case of slices equally spaced by small dx. In the case of an almost infinitely long slice, accurate estimates were still obtained for fairly small image samples (**Table 1.4**). This likely occurred because Eq. (21) involves only the coefficients of variation. The coefficient of variation of a variable often varies only slightly between small samples from a single population, even if the mean and the standard deviation vary, because these statistics vary largely in the same way (Dagnélie, 1973). Evidently, accuracy was lower with smaller samples or more approximate measures. With very small samples, Δ and cv_D could not even be calculated in some cases, but still, by setting them equal to zero, the method could provide approximate estimates of the mean diameter and of the number of particles.

The examples with bonbons largely confirmed the previous results, although there were some discrepancies between the estimated and real values. Most of these discrepancies could be explained by random variability because they were in the ranges expected from one hundred simulations made with sets of random diameters and random distances of the bonbons to the slice midpoint. The discrepancies in D_m and cv_D were greater in case E, probably because the numbers of images were smaller than in case F. However, a part of these discrepancies could be due to various approximations. The bonbons were not exactly spherical, and measurements of image diameters were therefore likely approximate: in case E, some of the images showed shaded zones because the lighting was not exactly perpendicular to the slices (**Fig. 1.6c**); in case F, some image contours were not very clear due to light diffusion and diffraction (**Fig. 1.6c**). In spite of these discrepancies, the estimates provided information about the D_m and cv_D of the two populations, as shown in case F (**Fig. 1.7**), which would likely prove useful. However, in case F for WB, the number of bonbons was greatly underestimated. This was likely due to underestimation of the observed number of images. Most probably, the slice portions were not sufficiently representative of the large-scale spatial variability of bonbon density. **Fig. 1.8** provides some indication of the number of images which would have to be obtained to achieve a given level of precision. Here, the number of images was limited by the minimal distance, $D_{max} \pm t$, between slice portions and by the direction of the slices, which was chosen to take heterogeneities in the cylinder axial direction into account. It was assumed that spatial variability along the axis was not related to any periodic variable harmonized with the distance between slices, which was not random, but constant.

If the diameter distribution, which is not generally known, is not perfectly or approximately symmetrical, the method will provide estimates of D_m and cv_D, the latter being possibly set equal to zero, but these might be very far from the true values. In this case, the image-length distributions calculated for a sample of circles assuming successively different types of diameter distribution (for example, a normal distribution) with the estimated values of cv_D^2 and D_m will not be very close to the observed image-length distribution. Therefore, it is important to verify that the image-length distribution predicted by these estimates is in agreement with the observed image length distribution. This is easy to check if the distribution is normal.

Certainly the proposed method provides estimates which do not converge exactly to the true values when the number of images is infinitely large, especially when t and L_S are nonzero because of the approximations made when c_1, c_2, and c_3 are factored to give Eqs. (15) to (20). However, both bias and estimate variability seem to be small enough to provide useful information with only a few dozen images.

It is important not to forget that the proposed method must be used with caution, especially if diameters are smaller than t or when images overlap. Suggestions have already been provided as to how

to overcome the first limitation, whereas the example with the bonbons, where only two images among 118 were found to overlap, suggested a low probability of completely overlapping images in a slice where the particles are widely enough dispersed (the ratio of bonbon volume to the total volume of resin and bonbons was 0.11). In the case of partly overlapping sphere images, or lobed images, it is possible to infer the circle diameters from their visible lobed parts.

5. Conclusions

The proposed method provides estimates of the number n of objects and of the mean, D_m, and the coefficient of variation, cv_D, of their diameters when the diameter distribution is symmetrical or approximately symmetrical. It works even with a small number of images, although cv_D may not be estimated if the number of images is very small. Evidently, the estimates are more precise on average when the spatial distribution of the objects in the volume is more homogeneous and when the number of slices and the number of objects are larger, or when the image-detection limit is lower, leading to a larger number of images. The accuracy depends also on the slice thickness and on the underlying distributions. In the simulated and real examples presented here, valuable predictions were obtained with several tens of images. Simulations can provide indications of the number of images which have to be obtained to achieve a given accuracy level.

The proposed method, which is based both on a geometric model and on a sampling design, and which is easily applicable using **Table 1.2,** will likely be very useful in many fields, especially for approximations when only a small number of images (evidently not too small) is available and when the distribution is approximately normal.

In a number of cases, the diameter distribution is not of a simple type or is not perfectly or approximately symmetrical, or the objects are not perfect circles, cylinders, or spheres. The present method plays a large part in methods under development for any diameter distribution or for only approximately circular objects with an equivalent diameter which can be estimated. These methods will play a role in further research to estimate the size of phloem pores.

Acknowledgements

The author thanks B. Delécolle for her help in making electron microscopy observations and in solving image interpretation problems, C. Vigne for his very competent contribution in making the bonbon slices, and anonymous reviewers for their many comments and suggestions.

References

Antoniadis, A., Fan, J., Gijbels, I. 2001. A wavelet method for unfolding sphere size distributions. *Can. J. Stat*. 29, 251–258.

Baddeley, A., Jensen, E. 2005. Stereology for Statisticians. Boca Raton, USA: Chapman and Hall-CRC.

Bussières, P. 2002. Water import in the young tomato fruit limited by pedicel resistance and calyx transpiration. *Funct. Plant Biol*. 29, 631–641.

Cau, P. 1990. Microscopie Quantitative: Stéréologie, Autoradiographie et Immunocytologie Quantitatives. Paris, France: Editions INSERM.

Coleman, R. 1983. The sizes of spheres from profiles in a thin slice: II. Transparent spheres. *Biom. J*. 25, 745–755.

Cruz-Orive, L.M. 1983. Distribution-free estimation of sphere size distribution from slices showing overprojection and truncation, with a review of previous methods. *J. Microsc*. 131:265–290.

Cruz-Orive, L.M. 1997. Stereology of single objects. *J. Microsc*. 186, 93–107.

Dagnélie, P. 1973. Théorie et Méthodes Statistiques. Vol. 1 and 2. Gembloux, Belgium: Les Presses Agronomiques de Gembloux.

Davtian, A., Hahn, U., Ohser, J., Stoyan, D. 2000. Estimating the number density N_V: a comparison of an improved Saltykov estimator and the dissector method. *Image Anal. Stereol*. 19, 209–214.

Feuerverger, A., Hall, P. 2000. Methods for density estimation in thick-slice versions of Wicksell's problem. *J. Am. Stat. Assoc*. 450, 535–546.

Feuerverger, A., Menzinger, M., Atwood, H.L., Cooper, R.L. 2000. Statistical methods for assessing the dimensions of synaptic vesicles in nerve terminals. *J. Neurosci. Meth*. 103, 181–190.

Fleischer, K. 1994. The tomato salad problem reconsidered. *Biom. J*. 36, 193–203.

Hedreen, J.C. 1998. Lost caps in histological counting methods. *Anat. Rec*. 250, 366–372.

Howard, C.V., Reed, M.G. 1998. Unbiased Stereology. Three-Dimensional Measurement in Microscopy. Oxford, England: BIOS Scientific Publishers.

Jastrow, H., Von Mach, M.A., Vollrath, L. 1997. Adaptation of the dissector method to rare small organelles in TEM sections exemplified by counting synaptic bodies in the rat pineal gland. *J. Anat*. 191, 399–405.

Kok, L.P. 1990. 100 Problems of My Wife and their Solution in Theoretical Stereology. Leiden, The Netherlands: Coulomb Press.

Kopp-Schneider, A. 2003. Biostatistical evaluation of focal hepatic preneoplasia. *Toxicol. Pathol*. 31, 121–125.

Mase, S. 1995. Stereological estimation of particle size distributions. *Adv. Appl. Prob*. 27, 350–366.

Sahagian, D.L., Proussevitch, A.A. 1998. 3D particle size distributions from 2D observations: stereology for natural applications. *J. Volcanol. Geoth. Res.* 84, 173–196.

Silverman, B.W, Jones, M.C, Wilson, J.D., Nychka, D.W. 1990. A smoothed EM approach to indirect estimation problems, with particular reference to stereology and emission tomography. *J. R. Statist. Soc*. *B* 52, 271–324.

Stoyan, D, Kendall, W.S., Mecke, J. 1995. Stochastic Geometry and its Applications. Chichester, England: John Wiley and Sons.

Weibel, E.R. 1980. Stereological Methods. Vol. 2: Theoretical Foundations. London, England: Academic Press.

Wicksell, S.D. 1925. The corpuscle problem: a mathematical study of a biometric problem. *Biometrika* 17, 84–99.

Wilson, J.D. 1989. A smoothed EM algorithm for the solution of Wicksell's corpuscule. *J. Statist. Comput. Simul*. 31, 195–221.

Xu, Y.H., Pitot, H.C. 2002. An improved stereologic method for three-dimensional estimation of particle size distribution from observations in two dimensions and its application. *Comput. Meth. Prog. Bio*. 72, 1–20.

Annex

When the distribution of a variable is symmetrical, the third central moment (relative to the mean diameter) is nil. Based on the relation which exists between this moment and the three first moments relative to the origin (Dagnélie, 1973), it follows that:

$$(D^3)_m = 3\, D_m\, (D^2)_m - 2\, D_m{}^3 \qquad (24)$$

Therefore, by letting cv_D represent the coefficient of variation of the diameter, Eq. (18) yields Eq. (21), after multiplying the numerator and the denominator by D_m and noting that $3\ cv_D^2 + 1$ is equal to $3\ (cv_{L,\ Dlm}^2 + 1) - 2$.

CHAPTER 2

Estimating the numbers and diameters of objects from their images in slices: case of any diameter distribution treated as a set of symmetrical distributions

Abstract

A method has been recently proposed to estimate the numbers and the diameter distributions of circular, cylindrical, or spherical objects included in a matrix from their images generated by slices when the diameter distribution is perfectly or approximately symmetrical. Here a method is proposed for any distributions. The object population is considered to be composed of various populations in juxtaposed size classes, each with a perfectly or approximately symmetrical diameter distribution. These size classes, called macro-classes as composed of smaller classes, are defined so that the largest images of the objects of a single population fall into a single macro-class. The mean and coefficient of variation of the diameters in the population of the largest objects are estimated from those of the image lengths in the largest macro-class using the recently developed method for symmetrical distributions. For that, the lower image-detection limit is set equal to the lower limit of the macro-class. The same calculations are performed successively for each population of smaller objects, the number of images in each size class being estimated by the observed number of images minus the numbers of images generated by the populations of larger objects calculated assuming their diameter distributions to be normal. The calculations are formulated in a spreadsheet available online. Valuable predictions were obtained for both simulated and real examples.

1. Introduction

Estimation of the numbers and diameter distributions of circular, cylindrical, or spherical objects included in a matrix from their images obtained by slices has been the purpose of many research studies, a great number of these originating in microscopy. Most of these are cited in the references of Weibel (1980), Cruz-Orive (1983), Stoyan et al. (1995), and Baddeley and Jensen (2005). This problem has been recently reconsidered (see Chapter 1) from a general viewpoint, including the cases of both opaque and transparent objects, of possible image-detection limit, and of thick slices (which are less thick than the smallest circle diameters), but only for perfectly or approximately symmetrical diameter distributions.

However, in many cases, the diameter distribution is not perfectly or even approximately symmetrical. It can be strongly unbalanced either on the right or on the left, or highly irregular with several local frequency maxima. It is important to be able to estimate the diameter distribution in such cases, especially because it may reveal different object populations. Kim et al. (2000) proposed a method for this problem based on subdividing the population of the images in sets which contain normal deflections in the

distribution. Here, this approach is used in a new method applicable to any diameter distributions which is based largely on the relations and the method developed for symmetrical distributions (see Chapter 1). These are briefly presented hereafter.

First, the case of circles on a plane is initially considered because the cases of spheres or cylinders are then easily derived from it. Assuming therefore a circle of diameter D on a plane and a slice of thickness t perpendicular to the plane at a distance x from the circle center, two cases of images of the possible intersection between the circle and the slice, which is a circle segment, were considered. In one case, the circle is more transparent than the slice matrix (**Fig. 2.1a**) and the image length is L_1 (case E), and in the other case, it is more opaque than the slice matrix and the image length is L_2 (case F). However, no image is obtained if the image length is shorter than the image-detection limit L_S. Assuming circles with possibly different diameters randomly positioned in a part of the plane with area $\mathcal{A}$, images of these circles are generated using a set of slices perpendicular to the plane and equally spaced by a very small distance dx relative to the smallest diameter. When only one almost infinitely long slice of length $\mathcal{L}$ sections the plane, only a certain number of these circles yields an image. Similar to this latter case is the case of a set of slice portions distant from each other by a value greater than $D_{max} \pm t$ (minus sign in case E and plus sign in case F), D_{max} being the diameter of a fairly large circle of the population. In all these cases, when the diameter distribution is perfectly or approximately symmetrical, the mean D_m and coefficient of variation cv_D of the circle diameters as well as the number n of circles can be estimated from the number of images and the mean l_m and coefficient of variation cv_{length} of their lengths which fall into the size classes greater than L_S, using equations which are described in the **Annex**. Also, in the cases of circles in different planes or of spheres or cylinders, the previous estimates can be derived from these equations by replacing $\mathcal{L}$ and $\mathcal{A}$ by S_A and $\mathcal{V}$ respectively, S_A being the area of the slice which sections the volume $\mathcal{V}$ which contains the n circles.

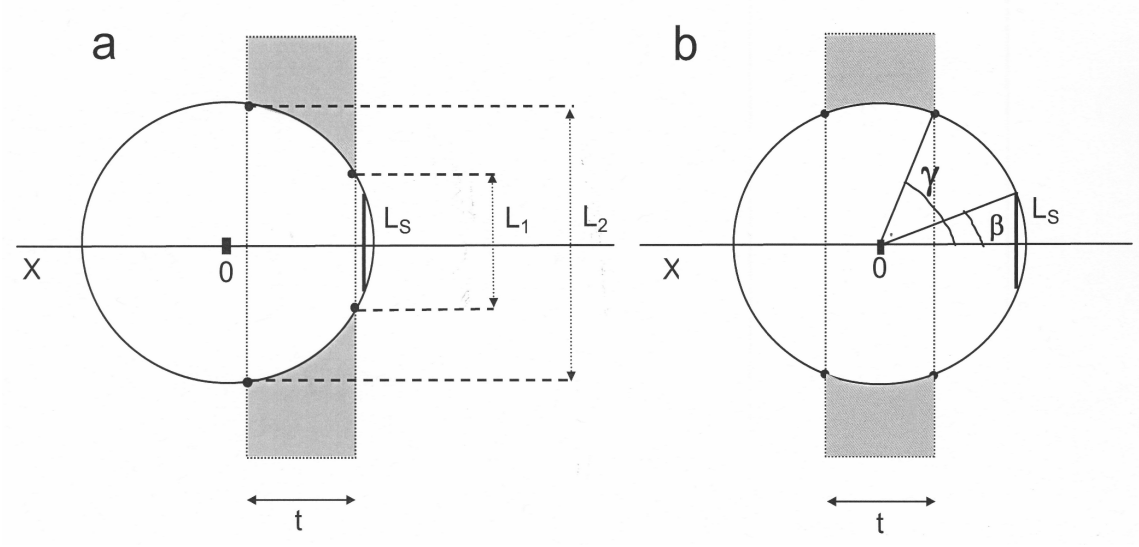

Fig. 2.1. . Circle of diameter D cut by a slice of thickness t.

(a) If the circle is transparent relative to the slice (the case shown in the figure), the image length is L_1; if the circle is opaque relative to the slice, the image length is L_2. An image smaller than L_S cannot be observed. (b) When the middle of the slice passes through the circle center, the angles β and γ are equal to asin(L_S / D) and acos (t / D) respectively.

2. Proposed Method

As for the case of symmetrical distributions, consider the case of images of circles in a part of a plane with area $\mathcal{A}$. The cases of cylinders or spheres are easily derived from this case when the images of the spheres are diameters of circular sections observed on planes which section the spheres, or when the images of the cylinders are chords of cylinder cross-sections on planes parallel to the cylinder axis which section the cylinders.

Consider images of these circles which are obtained either from a set of slices of thickness t and equally spaced by a very small distance dx or from only one almost infinitely long slice of thickness t. When a set of slice portions is considered in this latter case, the slice portions must be chosen at random in the area $\mathcal{A}$, but must be distant from each other by more than $D_{max,\ max} \pm t$ (minus sign in case E and plus sign in case F), $D_{max,\ max}$ being the diameter of one fairly large circle of the population. Because the diameters are unknown, $D_{max,\ max}$ must be evaluated based on previous knowledge, for example from the longest image length, L_{max}, observed in a preliminary slice sample which estimates the diameter by $(L_{max}^2 + t^2)^{0.5}$ in case E or L_{max} in case F. Then it is necessary to verify *a posteriori* that the distance between slices is greater than $(L_{max}^2 + t^2)^{0.5} - t$ in case E or $L_{max} + t$ in case F.

Assume that i) the images of two or several circles obtained by a slice do not overlap in case F (this is not possible in case E), ii) only images longer than L_S (possibly equal to zero) can be measured, and iii) the circle diameters are not smaller than the largest of t or L_S in case F or $(L_S^2 + t^2)^{0.5}$ in case E.

The method proposed to estimate the number of circles and the diameter distribution is as follows.

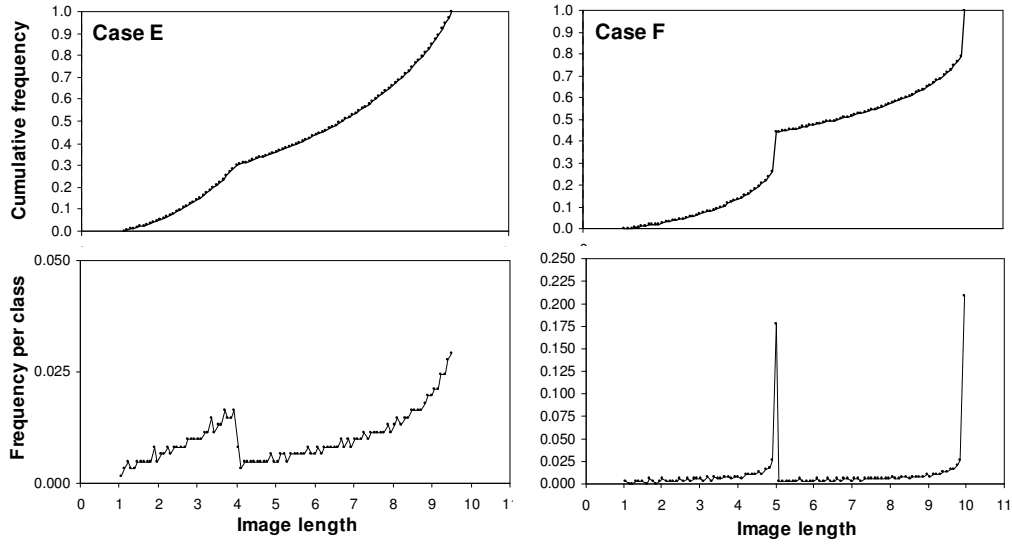

Fig. 2.2. Variations in the cumulative frequency and the frequency per class of the lengths of the images of two circles with different diameters (5 and 10 mm) generated by equally spaced slices, t and L_S being 3 and 1 mm respectively. Cases E and F are shown.

The slices are equally spaced by 0.0072 and 0.03 mm in cases E and F respectively, values chosen for the same number (131) of images of the larger circle in the two cases E and F. There are 581 and 215 images of the circle of diameter 10 mm in cases E and F respectively, distributed into one hundred classes. With smaller numbers of images, the curves were more irregular. With larger classes, the curves are smoother, but the variations around 4 or 5 mm were reduced.

First, the images are arranged into image length classes which are grouped into larger classes named macro-classes (labeled C_1, C_2, … C_i, …, C_P in descending order of size). Each macro-class C_i is defined to contain the largest image of each circle of the population P_i (i varying from 1 to P) in which the diameter distribution can be approximated by a symmetrical distribution. Because this population also generates images in all the smaller macro-classes, each macro-class (except the largest) contains also images of circles which generate their largest images in one or several larger macro-classes. When the frequency varies slowly with the image length, equally large arbitrary macro-classes can be created. When it varies suddenly, the macro-classes are defined in agreement with the observed image length variations. A basis for this definition is provided by the fact that the frequency of the images generated by a circle is lower in classes of shorter images (**Fig. 2.2**). Thus, a higher image frequency in a smaller class with upper limit λ reveals the existence of circles having diameters in this class, in case F, or in a class with upper limit $(\lambda^2 + t^2)^{0.5}$, in case E. In case F, because all the circles of which the center is at a shorter than t / 2 from the slice midpoint generate images with length equal to the diameter D, the image frequency in the class which contains D is high when t is large. Therefore, the upper limit of a macro-class can be identified as the lower limit of a class in which the image frequency is locally minimal. Evidently, minimal values suspected to be due to random variability should be neglected. Each circle population must be sufficiently large so that each macro-class C_i contains sufficiently large samples of images of all the populations of larger circles. With a sufficiently large image sample, large numbers of macro-classes and classes per macro-class are preferred if the frequency varies suddenly with image length, whereas with a small sample, these numbers are limited. At a given frequency, more macro-classes must be created for the larger image sizes because the number of images generated by larger circles is greater.

As a first step, L_S is set equal to the lower limit of C_1. From the m_1 images of C_1, the mean ($D_{m,1}$) and coefficient of variation ($cv_{D,1}^2$) of the diameters of P_1 are estimated by the method proposed for symmetrical diameter distributions. Then a sample of circles - for example, 100 circles - is taken from the normal distribution defined by $cv_{D,1}$ and $D_{m,1}$. The image frequencies for this sample in each of the smaller classes are calculated as described in Chap. 1, and the numbers of images are calculated from these frequencies and the numbers of images m_1. The total number $m_{D\max,\,1}$ (case of slices equally spaced by dx) or $m_{D\max,\,\text{one},\,1}$ (case of one almost infinitely long slice) of images expected to be generated by P_1 is equal to m_1 plus the numbers of images in the previously calculated smaller classes.

As a second step, L_S is set equal to the lower limit of C_2. In each class of C_2, the number of images m_2 generated by circles of P_2 is calculated as the observed number of images minus the previously calculated number of images generated by P_1. From the lengths of the m_2 images in all the classes of C_2, the values of $cv_{D,\,2}$ and $D_{m,\,2}$ of P_2 are estimated as for C_1. Then, also as for C_1, the numbers of images generated by the circles in each smaller class are calculated, as well as the number $m_{D\max,\,2}$ or $m_{D\max,\,\text{one},\,2}$.

In subsequent steps, similar calculations are carried out for each macro-class, taking the images generated by the circles of all the larger macro-classes into account.

Because of the random variability of the diameters and of the distances between slices and circles, the observed numbers of images in some classes of C_i may be less than the sum of the calculated numbers of images of the circles of the populations P_1 …P_{i-1} in this class. Therefore, the estimated number of images generated by circles of P_i in these classes may be negative. Such cases are acceptable because it is expected, on average, that the observed numbers of images in neighboring classes may be overestimated. However, it may be better to create larger classes, each with greater numbers of images.

The numbers n_i of circles are calculated using Eqs. 17 or 18 in **Table 2.1** according to the images are obtained from slices equally spaced by small dx or from almost infinitely long slice. In both cases, the proportion G_i of circles of each population P_i among all the circles, the total number of circles $\mathcal{N}$ and the mean $\mathcal{D}_m$ and coefficient of variation $\mathcal{CV}_D$ of the diameters are obtained using Eqs. 19 and 22 in **Table 2.1**.

This method with its calculations is formulated in the file 'diameters-slices.xls' (which is online freely on the website http://www.diameters-slices.org) which can function either with individual images (up to 10,000) or with image classes (up to 100). An alarm message is displayed if the observed number of images in any macro-class is less than that calculated from the populations of larger circles. This indicates that the image sample is too small and that the number of macro-classes must be decreased. **Fig. 2.3** shows the main sheet of this file.

Table 2.1. *Equations for estimating the number and the diameter distribution of circles in a population with any distribution composed of a mixture of P populations, each with a perfectly or approximately symmetrical diameter distribution.*

Note that the numbers of some equations follow those of Table 2 in Chap. 1.

The sign $\sum$ indicates the sum over all populations, with i varying from 1 to P.

			Eqs.
Case of slices equally spaced by small dx			
$n_i =$	$m_i / q\, c_{1,Dm,i}\, D_{m,i}$		T2-17
Case of one almost infinitely long slice			
$n_i =$ case of a surface:	$m_{Dmax,one,i}\, \mathcal{A} / \mathcal{L}\, c_{1,Dm,i}\, D_{m,i}$		T2-18
$n_i =$ case of a volume:	$m_{Dmax,one,i}\, \mathcal{V} / S_A\, c_{1,Dm,i}\, D_{m,ii}$		T2-18
Both cases			
$\mathcal{N} =$	$\sum n_i$		T2-19
$G_i =$	$n_i / \mathcal{N}$		T2-20
$\mathcal{D}_m =$	$\sum (G_i\, D_{m,i})$		T2-21
$\mathcal{CV}_D^2 =$	$\sum\{G_i\, D_{m,i}^2\, (1 + cv_{D,i}^2)\} / \mathcal{D}_m^2 - 1$	with $\sum G_i = 1$	T2-22

3. Validation of the proposed method with examples

The online file 'diameters-slices.xls' was used for the following examples.

3.1. Examples from Wicksell (1925) where both the diameter distribution and the image distribution are exactly theoretically known, t and L_S are equal to zero, and the objects are opaque

The method was applied to the two examples numbered 1 and 3 by Wicksell (1925), in which both the diameter distribution and the image distribution are exactly theoretically known and the diameter distribution is either almost symmetrical (Example 1) or highly asymmetrical (Example 3). The classes of images which were considered by Wicksell in Examples 1 and 3 (**Fig. 2.4**) were arranged into eight macro-classes with limits 15.5, 13.5, 11.5, …, 3.5, 1.5, and 0 or 13.5, 11.5, 9.5, …, 3.5, 1.5, 0.5, and 0 in Examples 1 and 3 respectively. The estimated values of $\mathcal{D}_m$ (6.27 and 2.11 respectively) were almost equal to the theoretical values (6.27 and 2.12) and were closer to the theoretical values than the values found by Wicksell (6.22 and 2.01). In Example 1, $\mathcal{D}_m$ was closer to the theoretical value than the value

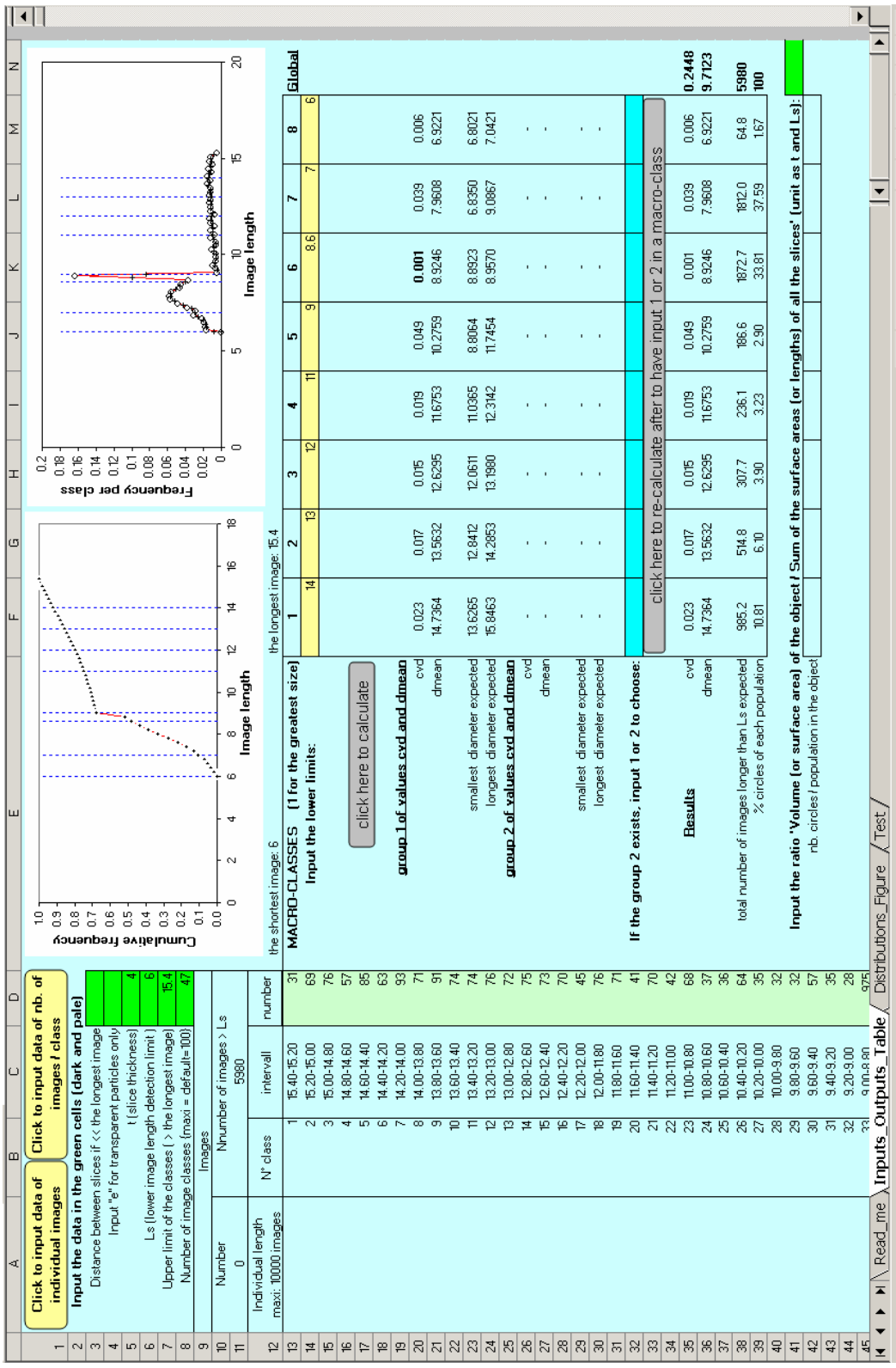

Fig. 2.3. Main sheet of the on line file diameter-slices.xls.

(6.11) found by the method for symmetrical distributions, which was also tried. The estimated values of CV_D (0.51 and 0.88 respectively) were almost equal to the theoretical values (0.50 and 0.86). Moreover, in Example 3, which was highly asymmetrical, 54 equally wide image subclasses were defined. With this number of classes (the number of classes is theoretically unlimited) and the eight previously defined macro-classes, the estimated diameter distribution was fairly smooth and very close to the theoretical distribution (**Fig. 2.4**), with $\mathcal{D}_m$ and CV_D being 2.14 and 0.87 respectively

.

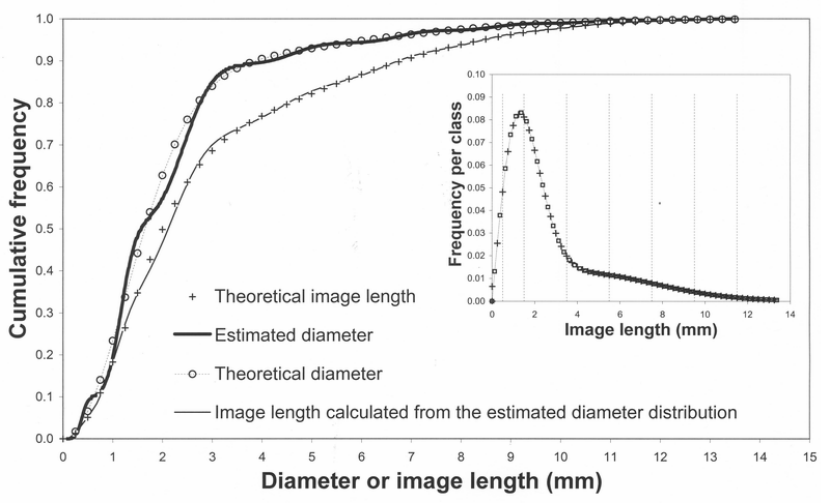

Fig. 2.4. Application of the proposed method to Example 3 from Wicksell (1925).
In the inset figure, the vertical dotted lines show the macro-class limits. The image frequencies per subclass are indicated at the subclass midpoints by squares. The cross symbols show the limits of the 54 subclasses which were created.

3.2. Examples with slices equally spaced by small d**x**, **t** *and* $\mathbf{L_S}$ *possibly >0, and opaque or transparent objects*

An artificial population of one hundred circles was created with an asymmetrical diameter distribution (**Fig. 2.5**), with 27%, 30%, and 43% of the circles taken from normal populations with means and standard deviations of 13.30 µm and 0.117, 8.99 µm and 0.0007, and 7.97 µm and 0.055 respectively. The mean and the coefficient of variation of the diameter were 9.71 µm and 0.246 respectively. The chosen values of t and L_S were 4 and 6 µm respectively.

The circles were first assumed to be opaque in a transparent matrix (case F). Using slices spaced by one-hundredth of the radius of the largest circle plus t / 2 resulted in 5980 virtual images. The image lengths were regarded as being measured and grouped into 47 subclasses 0.2 µm wide **(Fig. 2.5a)**. The method was first used to create three macro-classes (C_1, C_2, and C_3, with limits of 15.4 and 9.0, 9.0 and 8.6, and 8.6 and 6 µm respectively) based on variations in image frequency (**Fig. 2.5a** and **Table 2. 2**). The estimated diameter distribution was very close to the real diameter distribution (**Fig. 2.5a**), with CV_D and $\mathcal{D}_m$ being 0.244 and 9.71 µm respectively and the estimated percentages of the three circle populations 1, 2, and 3 being 26.4%, 34.3%, and 39.2% respectively. The estimated number of circles was 100.8. The distribution of calculated image lengths generated by this circle population was very close to the true distribution (**Fig. 2.5a**).

However, there were some discrepancies for the largest circles. Therefore, another set of eight macro-classes was created, of which four covered the largest sizes, neglecting one of the two principal minima of

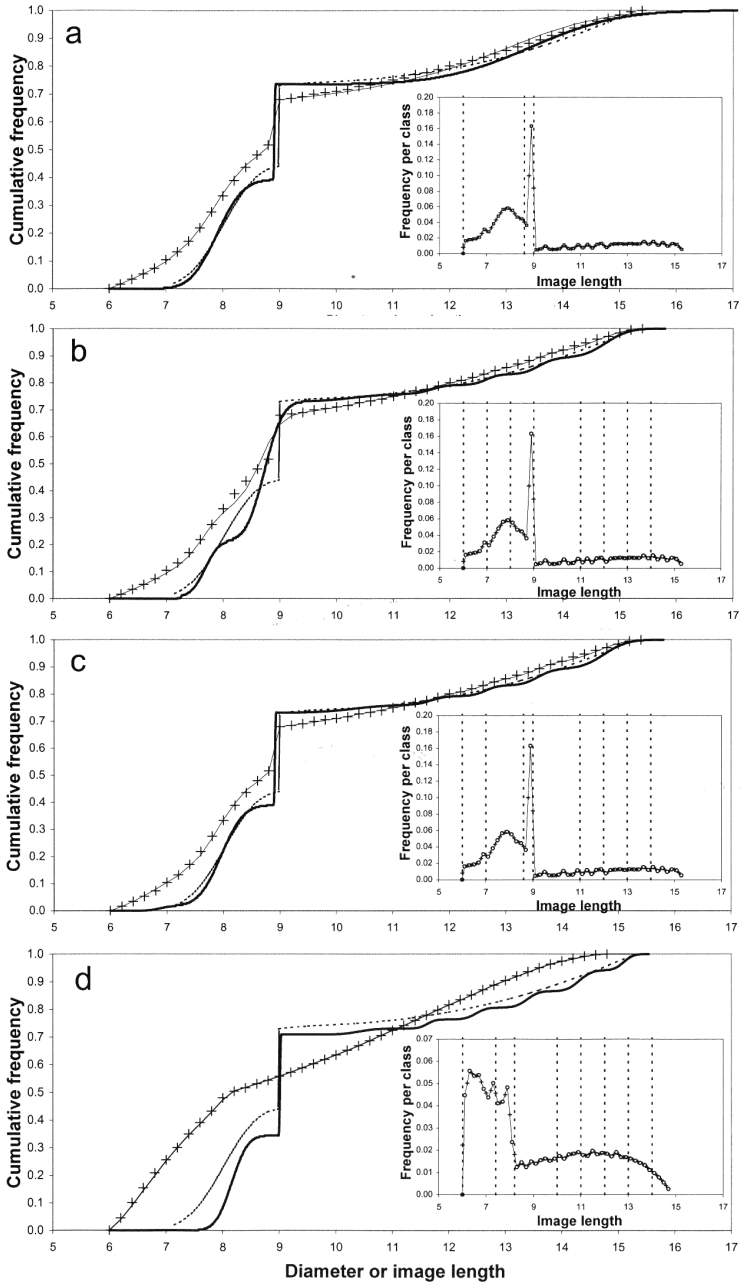

Fig. 2.5. Application of the proposed method to a mixture of populations of opaque (**a**, **b**, and **c**) and transparent (**d**) circles:

(a) Three macro-classes were created based on the two principal minima of the image frequency per image length class. **Table 2.2** gives details of the calculations. (b) Eight macro-classes were created, neglecting one of the two principal minima of the image frequency. (c) and (d) Eight macro-classes were created, three of them based on the two principal minima of the image frequency per image length class.

Main figures: Estimated diameter distribution: heavy lines. Image lengths: cross symbols in the main figures. Distribution of the image length calculated for one hundred circles having the estimated diameter distribution: fine line close to the cross symbols. Real diameter distribution: fine dotted lines.

Inset figures: image frequency per length subclass indicated at the subclass midpoints by squares and at the limits of the one hundred subclasses, which were indicated by crosses. The vertical dotted lines show the macro-class limits.

the image frequency **(Fig. 2.5b)**. The discrepancies were greatly reduced, but there were still some discrepancies around 8–9 µm. Finally, the best fit was obtained when the eight macro-classes were defined to include the two principal minima of the image frequency, the limits being 9–8.6 and 8.6–7 rather than 9–8 and 8–7 **(Fig. 2.5c)**.

Table 2.2. *Application of the proposed method to calculated image lengths of a population of opaque circles in a transparent matrix (case F).*

*Based on the principal minima of the image frequency per length subclass (***Fig. 2.**5a*), three macro-classes C_1, C_2, and C_3 of images of three populations P_1, P_2, and P_3 were distinguished, defined by the limits 15.4–9.0 μm, 9.0–8.6 μm, and 8.6–6 μm respectively.* L_S *was first set equal to 9.0 μm. The mean* l_m *and the coefficient of variation* $cv_{lengths}$ *of the lengths of the* m_1 *(1919) images of all the subclasses of* C_1 *were calculated (bottom part of table), the mean image length in a subclass being the mean of its upper and lower values. From* l_m, L_S, *and* t, *the diameter* D_{lm} *was estimated to be 0.930. Using the equations in the Appendix, the mean* $D_{m,1}$ *and the coefficient of variation* $cv_{D,1}$ *of the diameters of the circles of* P_1 *were estimated (bottom part of table). Using a sample of one hundred circles having the normal diameter distribution defined by* $cv_{D,1}$ *and* $D_{m,1}$, *sectioned by one hundred equally spaced slices, the proportions and the numbers of images obtained in* C_1 *and in each subclass smaller than 9.0 μm were calculated (columns c and d). Then* L_S *was set equal to 8.6 μm. In each image subclass of* C_2, *the number of images (column e) generated by circles which generated no image in* C_1 *was calculated to be equal to the observed number of images (column b) minus the previously calculated number of images generated* (legend continues on the following page)

Length classes (μm)	Observed images	Images estimated to be generated by circles which have:					
		the normal distribution defined by the estimated values of $cv_{D,1}$ and $D_{m,1}$ indicated at the bottom of this table		do not generate images in C_1	the normal distribution defined by the estimated values of $cv_{D,2}$ and $D_{m,2}$ indicated at the bottom of this table		do not generate images in either C_1 or C_2
	Number	Frequency	Number	Number	Frequency	Number	Number
(a)	(b)	(c)	(d) = (c) x 1919 / 0.776	(e) = (b) – (d)	(f)	(g) = (c) x 1141.5 / 0.494	(h) = (b) – (d) – (g)
macro-class C_1							
15.4 – 15.2	31						
15.2 – 15.0	69						
……	……						
9.2 – 9.0	28						
9.0 < total < 15.4	***1919***	***0.776***					
macro-class C_2							
9.0 – 8.8	975	0.011	26.42	948 .6			
8.8 – 8.6	217	0.010	24.09	192 .9			
8.6 < total < 9.0				***1141.5***	***0.494***		
macro-class C_3							
8.6 – 8.4	266	0.10	23.80		0.049	113.43	128.76
8.4 – 8.2	279	0.09	23.22		0.039	90.56	165.22
……	……	……	……		……	……	……
6.2 – 6.0	97	0.06	14.22		0.011	24.72	58.06
6.0 < total < 8.6							***1869.8***

Parameters estimated from the numbers of images of P_1 observed in the classes of the macro-class C_1 (column b) or of images of P_2 or P_3 estimated in the classes of the macro-classes C_2 or C_3 (columns e and h).

	l_m (μm)	$cv_{lengths}$	cv_D	D_m (μm)
population P_1	12.550	0.136	0.091	13.430
population P_2	8.866	0.008	0.001	8.910
population P_3	7.581	0.082	0.046	7.898

by the circles of P_1 (column d). The mean l_m and the coefficient of variation $cv_{lengths}$ of the lengths of the m_2 (1141.5; column e) images obtained in all the subclasses were calculated (bottom part of table). Using the equations in the Appendix, $cv_{D,2}$ and $D_{m,2}$ were estimated (bottom part of table). Finally, L_S was set equal to 6 μm. In each image subclass of C_3, the number of images (column h) generated by circles which generated no image in either C_1 or C_2 was calculated to be equal to the observed number of images (column b) minus the previously calculated numbers of images generated by the circles of P_1 and P_2 (columns d and g). The mean l_m and the coefficient of variation $cv_{lengths}$ of the lengths of the m_3 (1869.8; column h) images obtained in all the subclasses were calculated (bottom part of table). Using the equations in the Appendix, $cv_{D,3}$ and $D_{m,3}$ were estimated (bottom part of table). The percentages of the three populations of circles P_1, P_2, and P_3 were calculated as 26.5%, 34.3%, and 39.2% respectively. The diameter distribution of a sample of one hundred circles taken from this total population is shown in **Fig. 2.**5a*, which shows also the distribution of the calculated lengths of the images generated by this circle population.*

Then the circles were assumed to be transparent in an opaque matrix (case E). In this case, 3089 images were obtained. The method for case E was used. Based on the principal minima of the image frequency for each length class (**Fig. 2.5d**), eight macro-classes were defined taking into account the two principal minima of the image frequency, 8.2 and 7.4. The estimated diameter distribution was fairly close to the real diameter distribution (CV_D and $\mathcal{D}_m$ were equal to 0.235 and 9.99 μm respectively), but the frequencies in the classes smaller than 9 mm were underestimated. The estimated number of circles was 107. Differences similar (not shown) to those indicated for case F were obtained with three or eight different macro-classes.

3.3. Cases of an almost infinitely long slice or slices spaced by more than $D_{max,max} \pm t$

3.3.1. Example with simulated data in cases E and F

The method was applied to the previous example of the population of one hundred circles, taking only the image of each circle possibly generated by a slice with its midpoint at a random distance from the circle center, which was less than or equal to the radius of the largest circle minus $t / 2$ in case E or plus $t / 2$ in case F. The calculations were replicated ten times according to a Monte Carlo design. The number of images varied between 25 and 38 in case E and between 52 and 90 in case F. Only images longer than 6 μm were considered, and the value of L_S was set equal to the length of the smallest image. Three macro-classes were almost always distinguished (results not shown but close to those shown in **Fig. 2.5a**). In case E, CV_D varied between 0.21 and 0.27 (mean = 0.24; sd = 0.02), and $\mathcal{D}_m$ varied between 9.20 and 10.88 (mean 10.00; sd = 0.50). In case F, CV_D varied between 0.21 and 0.27 (mean = 0.23; sd = 0.02), and $\mathcal{D}_m$ varied between 9.38 and 10.02 (mean 9.75; sd = 0.22).

3.3.2. Example with real circular coins in case F

The method was applied to a mixture of three populations of coins: 17, 20, and 8 coins of 1, 2, and 5 centimes of euros respectively, thus 38%, 44%, and 18% of the total coin population, with diameters of 16.19,, 18.73 and 21.22 mm respectively. The mean and coefficient of variation of the diameters of the 45 coins were 18.21 mm and 0.100. Each coin was placed randomly on a scanner and scanned five times, with the coin's position on the scanner varied randomly each time. In this way, 225 coin scans were obtained, spread out over five photos 204 mm wide and 297 mm long.

On each photo (**Fig. 2.6**), seven slices 204 mm long and 5 mm thick were drawn, the slices being

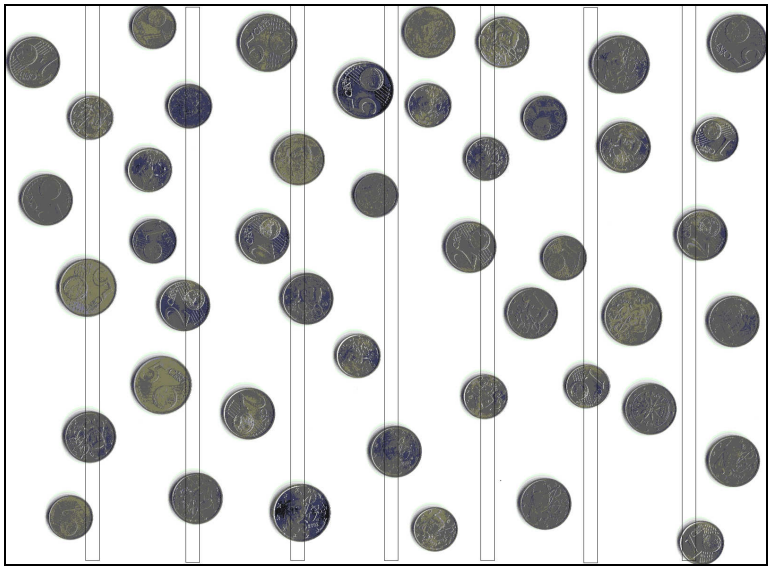

Fig. 2.6. Photo showing a mixture of three populations of coins (8, 20, and 17 coins of 5, 2, and 1 euros) and their intersections with slices 5 mm thick, perpendicular to the coins and having for sections the strips shown on the plane. The image lengths were those of the longest coin sections into the slices, neglecting shadows around the coins.

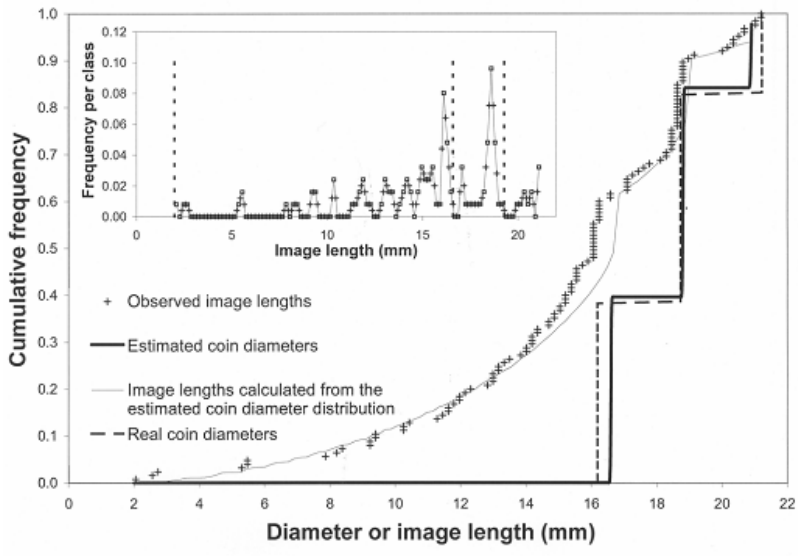

Fig. 2.7. Application of the proposed method to images of a mixture of three populations of coins, obtained using slices 5 mm thick.

In the inset figure, the vertical dotted lines show the macro-class limits; the image frequencies per subclass are indicated at the subclass midpoints by squares; the cross symbols show the limits of the one hundred subclasses which were created.

parallel and spaced by at least 30 mm. The longest side of each coin section present in a slice was measured and considered to be an image of the coin. The shortest and longest of the 125 images obtained were 2.05 and 21.20 mm long. Thus, $L_{max} + t$ was less than the distance between slices.

The values of t and L_S were set equal to 5 mm and 2 mm respectively. Based on the principal variations of the cumulative image frequency and of the frequency per class (**Fig. 2.7**), three macro-classes were created, defined by the values 19.3 and 16.6 mm. The estimated diameter distribution (**Fig. 2.7**) indicated clearly three circle populations with mean diameters of 20.87, 18.79, and 16.58 mm, containing respectively 16%, 45%, and 39% of the total number of coins, which was estimated to be equal to 229. $\mathcal{D}_m$ and $\mathcal{CV}_D$ were 18.24 mm and 0.084 respectively. These estimates generally agreed with the real data.

3.3.3. Example with real spherical bonbons in cases E and F.

The two populations of bonbon images previously studied (Chapter 1) were considered together. Briefly, two populations of approximately spherical bonbons, white (WB) or yellow-orange (YB), consisting of 100 and 150 bonbons respectively, which had been measured using a caliper (**Table 2. 3 and Fig. 2.8**), were mixed and included in a semi-transparent resin placed in a transparent tube (52 mm internal diameter) 195 mm in length. Slices 3.00 ± 0.01 mm in thickness, spaced by 15 mm, were made perpendicular to the cylinder axis. The slices were then scanned, and the bonbon image diameters (case F) were obtained using the Image J software. Then the slices were left in water until the bonbons dissolved, leaving spherical holes. The slices were then rescanned and the hole image diameters (case E) were obtained as before. There were 118 and 54 images in cases E and F respectively. The largest image diameters as measured were 7.87 mm in case E and 9.83 mm in case F. Therefore, $(L_{max}^2 + t^2)^{0.5} - t$ and $L_{max} + t$ were less than the distance between the slice portions. The smallest image diameters as measured were 1.36 mm in case E and 1.91 mm in case F. The value of t was set equal to 3 mm, and L_S was set equal to the smallest image diameter.

In case F, two macro-classes were first distinguished, separated by a limiting value of 6.45 mm and therefore including the peak between 6.5 and 7 mm in the greatest macro-class (**Fig. 2.8a**). $\mathcal{D}_m$, $\mathcal{CV}_D$, and $\mathcal{N}$ were close to their true values (**Table 2.3**). The mean diameters of the two populations P_1 and P_2 were close to the true values, but the coefficients of variation of the diameter were greater and the number of bonbons in P_2 was less than that of WB (**Table 2.3**). The calculated image length distribution was fairly close to the observed distribution (not shown). With three macro-classes**,** a small population appeared between the two others (**Fig. 2.8a** and **Table 2.3**). When two macro-classes were distinguished by a limiting value of 6.90 mm, the results were only slightly changed.

In case E, two macro-classes were also distinguished, separated by a limiting value of 5.21 mm (**Fig. 2.8b and Table 2.3**). $\mathcal{D}_m$ was close to the true value, but $\mathcal{CV}_D$ and $\mathcal{N}$ were overestimated. The estimated diameter distribution indicated two bonbon populations P_1 and P_2 (**Fig. 2.8b** and **Table 2.3).** In P_1, the mean diameter was close to that of YB, but the coefficient of variation of the diameter was set to 0.001 because calculations gave a negative value. In P_2, the mean diameter was less than that of WB, and the coefficient of variation of the diameter was greater than that of WB (**Table 2.3**). However, the calculated image length distribution was fairly close to the observed distribution (not shown). When only one macro-class was defined, the results were: $\mathcal{D}_m$ = 7.20 mm, $\mathcal{CV}_D$ = 0.240 and $\mathcal{N}$ = 249, but the calculated image length distribution was considerably different from the observed distribution for larger circle sizes.

Estimations were tried using several macro-classes and taking the peaks for the larger sizes into account, but no better agreement with the data was obtained. It is probable that the number of images (54) generated by slices at random distances from the sphere centers was too small in case E to obtain more accurate estimates.

Table 2.3. *Application of the proposed method to the images of the mixture of two populations of yellow-orange (YB) and white (WB) bonbons obtained from slices 3 mm thick.*

Two or three macro-classes were created, giving two or three circle populations P_1, P_2, and P_3.

Parameters	**Case E**	**Case F**		
		Numbers of images		
	54	118		
		Number of macro-classes		
	2	2	3	2
		Lower limits of the macro-classes		
	5.21	6.45	6.90	6.90
	1.35	1.90	6.4	1.90
			1.90	
	Real values	Estimated values		
WB and YB				
$\mathcal{D}_m$ (mm)	6.93	6.65	7.15	7.15	7.14
$C\mathcal{V}_D$	0.189	0.304	0.214	0.213	0.213
$\mathcal{N}$(number of bonbons)	250	290	224	224	225
P_1					
D_m (mm)	8.45	8.37	8.55	8.80	8.80
cv_D	0.055	0.001*	0.080	0.052	0.052
number of bonbons	100	143	108	92	92
P_2					
D_m (mm)	5.91	4.98	5.85	6.84	6.00
cv_D	0.060	0.309	0.128	0.001*	0.125
number of bonbons	150	147	116	19	132
P_3					
D_m (mm)				5.86	
cv_D				0.126	
number of bonbons				113	

* Value imposed because cv_D^2 was calculated to be negative.

4. Discussion

The method developed here provided accurate estimates, even for highly irregular diameter distributions, both for t and L_S equal to zero (as in the examples from Wicksell (1925)) and for nonzero values, and both for slices equally spaced by small dx and for one almost infinitely long slice when the number of images was large enough. This good agreement probably results mainly from the fact that the

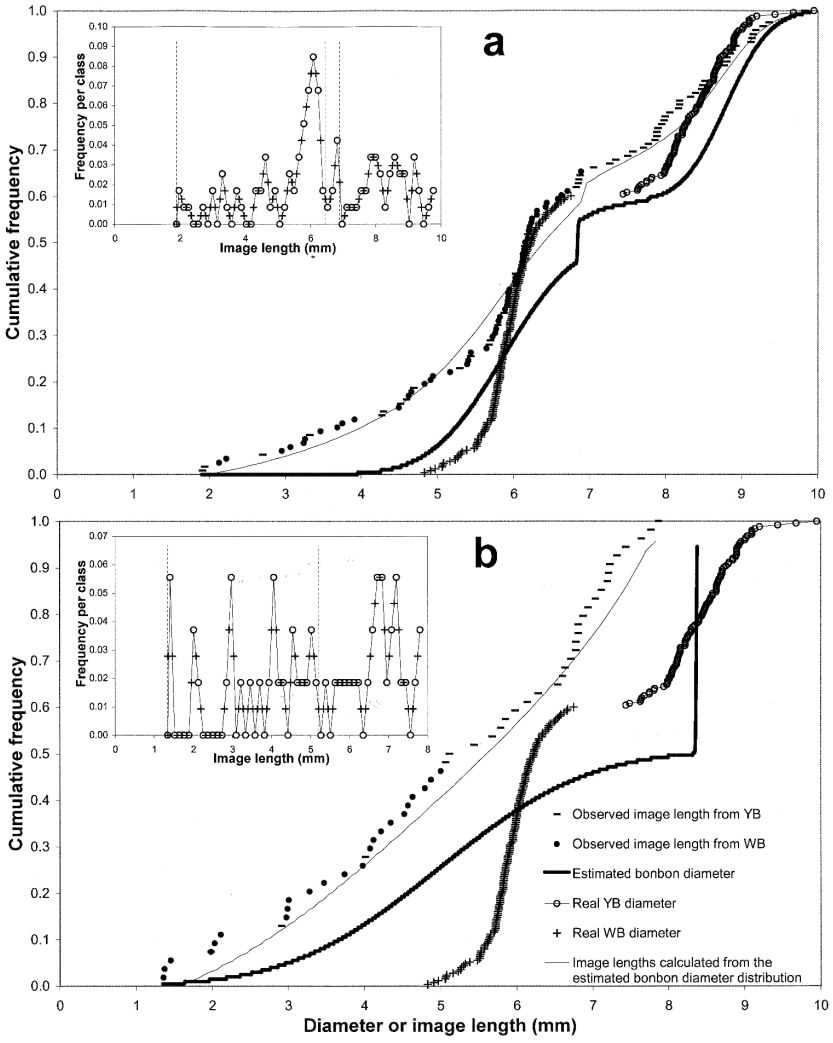

Fig. 2.8. Application of the proposed method to images of bonbons (a) or bonbon holes (b) included in a transparent resin and obtained using slices 3 mm thick.

In the inset figure, the vertical dotted lines show the macro-class limits; the image frequencies per subclass are indicated at the subclass midpoints by squares; the cross symbols show the limits of the one hundred subclasses which were created.

proposed method considers the object population as a set of juxtaposed populations, each in its own restricted class with a symmetrical diameter distribution. Therefore, D varies only slightly relatively to t and L_S within each population, and the approximations made in the relations specific to symmetrical distributions (see Chapter 1) are close to the exact values.

The choice of the number of macro-classes and their limits may be somewhat arbitrary in certain cases, especially with small samples when it is difficult to determine whether a given local image-frequency variation is random. Some cases may have to be extensively tested to obtain the best fit between the calculated and observed image length distributions. Indeed, it is believed that a given image

length distribution can result from only one circle diameter distribution. A proof of this would be desirable. The online spreadsheet, 'Diameter_Distribution.xls', can be used to test such cases easily. It can accommodate up to one hundred subclasses and eight macro-classes, although these numbers are theoretically unlimited.

Negative values of the estimated number of images may possibly occur in classes or macro-classes because the number of images is too small. Xu and Pitot (2003) proposed to "neutralize" such values by adding these numbers into the smaller classes. The same operation is performed here within each population: l_m and cv_{length} are estimated in each macro-class from the sum of the estimated positive and negative numbers of images in each class multiplied by the image length or the squared image length in the class.

In the case of the bonbon holes (case E), the estimates were highly inaccurate, probably because the number of images was small (54) due to the small number of bonbons from which images were obtained, and therefore the samples of bonbon sizes and of distances between slice and bonbon were also small. Moreover, the relative measurement errors were probably higher than in case F because the images were smaller. In addition, some shadow effects were observed (see Chapter 1).

5. Conclusions

The proposed method, which is easily applicable using the online file, 'Diameter_Distribution.xls', will probably be useful in many fields. However, it is important not to forget that the object shape needs to be close to a circle, cylinder, or sphere. Moreover, the method must be used with caution if images may overlap or if diameters are smaller than t or L_S in case F or $(L_S^2 + t^2)^{0.5}$ in case E. The suggestions which were provided to overcome these limitations in many cases for symmetrical populations (see Chapter 1) are valuable here. When slice portions are sampled, it is important that their distance from each other be greater than $D_{max,max} \pm t$ (minus sign in case E and plus sign in case F), which may be evaluated by preliminary observations or verified *a posteriori* using the largest observed image.

It is expected that the method will be useful even for only approximately circular objects, for which the author will present an extension of the previous method for circles (see Chapter 1).

Acknowledgements

The author thanks C. Vigne for his very competent contribution in making the bonbon slices and N. Bertin for her advices.

References

Baddeley, A., Jensen, E. 2005. Stereology for Statisticians. Boca Raton, USA: Chapman and Hall-CRC.

Bussières, P. 2013. File "diameters-slices.xls" on the website http://www.diameters-slices.org.

Cruz-Orive, L.M. 1983. Distribution-free estimation of sphere size distribution from slices showing overprojection and truncation, with a review of previous methods. *J. Microsc*. 131:265–290.

Kim, S., Atwood, H.L., Cooper, R.L. 2000. Assessing accurate sizes of synaptic vesicles in nerve terminals. Brain Res 877:209-217.

Stoyan, D., Kendall, W.S., Mecke, J. 1995. Stochastic Geometry and its Applications. Chichester, England: John Wiley and Sons.

Weibel, E.R. 1980. Stereological Methods. Vol. 2: Theoretical Foundations. London, England: Academic Press.

Wicksell, S.D. 1925. The corpuscle problem: a mathematical study of a biometric problem. *Biometrika* 17, 84–99.

Xu, Y.H., Pitot, H.C. 2002. An improved stereologic method for three-dimensional estimation of particle size distribution from observations in two dimensions and its application. *Comput. Meth. Prog. Bio.* 72, 1–20.

Annex: Principal relations for estimating the numbers and diameters of objects from their images generated by slices when the diameter distribution is perfectly or approximately symmetrical

Consider circles with possibly different diameters on a part of a plane with area $\mathcal{A}$. The number of images of these circles is labeled as m when they are generated by a set of slices equally spaced by a very small distance $1 / q$, or $m_{D\max,\,\mathrm{one}}$ when they are generated by one almost infinitely long slice of length $\mathcal{L}$, such that the circle centers are at random distances from the slice. The mean and coefficient of variation of the image lengths are labeled as l_m and cv_length.

The diameter $D_{l\mathrm{m}}$ of a circle of which the mean L_m of the image lengths L is equal to l_m is estimated from l_m, t, and L_S based on the following equations:

$$\gamma_{Dl\mathrm{m}} = \mathrm{acos}\,(t / D_{l\mathrm{m}}) \tag{1}$$

$$\beta_{Dl\mathrm{m}} = \mathrm{asin}\,(L_\mathrm{S} / D_{l\mathrm{m}}) \tag{2}$$

$$c_{1,\,Dl\mathrm{m}} = \cos\beta_{Dl\mathrm{m}} \pm \cos\gamma_{Dl\mathrm{m}} \qquad \text{(minus sign in case E and plus sign in case F)} \tag{3}$$

$$c_{2,\,Dl\mathrm{m}} = 2\gamma_{Dl\mathrm{m}} - 2\beta_{Dl\mathrm{m}} - \sin 2\gamma_{Dl\mathrm{m}} + \sin 2\beta_{Dl\mathrm{m}} \qquad \text{(case E)} \tag{4}$$

or:

$$c_{2,\,Dl\mathrm{m}} = \pi - 2\beta_{Dl\mathrm{m}} + 4\cos\gamma_{Dl\mathrm{m}} + \sin 2\beta_{Dl\mathrm{m}} \qquad \text{(case F)} \tag{5}$$

$$L_\mathrm{m} = D_{l\mathrm{m}}\, c_{2,\,Dl\mathrm{m}} / (4\, c_{1,\,Dl\mathrm{m}}) \tag{6}$$

By successive approximations, entering values of $D_{l\mathrm{m}}$ in Eq. 6 increasing from l_m, up to the predicted value of L_m becomes very close to l_m.

The coefficient of variation of the lengths of images of this circle generated by slices at distances varying by small values dx from the circle center can be calculated as:

$$cv_{L,\,Dl\mathrm{m}} = [16\, c_{1,\,Dl\mathrm{m}}\, c_{3,\,Dl\mathrm{m}} / (3\, c_{2,\,Dl\mathrm{m}}{}^2) - 1]^{0.5} \tag{7}$$

with:

$$c_{3,\,Dl\mathrm{m}} = (3 - \cos^2\beta_{Dl\mathrm{m}})\cos\beta_{Dl\mathrm{m}} - (3 - \cos^2\gamma_{Dl\mathrm{m}})\cos\gamma_{Dl\mathrm{m}} \qquad \text{(case E)} \tag{8}$$

or:

$$c_{3,\,Dl\mathrm{m}} = (3 - \cos^2\beta_{Dl\mathrm{m}})\cos\beta_{Dl\mathrm{m}} - 3\cos\gamma_{Dl\mathrm{m}} \qquad \text{(case F)} \tag{9}$$

When the diameter distribution is perfectly or approximately symmetrical, cv_D is estimated from one of the two roots (generally the smaller, see Chapter 1) of the quadratic equation:

$$(cv_{\mathrm{lengths}}{}^2 + 1)\,(cv_D{}^2 + 1)^2 - 3\,(cv_{L,\,Dl\mathrm{m}}{}^2 + 1)\,(cv_D{}^2 + 1) + 2\,(cv_{L,\,Dl\mathrm{m}}{}^2 + 1) \approx 0 \tag{10}$$

D_m is estimated by the equation:

$$D_\mathrm{m} = 4\, c_{1,\,Dl\mathrm{m}}\, l_\mathrm{m} / c_{2,\,Dl\mathrm{m}}\,(cv_D{}^2 + 1) \tag{11}$$

and the number n of circles within area $\mathcal{A}$ is estimated by the equation:

$$n = m / q\, c_{1,\,D\mathrm{m}}\, D_\mathrm{m}. \qquad \text{(case of equally spaced slices)} \tag{12}$$

or:

$$n = m_{D\max,\,\text{one}}\, \mathcal{A} / \mathcal{L}\, c_{1,\,D\text{m}}\, D_\text{m}. \qquad \text{(case of one almost infinitely long slice)} \qquad (13)$$

with:

$$c_{1,\,D\text{m}} = \cos \beta_{D\text{m}} \pm \cos \gamma_{D\text{m}} \qquad \text{(minus sign in case E and plus sign in case F)} \qquad (14)$$

where:

$$\gamma_{D\text{m}} = \operatorname{acos}\,(t / D_\text{m}) \qquad (15)$$

$$\beta_{D\text{m}} = \operatorname{asin}\,(L_\text{S} / D_\text{m}) \qquad (16)$$

CHAPTER 3

Estimating the equivalent diameter distribution of approximately circular objects from their images in slices when the distribution is roughly symmetrical

Abstract

This paper proposes a method for estimating the distribution of the equivalent diameters of planar objects only approximately circular from their images generated by slices perpendicular to the object plane when the distribution is roughly symmetrical, the object shape is known and the smallest diameter is greater than the slice thickness. The cases of opaque and transparent objects relative to the slices and a possible image detection limit are considered. In a first step, the method estimates the mean and coefficient of variation of the image lengths that would be obtained if each object was a circle with the same area as the object, its diameter being the equivalent diameter of the object. These estimates are obtained by successive approximations, measuring the lengths of images of a fictive object having the same shape as the studied objects. In a second step, the mean and coefficient of variation of the equivalent diameters are estimated using a recent method for circles. Valuable predictions were obtained for ellipses in numerical simulations and for cross sections of pores observed in a plant phloem sieve plate.

1. Introduction

Estimating the size of inclusions is an important problem in several fields. When slices are made through a matrix with inclusions, inclusion sections are obtained. It is expected that these sections generate images, when they are exposed to light, from which the inclusion size distribution is researched. There are various cases according to slice thickness and the relative transparency of the inclusions and matrix. Briefly, the image of an opaque inclusion section in a transparent matrix (case denoted F, for "full") will depend on the greatest dimension of the section while the image of a transparent inclusion in an opaque matrix (case denoted E, for "empty") depends on the smallest dimension which delimits the direct light path (**Fig. 3.1a-b**). The two cases are similar when the slice thickness is zero. This problem is important also for the particular case of planar objects (for examples disks) sectioned by perpendicular slices which determine strips at their intersections (**Fig. 3.1a-b** represents now the object plane). Cross-sections of tube-shaped pores in certain plant tissue are such planar objects.

Object size may be measured in terms of volume, surface area, or linear dimensions. For objects which do possess not a simple geometrical shape such as a sphere or a circle, a useful linear dimension is the "equivalent diameter", that is the diameter of the sphere or circle having the same volume or surface area as the object.

Various methods have been proposed for spherical inclusions when slices are of zero or finite

thickness (see references in Chapter 1), and for ellipsoidal inclusions when the slice thickness is zero (Wicksell, 1926; Cruz-Orive, 1976, 1978). Recently, I proposed a method for circles which is applicable to cross-sections of cylinders and spheres with diameters larger than the slice thickness (See Chapter 1). It works, even if there is a detection limit L_S (i.e., image lengths smaller than L_S cannot be observed), in the two previously described cases E and F. Assuming that the diameter distribution is approximately or perfectly symmetrical, the mean D_m and the coefficient of variation cv_D of the diameters can be estimated from the mean l_m and the coefficient of variation cv_{length} of the image lengths.

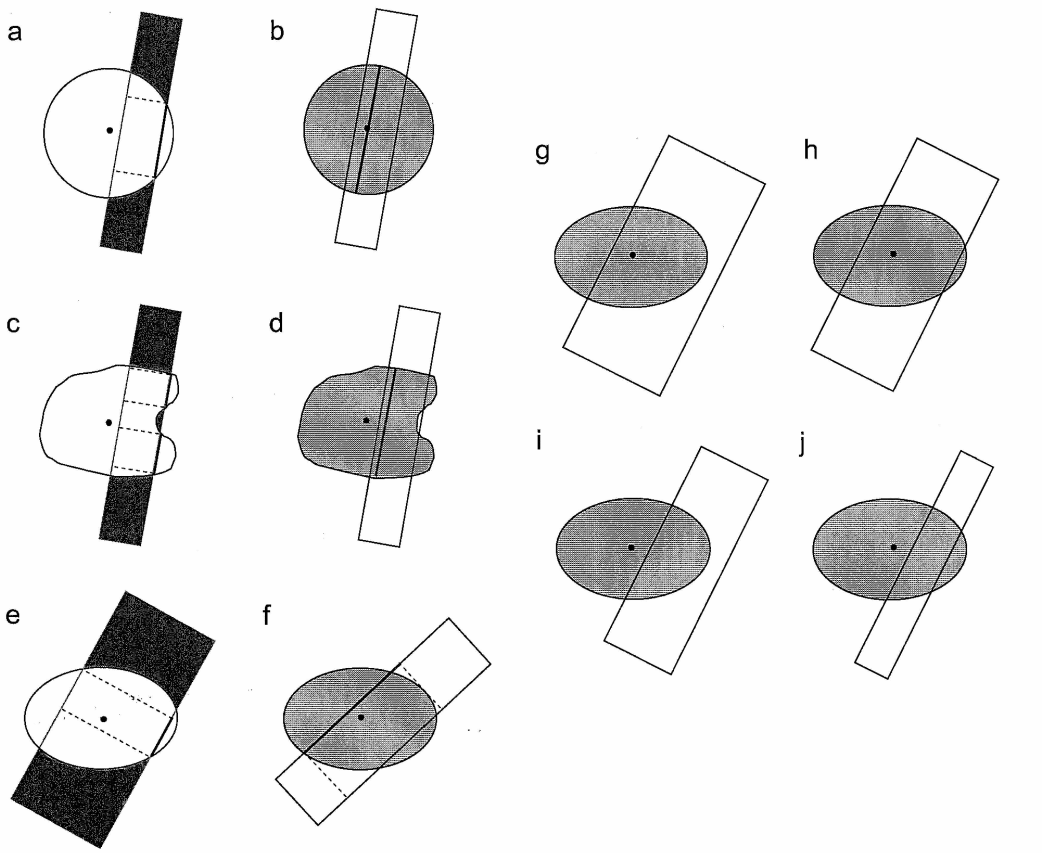

Fig. 3.1. Various cases of planar objects and their images obtained from a perpendicular slice.

Case "E" denotes a transparent object embedded in an opaque matrix: circle (a), irregular with concavities (c), ellipse (e). Case "F" denotes an opaque object embedded in a transparent matrix: circle (b), irregular with concavities (d), ellipse (f). Graphs (g) through (j) depict various relative positions and sizes of the objects and slices.

Many inclusions of interest are natural objects which are approximately, but only approximately, circular, cylindrical or spherical. For example, plant phloem pores are short, only approximately cylindrical tubes that pass through the plate between two sieve cells. The cross-section of each tube, as shown in **Fig. 3.2**, is an important parameter of flow rates. As views perpendicular to the tube axis showing the pore cross-sections are scarce, it would be desirable to estimate the pore size from the lengths of images of their sections visible in longitudinal slices, as portrayed in **Fig. 3.1a-c-e**.

When t and L_S are zero, the sum of the measured image lengths depends only on the total cross-sectional area of the pores. That becomes clear if we consider a large number of slices separated by a very small distance dx as the sum of the measured lengths times dx is equal to the area occupied by the pores. However, the mean and the coefficient of variation of the lengths vary with the object shape and they vary with t and L_S when they are nonzero. Therefore, it is not possible to estimate the mean and the coefficient of variation of the equivalent diameter of the objects from the mean, here denoted $l_{m,\,0}$, and the coefficient of variation, here denoted $cv_{length,\,0}$, of the image lengths alone using directly the previously described method for circles. For example, when the pores depicted in **Fig. 3.2** are sectioned by a great systematic sample of slices 0.07 µm thick, the values of $l_{m,\,0}$ and $cv_{length,\,0}$ are 0.303 µm and 0.399 respectively when L_S is equal to 0.094 µm. Applying my previous method for circles predicts the values 0.352 µm and 0.356 for D_m and cv_D but the true values relative to the equivalent diameter are 0.405 µm and 0.272. Another reason for developing a method suitable for objects other than circles is that the image formation is more complex (see below).

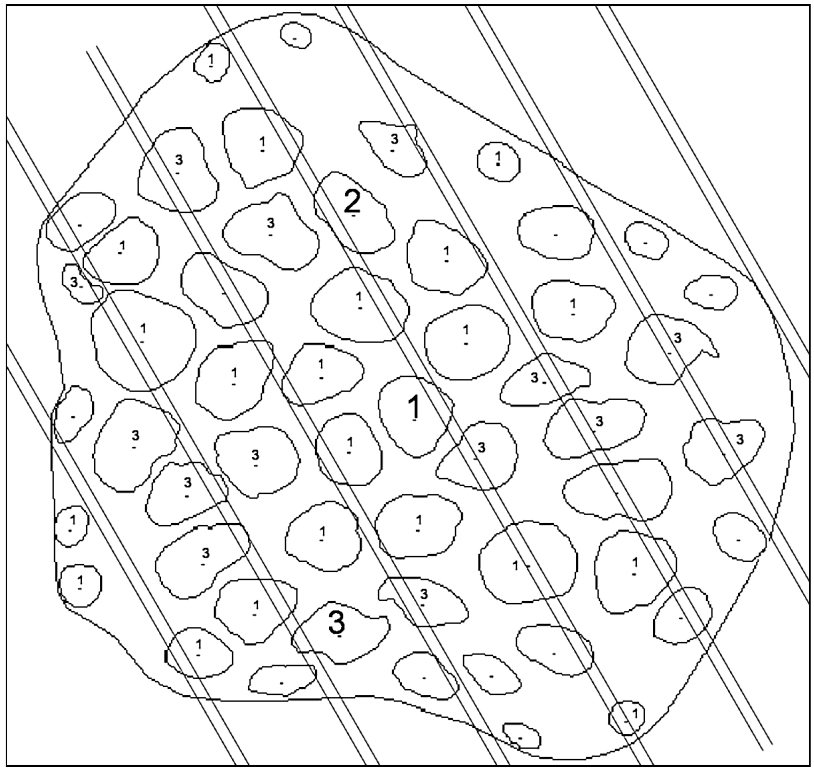

Fig. 3.2. Contours of a phloem plate and pore cross-sections drawn from an electron microscopy micrograph by Fisher (1975; see his Fig. 18).

A grid of slice section edges is superimposed on the contour plot. The lengths of the plate projections along axis x and axis y are 4.79 and 4.75 µm respectively. The number of pores is 53. The equivalent diameter of the plate is 4.647 µm. The mean and coefficient of variation of the equivalent pore diameters are 0.405 µm and 0.272. The slices are 0.070 thick and separated by a distance greater than the greatest pore dimension minus the slice thickness. Three pores labelled 1, 2 and 3 in bold type were selected as having representative shapes, as described in the text. The pores with small figures (1 or 3) and unlabelled pores are classified as similar to one of the three representative pores 1, 3 and 2 respectively; there are 22, 16 and 15 pores in classes 1, 2 and 3 respectively.

In order to obtain information about the particle size distribution from sectional data without making any assumptions about the object shape, Pawlas, Nyengaard and Jensen (2009) recently presented a method based on the components of the size variance, that due to the variability of the particle sizes and that due to local stereological estimation procedure. This method indicates the type of shape of the objects, among a number of types (for example, ellipsoid with the ratio of the semi-axe lengths). However, by this method each sampled object has to be observed at a same reference point (for example, the nucleus for cells).

In a number of cases, only sections from slices with random distances between slices and particles can be obtained whereas the object shape is known. Therefore, relations and a method were researched and are here proposed for estimating the equivalent diameter distribution of planar objects which are only approximately circular and whose the shape is known. The objects are sectioned by slices perpendicular to the object plane with a thickness t and images are obtained with a detection limit L_S. The distribution of the equivalent diameter is assumed to be approximately or perfectly symmetrical. The method is still limited to objects greater than t.

The method validity was studied with images of ellipses having various axial ratios in cases E and F and with images of the real population of pores depicted in **Fig. 3.2** under case E.

2. Materials and methods

2.1 Models of image formation

Multiple images may be obtained from a single concave object, especially in case E or when t is small in case F (**Fig. 3.1c-d**). Only the case of convex objects is here considered. The image length depends on the position and asymmetry of the object (**Fig. 3.1e-f**). In case E (**Fig. 3.1e**), the image length is equal to the direct light window width. It is less than or equal to the shorter slice side. In some geometries, the window may not even exist. In case F, the image length is equal to the length of projection of the object along the slice. Different figures are obtained depending on the relative locations and sizes of the slice and object (**Fig. 3.1g to j**).

2.2. Relations and models developed

In a first step, the method proposed here for planar objects that are only approximately circular estimates, from the mean $l_{m,\,0}$ and the coefficient of variation $cv_{length,\,0}$ of the image lengths, the mean l_m and coefficient of variation cv_{length} of the image lengths that would be obtained if each object was a circle with the same area as the object, its diameter being thus the equivalent diameter of the object. In a second step, it estimates D_m and cv_D from l_m and cv_{length} using the method previously proposed for circles (see Chapter 1).

In this method previously proposed for circles with a perfectly or approximately symmetrical distribution of diameters, D_m and cv_D are estimated by considering a fictive circle of diameter D_{lm}. This diameter D_{lm} is calculated such that the mean image length L_m of this circle over all possible configurations of the section is equal to mean length l_m of the images given by all the circles of the population. Given values of t and L_S, D_{lm} is calculated from l_m by of a series of approximations (see Chapter 1). The coefficient of variation of the image lengths of the D_{lm}-diameter circle is denoted $cv_{L,\,Dlm}$.

Here it is assumed that if the objects are sufficiently approximately circular, a fictive object which has the same shape as these objects and which generates a mean image length equal to $l_{m,0}$ has a surface area approximately equal to the surface area of a fictive D_{lm}-diameter circle which generates a mean image length equal to the mean length l_m of the images generated from all the circles having the same areas as the objects.

Therefore, the length l_m is estimated as it follows. A fictive object which generates the mean image length $L_{m,F}$ equal to the mean length $l_{m,0}$ of the images generated from all the objects is considered (note that the index F stands for "Form only approximately circular"). A fictive circle with the same area is considered. Its diameter is denoted D_{lm} and the mean length L_m of the images which are generated from this circle is hypothesized be equal to the mean image length l_m which would be generated by the circles with the same areas as all the objects.

As the relation between object area and mean image length is not known for any object shapes and values of t and L_S whereas the relation between circle diameter and mean image length is known, the sequence of the steps to estimate D_{lm} and then l_m is as follows (briefly summarized in **Fig. 3.3** and applied in **Table 3.1**):

i) A first approximate of D_{lm}, denoted $D_{lm,0}$ is derived from the mean image length $l_{m,0}$, t and L_S, assuming the object to be a circle.

ii) One object shaped like the planar objects with the same area as a $D_{lm,0}$-diameter circle is drawn by hand (or described by its equation in the case of a simple geometric form and computational simulations). The lengths of the images of this object obtained from a series of representative slices with equally spaced positions and orientations (i.e., the slices are distinguished by small parallel displacements and small angular shifts from zero to 180 degrees) are measured (or calculated). Their mean, $L_{m,F,0}$, is calculated, as well as their coefficient of variation $cv_{L,F,0}$ if necessary (see below).

iii) The ratio between the mean image length and the circle diameter is assumed to be constant when the diameter varies from $D_{lm,0}$ to D_{lm}. Therefore, as the object with the equivalent diameter $D_{lm,0}$ gives the length $L_{m,F,0}$, the equivalent diameter D_{lm} of the object which would give the length $l_{m,0}$ is estimated to be:

$$D_{lm} = D_{lm,0} \frac{l_{m,0}}{L_{m,F,0}} \tag{1}$$

This second approximate can be sufficiently accurate in a number of cases. If the previous ratio is not very constant (especially if t and L_S are great), successive approximations from ii) to iii) can be made.

iv) The mean length L_m of the images expected from this D_{lm}-diameter circle is calculated from D_{lm}, t and L_S as before. The mean length l_m of the images expected from the circles having the same areas as the planar objects is then estimated by L_m.

Then, cv_{length} is estimated as it follows. In the case of circles, when the circle diameter distribution is symmetrical, the following equation has been found (see Chapter 1):

$$(cv_{lengths}^2 + 1)(cv_D^2 + 1)^2 - 3(cv_{L,Dlm}^2 + 1)(cv_D^2 + 1) + 2(cv_{L,Dlm}^2 + 1) \approx 0 \tag{2}$$

$cv_{lengths}$ and cv_D being the coefficients of variation of the image length from all the circles and of the circle diameter, respectively. Eq. (2) can be written also:

$$(cv_{length}^2 + 1)(cv_D^2 + 1)^2 \approx (3\,cv_D^2 + 1)(cv_{L,Dlm}^2 + 1) \tag{3}$$

It is hypothesized by analogy that the following approximate equation exists if the objects are only slightly different from circles:

$$(cv_{\text{length, 0}}^{\ 2} + 1)\,(cv_{\text{D}}^{\ 2} + 1)^2 \approx (3\,cv_{\text{D}}^{\ 2} + 1)\,(cv_{\text{L, F}}^{\ 2} + 1) \quad (4)$$

where $cv_{\text{length, 0}}$ and $cv_{\text{L, F}}$ are, respectively, the coefficient of variation of the image length from all the objects and the coefficient of variation of the image length from an object which has the same surface area as the D_{lm}-diameter circle. The coefficient $cv_{\text{L, F}}$ is estimated from a surface shaped like the planar objects and having the same area as that of the D_{lm}-diameter circle like previously made for measuring $L_{\text{m, F, 0}}$. Practically, it is equal or close to $cv_{\text{L, F, 0}}$ when D_{lm} is close to $D_{\text{lm, 0}}$ and when t and L_S are not too great.

From Eqs. (3) and (4), it follows that:

$$cv_{\text{length}} \approx [(cv_{\text{length, 0}}^{\ 2} + 1)\,(cv_{\text{L, Dlm}}^{\ 2} + 1) / (cv_{\text{L, F}}^{\ 2} + 1) - 1\,]^{0.5} \quad (5)$$

If the equivalent diameter distribution is approximately or perfectly symmetrical, the mean D_{m} and coefficient of variation cv_{D} of the equivalent diameter can be estimated from l_{m} and cv_{length} by the previously proposed method for circles (see Chapter 1).

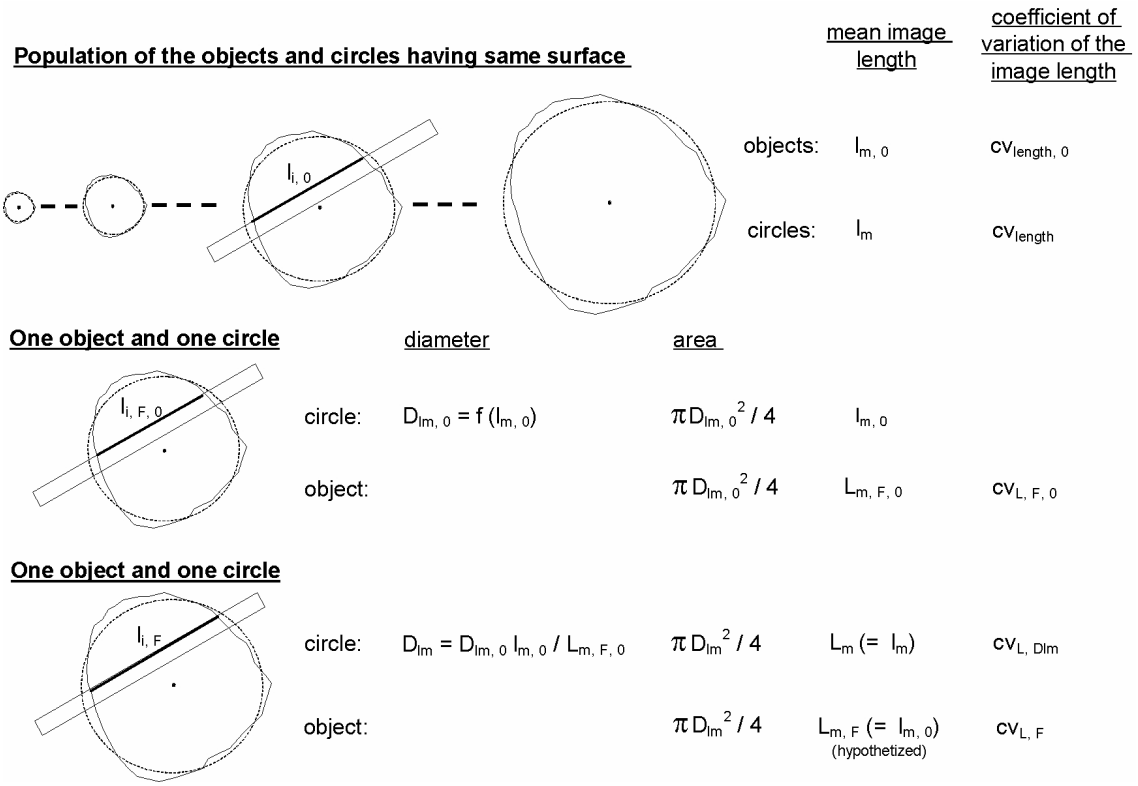

Fig. 3.3. Sequence of calculations for the proposed estimation method.

First, the mean and coefficient of variation of the image lengths ($l_{\text{m, 0}}$ and $cv_{\text{length, 0}}$) obtained from the approximately circular objects are calculated from individual image lengths such as $l_{i, 0}$. In order to estimate the mean and coefficient of variation of the image lengths (l_{m} and cv_{length}) which would be obtained from circles with the same areas as the approximately circular objects, one object with the same area as the $D_{\text{lm, 0}}$-diameter circle and one object with the same surface area as the D_{lm}-diameter circle are drawn. The image lengths from both objects which are drawn by a heavy line, in case E, are measured directly.

Table 3.1. *Image lengths and parameters estimated for a ellipse population (ES) in case F with the distribution 1 of the equivalent diameter, the axial ratio* a / b *equal to 1.5, and* t *and* L_S *equal to 3 (one replication), and for the population of the real phloem pores (P) shown in* ***Fig. 3.2****, in case E with* t *and* L_s *equal to 0.07 and 0.094µm, respectively.*

In the latter case, the coefficient of variation $cv_{L, F}$ *is estimated as* $cv_{L, F, 0}$ *and one of three shapes is assumed for the whole population: P1, P2 or P3.*

	Form	Diameter (µm)	Image mean length (µm)	Coefficient of variation (cv*)
Object population: values of $l_{m, 0}$ and cv^* ($cv_{length, 0}$) (calculated for ES, measured for P)	ES		8.28	0.285
	P		0.303	0.399
Circle giving the mean image length $l_{m, 0}$: diameter $D_{lm, 0}$ (estimated from $l_{m, 0}$, t, and L_S)	ES	9.62		
	P	0.398		
Shape having the same area as the $D_{lm, 0}$-diameter circle: mean ($L_{m, F, 0}$) and, eventually, cv^* ($cv_{L, F, 0}$) of the image lengths	ES		7.89	
	P1		0.289	0.307
	P2		0.274	0.321
	P3		0.268	0.342
Circle having the same area as the shape from which $l_{m, 0}$ would be obtained: diameter D_{lm} (estimated as $D_{lm, 0}\ l_{m, 0} / L_{m, F, 0}$), mean ($L_m$) and cv^* ($cv_{L, Dlm}$) of the image length	ES	10.11	8.67	0.212
	P1	0.417	0.318	0.260
	P2	0.440	0.336	0.262
	P3	0.451	0.344	0.264
Shape having the same area as the D_{lm}-diameter circle: cv^* ($cv_{L, F}$) of the image lengths	ES			0.278
Population of circles having the same surface areas as the ellipses or the pores:				
estimated mean ($l_m = L_m$) and cv^* (cv_{length}) of the image lengths	ES		8.67	0.220
	P1		0.318	0.396
	P2		0.336	0.385
	P3		0.344	0.366
estimated mean (D_m) and cv^* (cv_D) of the diameters	ES	10.08		0.059
	P1	0.373		0.345
	P2	0.401		0.315
	P3	0.419		0.273

2.3 Validation of the method

Populations of one thousand ellipses were constructed, each with a given approximately symmetrical equivalent diameter distribution and a given axial ratio a / b (a is the semi-major axis and b the semi-minor axis). The ellipses of each population were positioned at random distances from an almost infinitely long slice and with random orientations. The images generated by the ellipse population were calculated for cases E and F with different values of t and L_S. The real population of pores depicted in **Fig. 3.2** was also considered and images of these pores were measured in case E with t and L_S equal to

0.070 µm (a typical value of slice thickness in microscopy) and 0.094 µm (a value chosen for further reference). The method was applied to these images. As the pores have various forms, the estimation procedure was carried out three times for three shapes labelled in **Fig. 3.2**.

2.3.1. Population of ellipses

The equivalent diameter distributions were those previously studied, labelled 1 to 5 (see Chapter 1). Briefly, D_m was equal to 10 for all the distributions. Distributions 1 and 2 were Gaussian. Distribution 3 was derived from distribution 2, the diameter being equal to the mean (10) between 30% and 70%. Distributions 4 and 5 were concave and convex beta distributions respectively. Their values of cv_D varied from 0.100 to 0.243 (**Table 3.2a**). The axial ratios a / b were 1.25, 1.5, 2 or 3.

For each population, the area of each ellipse was calculated from each equivalent diameter. The values of a and b were calculated from the area, $\pi\, a\, b$, and the axial ratio a / b.

Different values of t and L_S were chosen: 0, 1, 3 and 5. However, only the values sufficiently small to obtain at least one image of the smallest ellipse of the population in positions parallel or perpendicular to the slice were considered. Thus, in case E, based on the ellipse equation ($b_0^2x^2 + a_0^2y^2 = a_0^2b_0^2$), t and L_S obeyed the relations $b_0^2\,(t/2)^2 + a_0^2\,(L_S/2)^2 < a_0^2\,b_0^2$ and $b_0^2\,(L_S/2)^2 + a_0^2\,(t/2)^2 < a_0^2\,b_0^2$, a_0 and b_0 referring to the dimensions of the smallest ellipse in the population. In case F, both t and L_S were smaller than $2b_0$.

The following calculations were made for each population.

As detailed in **Annex** with **Fig. 3.4**, each ellipse was positioned at a random distance from the slice and with a random angle between the major axis and the slice. For each ellipse giving an image, the image length was calculated. The mean, $l_{m,\,0}$, and coefficient of variation, $cv_{length,\,0}$, of the image lengths obtained from all the ellipses were calculated.

Next, $D_{lm,\,0}$ was calculated from $l_{m,\,0}$ by successive approximations.

The axial ratio being known, the dimensions a and b of an ellipse with the same area as a $D_{lm,\,0}$-diameter circle were calculated. A set of images of this ellipse was generated from one hundred equally spaced slices (the distance between the ellipse centre and the middle of the t-thickness slice being between 0 and $h_0 \cos\theta - t/2$ in case E or $h_0 \cos\theta + t/2$ in case F, with $h_0 = -(b^2 + a^2\,c^2)^{0.5}$ (see **Annex**), and one hundred orientations varying from zero to 180 degrees (thus 10^4 possible images). The mean image length $L_{m,\,F,\,0}$ was calculated.

D_{lm} was calculated according to Eq. (1) and L_m and $cv_{L,\,Dlm}$ were assessed based on Table 2 given in Chapter 1. Then, the dimensions a and b of an ellipse with the same area as a D_{lm}-diameter circle were calculated. A set of images was generated from this ellipse like previously described for the ellipse with the same surface area as the $D_{lm,\,0}$-diameter circle. The coefficient of variation of the image lengths $cv_{L,\,F}$ was calculated.

The value of l_m was estimated as L_m and the value of cv_{length} was estimated by Eq. (5). Based on these values, cv_D and D_m were calculated according to Chapter 1.

Ten replications of the previous calculations were made and the means and standard deviations of $l_{m,\,0}$, l_m, $cv_{length,\,0}$, cv_{length}, cv_D and D_m among these ten trials were calculated.

The previous calculations were also made for an axial ratio a / b equal to 1 (circles). The mean values of l_m and cv_{length} obtained in this case are denoted $(l_m)_1$ and $(cv_{length})_1$.

The mean values of $l_{m,0}$, l_m, $cv_{length,0}$ and cv_{length} obtained for various values of a / b were compared to those obtained in the case of the circle through the ratios $R_{lm,0} = l_{m,0} / (l_m)_1$, $R_{lm} = l_m / (l_m)_1$, $R_{cvlength,0} = cv_{length,0} / (cv_{length})_1$ and $R_{cvlength} = cv_{length} / (cv_{length})_1$.

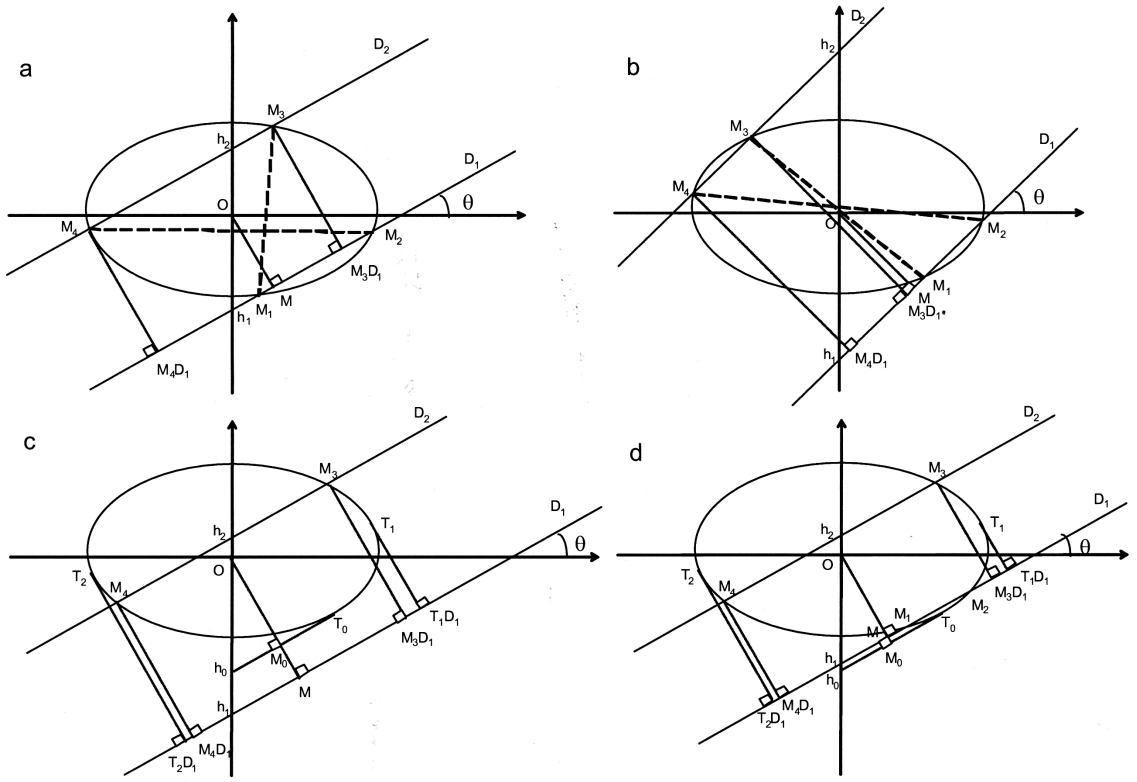

Fig. 3.4. Images of an ellipse generated by a slice (a / b is approximately 1.7) for cases E (a,b) and F (c, d).

D_1 and D_2 are the sides of the slice. As the object is symmetrical, only slices where D_1 is more distant from the ellipse centre than D_2 are considered. In case E, the image is M_1M_{3D1} in panel (a), as only this part of the section M_1M_2, which is smaller than M_3M_4, is facing M_3M_4. In panel (b) no image is obtained as the sections M_1M_2 and M_3M_4 do not overlap. In panel (c), the image is $M_4D_1T_1D_1$. In panel (d), the image is $T_1D_1T_2D_1$.

2.3.2. Population of phloem sieve plate pores

A transverse view of an entire phloem sieve plate was published by Fisher (1975) in his Fig. 18. **Fig. 3.2** depicts outlines taken from this view which shows an entire sieve plate with 53 pores. A series of parallel slices 0.07 µm thick and spaced 0.5 µm apart (about the diameter of the greatest pore minus t) was superimposed on the outlines. The pores were assumed to be transparent cylinders in opaque slices lit by a direct light (case E). Thus, whenever both sides of a slice section pass through a pore, the length of the window was measured. Only the lengths greater than 0.094 µm (L_S) were considered to be detectable. The process was repeated for five other orientations of the grid, each turned by an angle 30 degrees with respect to the last. The mean $l_{m,0}$ and the coefficient of variations $cv_{length,0}$ of the image lengths were

calculated.

The diameter $D_{lm,\,0}$ of the circle whose mean image length is expected to be $l_{m,\,0}$ was calculated. I then selected three pores of different shapes, which in **Fig. 3.2** are labelled P1 (more rounded), P2 (more oblong) and P3 (more irregular with some convexities). The following procedure was carried out for each of the three pores. First, the outline of the pore was copied to a "bmp" file. Second, using the "Image J" software, I counted the number of pixels in the pore area and determined the scale length that would give a pore area equal to that of the $D_{m,\,0}$-diameter circle. The height of the pore and its greatest dimension were measured on this scale. Third, the image was inserted into an Excel worksheet. Using Excel tools, the coordinates of several points along the pore outline were recorded to create one hundred copies of the pore. The scale length was determined by the height of the pore and the smallest and greatest ordinates. Each copy was positioned at a different distance from the middle of a slice 0.07 µm thick (the distance varying by one-tenth the greatest dimension of the pore minus the slice thickness) and rotated by an angle varying from 0 to 162 degrees in eighteen-degree intervals (**Fig. 3.5** shows all the copies of the shape 2). As previously made for the sieve plate, whenever both sides of a slice sectioned a pore, the length of the window was measured (using Image J). In some images of P3, where a multiple image was observed, only the longer image part was counted. Finally, I calculated the mean $L_{m,\,F,\,0}$ and coefficient of variation $cv_{L,\,F,\,0}$ of lengths longer than 0.094 µm (L_S).

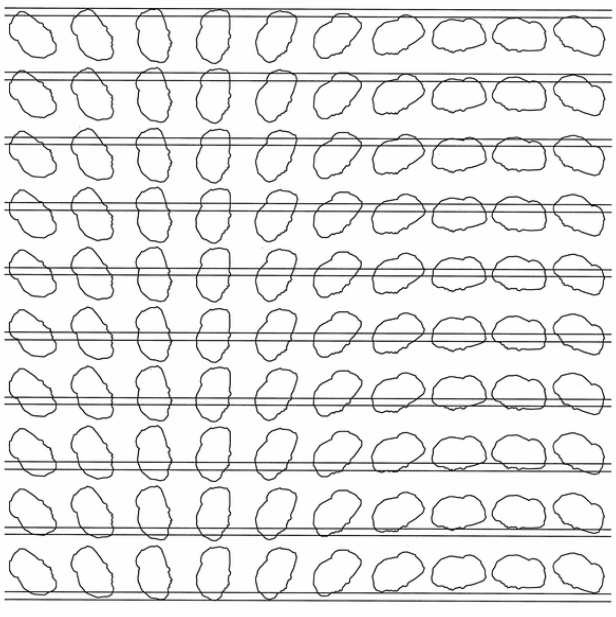

Fig. 3.5. One hundred identical shapes having the same area as the circle whose expected mean image length is equal to the measured mean length $l_{m,\,0}$ of the images of the pores in **Fig. 3.2**, shaped according to the shape P2.

The surfaces are placed at ten different distances from the slice, varying by one tenth of the longest dimension of the object minus t and rotated by an angle varying by 18-degrees steps from 0 to 162 degrees.

I calculated D_{lm} using Eq. (1) under hypothesis that all pores were shaped exactly the same (either P1, P2 or P3). I then calculated L_m and set l_m equal to L_m. The coefficient of variation cv_{length} was calculated using Eq. (5). D_m and cv_D were calculated according to the method laid out in Chapter 1.

The real pore areas (**Fig. 3.2**) were measured to calculate the equivalent pore diameters and the above estimates were compared to their target values. Moreover, the pores were fitted to ellipses using Image J which provided their ratio a / b.

3. Results

3.1. Population of ellipses

Table 3.1 shows the sequence of calculations made in case F for one simulation with an ellipse population constructed with the distribution 1, a / b equal to 1.5, and t and L_S equal to 3. The values of $(l_m)_1$ and $(cv_{length})_1$ obtained for the five distributions were close to those previously obtained in Chapter 1 from circles sectioned by equally spaced slices with the same values of t and L_S (not shown). The predicted values of cv_D and D_m were also close to the true values (**Table 3.2a-b**).

R_{lm} and $R_{cvlength}$ were much nearer to 1 than to $R_{lm,\,0}$ and $R_{cvlength,\,0}$ respectively (**Fig. 3.6** shows only the data for distribution 1). In case E, at a given value of a / b, $R_{lm,\,0}$ and $R_{cvlength,\,0}$ tended to be lower when L_S was higher.

The standard deviations of cv_D and D_m over the tens randomly generated image length distributions were 0.02 and 0.1 respectively in average. The estimates of cv_D and D_m were very close to the true values (**Table 3.2c-d**). However, when a / b and/or t were higher, the estimates were less close to the true values.

Table 3.2a. *Estimated values of* cv_D *when the axial ratio was 1 (circle). The two values are for cases E and F, respectively from left to right. No value was calculated if* t *or* L_S *was too large to obtain at least one image from the smallest ellipse. The real values of* cv_D *are indicated in line 2.*

t	L_S	Distribution 1	Distribution 2	Distribution 3	Distribution 4	Distribution 5
		0.100	0.200	0.196	0.171	0.243
0	0	0.10 - 0.11	0.21 - 0.20	0.20 - 0.20	0.16 - 0.15	0.26 - 0.27
0	1	0.11 - 0.08	0.20 - 0.21	0.18 - 0.18	0.17 - 0.15	0.26 - 0.28
0	3	0.09 - 0.10	0.19 - 0.19	0.20 - 0.18	0.15 - 0.15	0.25 - 0.25
0	5	0.09 - 0.09	-	-	-	0.23 - 0.23
1	0	0.09 - 0.10	0.21 - 0.21	0.20 - 0.20	0.14 - 0.16	0.27 - 0.25
1	1	0.11 - 0.11	0.22 - 0.19	0.20 - 0.18	0.18 - 0.16	0.26 - 0.26
1	3	0.10 - 0.08	0.18 - 0.18	0.19 - 0.18	0.13 - 0.15	0.26 - 0.25
1	5	0.09 - 0.09	-	-	-	0.23 - 0.23
3	0	0.10 - 0.09	0.23 - 0.19	0.22 - 0.19	0.16 - 0.16	0.30 - 0.25
3	1	0.10 - 0.07	0.23 - 0.20	0.22 - 0.20	0.17 - 0.15	0.29 - 0.27
3	3	0.10 - 0.08	- 0.19	- 0.18	0.14 - 0.15	0.27 - 0.25
3	5	0.08 - 0.09	-	-	-	0.23 - 0.23
5	0	0.13 - 0.10	-	-	-	0.36 - 0.26
5	1	0.12 - 0.09	-	-	-	0.34 - 0.26
5	3	0.12 - 0.08	-	-	-	0.31 - 0.24
5	5	- 0.09	-	-	-	- 0.24

Table 3.2b. *Estimated values of* D_m *when the axial ratio was 1 (circle). See* ***Table 3.2a*** *legend. The real value of* D_m *was 10 in all five distributions.*

t	L_S	Distribution 1	Distribution 2	Distribution 3	Distribution 4	Distribution 5
0	0	10.0 - 9.8	9.8 - 9.9	9.9 - 9.9	10.0 - 10.0	9.9 - 9.8
0	1	10.0 - 10.0	9.9 - 9.8	10.1 - 10.1	10.0 - 10.0	10.0 - 9.8
0	3	10.0 - 9.9	10.1 - 9.9	10.0 - 10.0	10.1 - 10.0	10.1 - 9.9
0	5	10.0 - 10.0	-	-	-	10.3 - 10.2
1	0	10.0 - 10.0	9.9 - 9.8	10.0 - 9.9	10.2 - 10.0	9.8 - 9.9
1	1	9.9 - 9.9	9.9 - 10.1	10.0 - 10.1	10.0 - 10.0	10.0 - 9.9
1	3	9.9 - 10.1	10.2 - 10.1	10.1 - 10.0	10.2 - 10.1	10.0 - 10.0
1	5	10.0 - 10.0	-	-	-	10.4 - 10.1
3	0	10.0 - 10.0	10.1 - 9.9	10.1 - 9.9	10.1 - 10.0	10.0 - 9.9
3	1	10.0 - 10.0	9.9 - 9.9	10.0 - 9.8	10.1 - 10.0	10.0 - 9.8
3	3	10.1 - 10.0	- 10.0	- 10.0	10.3 - 10.0	10.3 - 9.9
3	5	10.2 - 10.0	-	-	-	10.7 - 10.1
5	0	9.9 - 10.0	-	-	-	9.8 - 9.8
5	1	10.0 - 10.0	-	-	-	10.0 - 9.7
5	3	10.0 - 10.0	-	-	-	10.2 - 9.8
5	5	- 10.0	-	-	-	- 10.0

3.2. Population of phloem sieve plate pores

Table 3.1 shows the values of $l_{m,\,0}$ and $cv_{length,\,0}$ obtained with the 147 measured images. The image lengths varied with the position of the grid (**Table 3.3**). The axial ratios a / b of pore shapes P1, P2 and P3 which were fitted to ellipses by Image J were 1.12, 1.67 and 1.66 respectively. **Table 3.1** shows the sequence of the calculations and the estimates of D_m and cv_D for each of the three assumed pore shapes. The mean values of D_m and of cv_D obtained from this method, averaging over all three forms, were 0.398 µm and 0.310 respectively. The equivalent diameter distribution based on these parameters, assuming the distribution to be normal, is shown in **Fig. 3.7**. When D_m and cv_D were weighted by the number of pores of each shape (22, 16 and 15 respectively for P1, P2 and P3) their values were 0.394 µm and 0.314.

Based on the measured pore areas, the mean and the coefficient of variation of the equivalent pore diameter were 0.405 µm and 0.272 respectively. The equivalent diameter distribution was not quite symmetrical, longer diameters having higher frequencies (**Fig. 3.7**). When the pores were fitted to ellipses using Image J, the axial ratio a / b of 28, 40, 28 and 4% of the pores was into the classes]1.02 - 1.25],]1.25 - 1.5],]1.5 – 2] or]2 – 2.21] respectively, and the mean axial ratios were 1.22, 166 and 1.55 for the pores shaped like P1, P2 and P3 respectively.

4. Discussion

The proposed method involves two successive steps which assume the distribution of the equivalent diameters of the objects to be approximately or perfectly symmetrical. The first aims to estimate, from the mean $l_{m,\,0}$ and coefficient of variation $cv_{length,\,0}$ of the measured lengths of images of approximately circular objects, the mean l_m and coefficient of variation cv_{length} of the lengths of images that would be

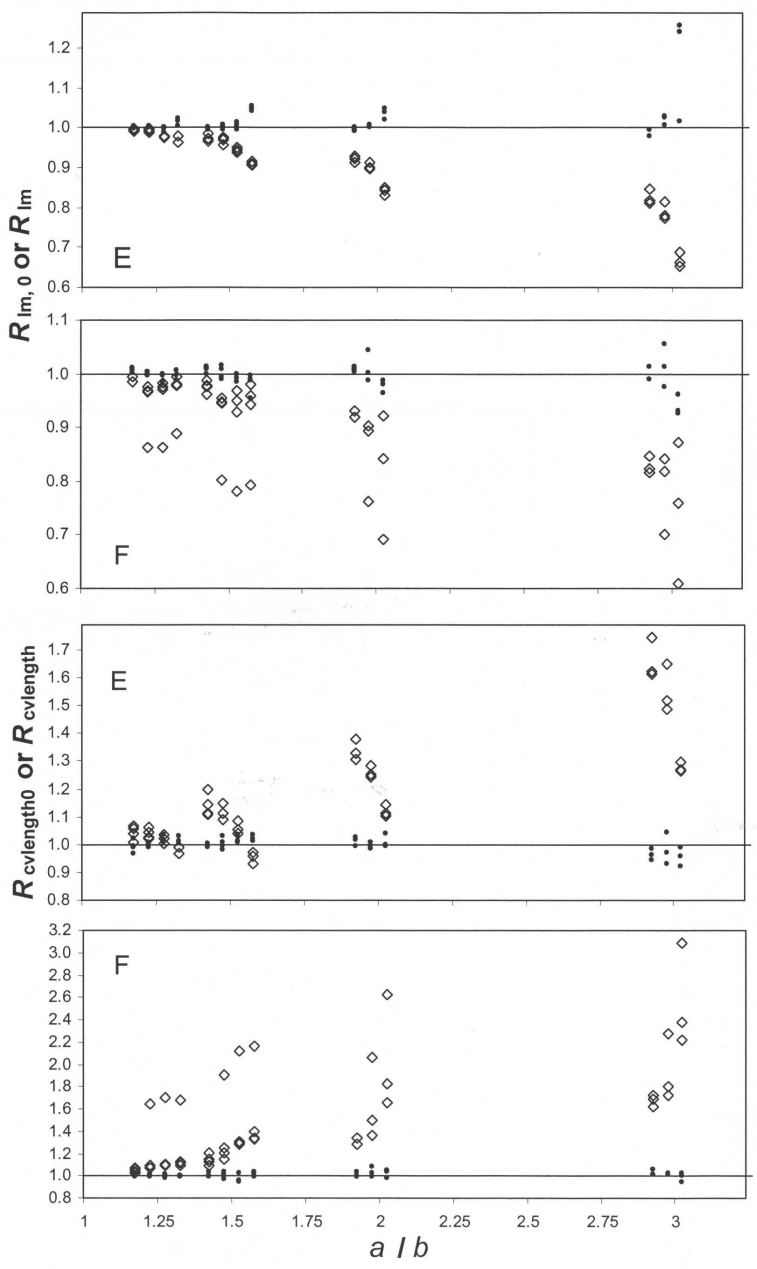

Fig. 3.6. Variations of $R_{lm,\,0}$, $R_{cvlength,\,0}$, R_{lm} and $R_{cvlength}$ with respect to the ratio a / b, for cases E and F in distribution 1.

$R_{lm,\,0}$ and $R_{cvlength,\,0}$ (empty losanges) are ratios of the mean ($l_{m,\,0}$) or coefficient of variation ($cv_{length,\,0}$) of the image length obtained from the ellipses to the mean or coefficient of variation of the image length obtained from circles having the same surface area. R_{lm} and $R_{cvlength}$ (dots) are ratios of the mean (l_m) or coefficient of variation (cv_{length}) of the image length estimated from $l_{m,\,0}$ or $cv_{length,\,0}$ to the mean or coefficient of variation of the image length obtained from circles having the same surface areas as the ellipses. The abscissas are all exactly 1.25, 1.5, 2 and 3, but have been slightly shifted to distinguish sub-groups with different values of L_S. In order from left to right, L_S is 0, 1, 3 or 5; the last sub-group is missing for abscissas 2 and 3.

***Table 3.2c**. Estimated values of* cv_D *for axial ratios > 1. The two values are for cases E and F, respectively from left to right. No value was calculated if* t *or* L_S *was too large to obtain at least one image from the smallest ellipse. Note that the lines with* t = *5 and* a / b *equal to 2 or 3 are not shown as no value was obtained. The real values of* cv_D *are indicated in line 2.*

a / b	*t*	L_S	Distribution 1	Distribution 2	Distribution 3	Distribution 4	Distribution 5
			0.100	0.200	0.196	0.171	0.243
1.25	0	0	0.10 - 0.10	0.20 - 0.19	0.19 - 0.21	0.17 - 0.15	0.25 - 0.26
1.25	0	1	0.07 - 0.10	0.20 - 0.21	0.19 - 0.18	0.16 - 0.16	0.27 - 0.26
1.25	0	3	0.10 - 0.09	0.19 - 0.19	0.19 - 0.18	0.15 - 0.15	0.24 - 0.25
1.25	0	5	0.09 - 0.09	-	-	-	0.22 - 0.23
1.25	1	0	0.10 - 0.09	0.19 - 0.19	0.20 - 0.18	0.16 - 0.12	0.27 - 0.26
1.25	1	1	0.10 - 0.11	0.20 - 0.20	0.20 - 0.20	0.15 - 0.16	0.27 - 0.26
1.25	1	3	0.10 - 0.09	- 0.19	- 0.18	0.16 - 0.13	0.26 - 0.25
1.25	1	5	0.09 - 0.09	-	-	-	0.23 - 0.22
1.25	3	0	0.12 - 0.08	0.22 - 0.22	0.22 - 0.20	0.19 - 0.13	0.32 - 0.24
1.25	3	1	0.12 - 0.08	- 0.19	- 0.18	0.16 - 0.15	0.32 - 0.24
1.25	3	3	0.10 - 0.09	- 0.19	- 0.18	- 0.14	0.29 - 0.23
1.25	3	5	0.10 - 0.09	-	-	-	0.24 - 0.22
1.25	5	0	0.13 - 0.09	-	-	-	0.39 - 0.26
1.25	5	1	0.15 - 0.09	-	-	-	0.38 - 0.25
1.25	5	3	0.12 - 0.08	-	-	-	0.31 - 0.25
1.25	5	5	- 0.08	-	-	-	- 0.23
1.5	0	0	0.10 - 0.09	0.19 - 0.21	0.21 - 0.18	0.17 - 0.16	0.26 - 0.27
1.5	0	1	0.10 - 0.11	0.20 - 0.20	0.20 - 0.21	0.15 - 0.16	0.27 - 0.27
1.5	0	3	0.09 - 0.08	-	-	0.14 - 0.14	0.24 - 0.24
1.5	0	5	0.09 - 0.08	-	-	-	0.22 - 0.23
1.5	1	0	0.13 - 0.13	0.19 - 0.22	0.22 - 0.22	0.17 - 0.17	0.27 - 0.30
1.5	1	1	0.10 - 0.07	0.21 - 0.20	0.19 - 0.20	0.17 - 0.15	0.26 - 0.26
1.5	1	3	0.10 - 0.09	-	-	0.15 - 0.15	0.26 - 0.24
1.5	1	5	0.08 - 0.09	-	-	-	0.23 - 0.21
1.5	3	0	0.11 - 0.05	-	-	0.17 - 0.13	0.31 - 0.25
1.5	3	1	0.11 - 0.09	-	-	0.17 - 0.14	0.32 - 0.26
1.5	3	3	0.12 - 0.10	-	-	- 0.15	0.29 - 0.23
1.5	3	5	0.10 - 0.08	-	-	-	0.24 - 0.22
1.5	5	0	0.15 - 0.12	-	-	-	0.42 - 0.25
1.5	5	1	0.15 - 0.08	-	-	-	0.48 - 0.23
1.5	5	3	0.12 - 0.10	-	-	-	0.35 - 0.22
1.5	5	5	- 0.09	-	-	-	- 0.21
2	0	0	0.10 - 0.11	0.21 - 0.20	0.18 - 0.18	0.16 - 0.15	0.27 - 0.27
2	0	1	0.13 - 0.10	0.18 - 0.18	0.20 - 0.18	0.14 - 0.15	0.27 - 0.27
2	0	3	-	-	-	0.15 - 0.15	0.24 - 0.27
2	0	5	-	-	-	-	-
2	1	0	0.10 - 0.10	0.21 - 0.23	0.21 - 0.21	0.16 - 0.21	0.28 - 0.30
2	1	1	0.10 - 0.10	0.19 - 0.20	0.20 - 0.19	0.15 - 0.17	0.27 - 0.26
2	1	3	-	-	-	-	-
2	1	5	-	-	-	-	-
2	3	0	-	-	-	-	-
2	3	1	-	-	-	-	-
2	3	3	-	-	-	-	-
2	3	5	-	-	-	-	-
3	0	0	0.06 - 0.11	0.23 - 0.19	0.20 - 0.22	0.13 - 0.17	0.26 - 0.25
3	0	1	0.06 - 0.12	0.13 - 0.21	0.20 - 0.17	0.15 - 0.17	0.27 - 0.25
3	0	3	-	-	-	-	-
3	0	5	-	-	-	-	-
3	1	0	0.05 - 0.12	0.20 - 0.27	0.19 - 0.20	0.17 - 0.18	0.26 - 0.29
3	1	1	0.08 - 0.12	0.19 - 0.18	0.19 - 0.20	0.17 - 0.16	0.27 - 0.22
3	1	3	0.12 - 0.09	-	-	-	0.28 - 0.23
3	1	5	-	-	-	-	-
3	3	0	0.05 - 0.10	-	-	-	0.42 - 0.14
3	3	1	0.05 - 0.09	-	-	-	0.35 - 0.19
3	3	3	0.08 - 0.10	-	-	-	0.30 - 0.18
3	3	5	0.06 - 0.11	0.23 - 0.19	0.20 - 0.22	0.13 - 0.17	0.26 - 0.25

Table 3.2d. *Estimated values of* D_m *for axial ratios > 1. See* ***Table 3.2c*** *legend. The real mean diameter was 10 in all five distributions.*

a / *b*	*t*	L_S	Distribution 1	Distribution 2	Distribution 3	Distribution 4	Distribution 5
1.25	0	0	10.0 - 10.0	10.0 - 10.0	10.0 - 9.9	10.0 - 10.1	10.0 - 10.0
1.25	0	1	10.1 - 10.0	10.0 - 10.0	10.0 - 10.1	10.0 - 10.0	9.9 - 10.0
1.25	0	3	10.0 - 10.0	10.0 - 10.1	10.1 - 10.2	10.1 - 10.1	10.1 - 10.1
1.25	0	5	10.1 - 10.0	-	-	-	10.3 - 10.3
1.25	1	0	10.0 - 10.0	10.1 - 10.1	10.1 - 10.1	10.1 - 10.2	9.9 - 10.0
1.25	1	1	10.0 - 9.9	10.1 - 9.9	10.0 - 9.9	10.1 - 10.0	9.9 - 9.9
1.25	1	3	10.0 - 10.0	- 10.0	- 10.1	10.1 - 10.2	10.1 - 10.0
1.25	1	5	10.1 - 10.0	-	-	-	10.3 - 10.4
1.25	3	0	10.0 - 9.8	10.1 - 9.6	10.1 - 9.6	10.0 - 9.9	9.8 - 9.8
1.25	3	1	9.9 - 10.0	- 9.8	- 10.0	10.2 - 9.9	9.8 - 9.9
1.25	3	3	10.0 - 10.0	- 9.9	- 9.9	- 10.1	10.1 - 9.9
1.25	3	5	10.0 - 10.0	-	-	-	10.6 - 10.1
1.25	5	0	10.1 - 9.9	-	-	-	9.7 - 9.6
1.25	5	1	10.0 - 9.9	-	-	-	9.8 - 9.8
1.25	5	3	10.1 - 10.0	-	-	-	10.4 - 9.8
1.25	5	5	- 10.1	-	-	-	- 10.0
1.5	0	0	9.9 - 10.0	10.0 - 10.0	9.8 - 10.1	10.0 - 10.1	10.0 - 9.8
1.5	0	1	10.0 - 9.9	10.0 - 10.0	10.0 - 9.9	10.1 - 10.0	9.8 - 9.9
1.5	0	3	10.0 - 10.0	-	-	10.1 - 10.2	10.1 - 10.1
1.5	0	5	10.0 - 10.1	-	-	-	10.4 - 10.3
1.5	1	0	9.9 - 10.1	10.1 - 10.1	9.9 - 10.1	10.0 - 10.2	9.9 - 9.9
1.5	1	1	10.0 - 10.0	10.1 - 9.9	10.1 - 9.9	10.0 - 10.1	10.0 - 9.9
1.5	1	3	10.0 - 10.0	-	-	10.2 - 10.2	10.0 - 10.0
1.5	1	5	10.0 - 9.9	-	-	-	10.4 - 10.5
1.5	3	0	10.1 - 10.0	-	-	10.2 - 9.9	10.0 - 9.7
1.5	3	1	10.0 - 9.8	-	-	10.2 - 10.0	9.9 - 9.8
1.5	3	3	10.1 - 9.9	-	-	- 10.0	10.1 - 10.1
1.5	3	5	10.1 - 10.0	-	-	-	10.8 - 10.2
1.5	5	0	10.3 - 9.4	-	-	-	9.7 - 9.4
1.5	5	1	10.3 - 9.8	-	-	-	9.3 - 9.7
1.5	5	3	10.4 - 9.9	-	-	-	10.3 - 9.9
1.5	5	5	- 10.0	-	-	-	- 9.9
2	0	0	10.0 - 10.0	10.0 - 10.0	10.1 - 9.9	10.1 - 10.1	9.9 - 10.0
2	0	1	9.8 - 10.0	10.0 - 10.1	9.9 - 10.1	10.1 - 10.0	9.9 - 9.9
2	0	3	9.9 - 10.0	-	-	10.1 - 10.1	10.0 - 10.0
2	0	5	-	-	-	-	-
2	1	0	10.0 - 10.4	10.0 - 10.3	10.0 - 10.3	10.1 - 10.2	9.9 - 10.2
2	1	1	10.0 - 9.9	10.0 - 10.1	10.0 - 10.0	10.1 - 10.1	10.0 - 9.9
2	1	3	9.9 - 9.8	-	-	- 10.1	10.0 - 9.9
2	1	5	-	-	-	-	-
2	3	0	10.3 - 9.8	-	-	10.5 - 9.9	10.0 - 9.1
2	3	1	10.4 - 9.6	-	-	- 9.9	10.1 - 9.7
2	3	3	10.3 - 9.8	-	-	- 10.1	10.2 - 10.1
2	3	5	-	-	-	-	-
3	0	0	10.0 - 9.9	9.9 - 10.1	9.9 - 9.9	10.1 - 10.0	9.9 - 10.1
3	0	1	10.0 - 10.0	10.2 - 9.9	9.8 - 10.1	9.9 - 10.0	9.8 - 10.1
3	0	3	9.8 - 9.8	-	-	-	10.0 - 9.8
3	0	5	-	-	-	-	-
3	1	0	10.4 - 10.5	10.2 - 10.1	10.4 - 10.4	10.3 - 10.5	10.2 - 10.1
3	1	1	10.2 - 10.0	10.2 - 10.1	10.2 - 10.1	10.2 - 10.0	10.2 - 10.1
3	1	3	9.9 - 9.8	-	-	-	9.9 - 10.0
3	1	5	-	-	-	-	-
3	3	0	12.4 - 9.2	-	-	-	11.0 - 9.8
3	3	1	12.2 - 9.3	-	-	-	11.3 - 9.4
3	3	3	10.3 - 9.5	-	-	-	11.2 - 9.9
3	3	5	-	-	-	-	-

Table 3.3. *Number of the pore images and mean and coefficient of variation of the image lengths obtained assuming case E from the view from Fisher (1975). These values are calculated for six orientations of the grid superimposed on the plate shown in* ***Fig. 3.2*** *separated by an angle of 30°.*

Grid positions (degrees)	0	30	60	90	120	150
Numbers of images	21	22	25	28	29	22
Mean image length	0.338	0.348	0.291	0.282	0.283	0.283
Coefficient of variation	0.406	0.369	0.436	0.360	0.450	0.471

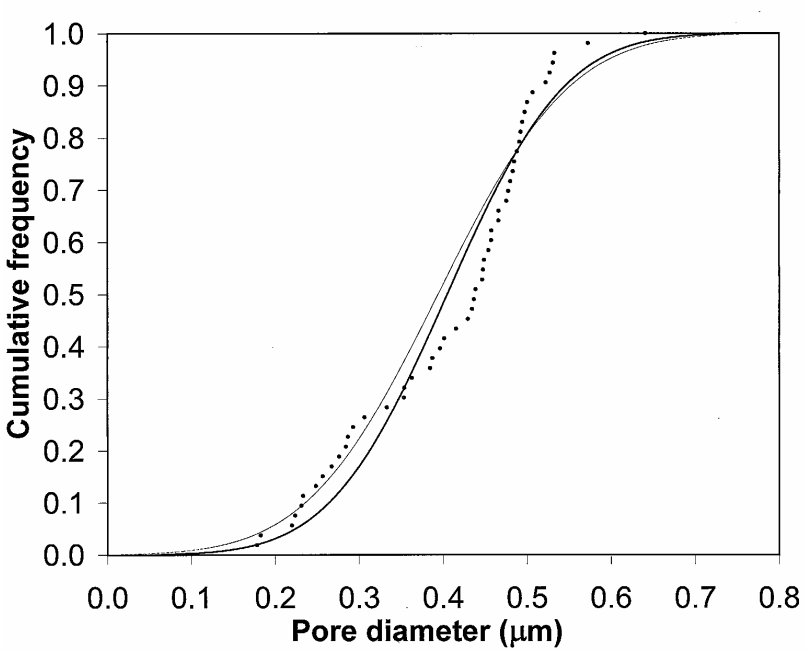

Fig. 3.7. Cumulative distribution of the equivalent diameters of the 53 pores of the sieve plate shown in **Fig. 3.2** (heavy dots) and corresponding normal distributions whose mean and coefficient of variation are based on the real pore areas (0.405 µm and 0.272; heavy line) or are equal to the values estimated from the estimated values of l_m and cv_{length} (0.394 µm and 0.314; fine line).

obtained if each object was a circle with the same area as the object. It needs measuring (or calculating in case of numerical simulations) the lengths of images of a fictive object. The second step consists to apply the previously proposed method to estimate the mean D_m and the coefficient of variation cv_D of the circle diameters.

The examples with ellipses showed that the estimations of l_m and cv_{length} obtained by this method were accurate as R_{lm} and $R_{cvlength}$ were much nearer to 1 than $R_{lm,\,0}$ and $R_{cvlength,\,0}$ (**Fig. 3.4**). The estimated values of D_m were very close to the true values (within 10%) except when both a / b and t were high (both equal to 3). The deviations in the estimations of D_m and cv_D which occurred when a / b and t increased were likely due to deviations in the estimations made in the two steps.

In the example with the pores, the axial ratio of almost all the pores was lower than 2. Therefore, although the number of images was not very high (147), the distribution of the equivalent pore diameters only very approximately symmetrical, and the shape more irregular than the ellipses with even some

convexities, the estimated values of D_m and cv_D (0.394 µm and 0.314) could be close to the true values obtained by directly measuring the areas of the 53 pores (0.405 µm and 0.272). The equivalent pore diameter distribution predicted from these estimated values seems sufficiently accurate to provide useful information for a number of questions (**Fig. 3.7**).

These results show that in the two cases E and F, the equivalent diameter distribution of approximately circular objects can be accurately assessed by the proposed method. The examples with ellipses indicate the range of shapes that can be considered approximately circular in this context. The method does need the object shape to be known. In the example with pores, a transverse section like that shown in **Fig. 3.2** can be extrapolated to infer the shape of other pores in the same tissue. Furthermore, the method assumes that all objects have the same shape. However, when two or more shapes occur and the shapes are not very different from one another, the example with the pores demonstrates that the method can be still applied by conducting the analysis on each form in succession. Compensations exist likely between the probable deviations which occur in the values estimated for each shape from the mean length of the images of all shapes. However, it is necessary to know about the relative frequencies of the different shapes for such estimations.

The method assumes that the equivalent diameter distribution is approximately or perfectly symmetrical. Generally, the distribution is not known. For simple shapes like ellipses, I recommend estimating the equivalent diameters from the normal distribution definite by cv_D and D_m, then calculating the values of a and finally calculating the distribution of the lengths of the images given by the population according to the calculations described previously for ellipses. Good agreement with the real distribution will support the hypothesis that the distribution is approximately normal (and thus approximately symmetrical).

Of course, the method will be generally less accurate when the number of images is small or when the distribution is very asymmetrical. Some other limitations have previously been indicated in the context of circular objects (see Chapter 1). However, the precise effects of variations in these parameters remain to be studied.

From the equivalent diameter distribution, the number of objects can be easily derived (see Chapter 1).

The proposed method is easily applicable and will be likely very useful in many fields, especially for estimating the size and number of pores in the phloem sieve plates of the fruit pedicel which limit likely the fruit growth (Bussières, 2002). The author is studying an extension of the method for approximately spherical objects.

5. Conclusions

The distribution of the equivalent diameters of approximately circular objects, opaque or transparent relative to the medium in which they are embedded, can be assessed from images of their sections in slices by the proposed method when the distribution is roughly symmetrical and the object shape is known.

Acknowledgements

I thank an anonymous translator for his advices and who found a small error of the logical development in the first manuscript.

References

Bussières, P. 2002. Water import in the young tomato fruit limited by pedicel resistance and calyx transpiration. *Funct. Plant Biol*. 29, 631–641.

Cruz-Orive, L.M. 1976. Particle size-shape distribution: the general spheroid problem. I Mathematical model. *J Microsc.* 107, 235–253.

Cruz-Orive, L.M. 1978. Particle size-shape distribution: the general spheroid problem. II Stochastic model and practical guide. *J. Microsc.* 112, 153–167.

Fisher, D.B. 1975. Structure of functional soybean sieve elements. *Plant Physiol.* 56, 555-569.

Pawlas, Z., Nyengaard, J.R., Jensen, E.B.V. 2009. Particles sizes from sectional data. *Biometrics* 65, 216-224.

Wicksell, S.D. 1926. The corpuscle problem. Second memoir. Case of ellipsoidal corpuscles. *Biometrika* 18, 151-172.

Annex

Each ellipse was positioned at a random distance from the slice and with a random angle between the major axis and the slice. For that, the value of a obtained for the greatest ellipse is denoted *amax*. The distance, denoted *dist*, between the centre of each ellipse with a given value of a and the middle of the t-thickness slice was taken to be a random value between 0 and $amax - t / 2$ in case E or $amax + t / 2$ in case F. The slice side farthest from the ellipse centre is labelled D_1 and the nearest side is labelled D_2. Referring to **Fig. 3.4**, the angle θ was taken to be a random value between 0 and 180 degrees. The absolute value of the ordinate at the origin, h_0, of line D_0 parallel to the slice and tangent at T_0 (showed only in **Fig. 3.4c-d**) was calculated to be $(b^2 + a^2 c^2)^{0.5}$, with $c = \tan \theta$. The distance OM_0 was $|h_0 \cos\theta|$. When OM_0 was shorter than $dist + t / 2$ in case E or $dist - t / 2$ in case F, the ellipse did not give image.

For each ellipse giving an image, the image length was calculated based on a) the equations of the ellipse ($a^2x^2 + b^2y^2 = a^2b^2$), the line D_1 ($y = c\,x + h_1$) and possibly the line D_2 ($y = c\,x + h_2$), b) the points of intersection M_1, M_2, M_3 and M_4 between lines D_1 and D_2 and the ellipse, c) the equations of the lines perpendicular to D_1 going through M_3 and M_4, d) the coordinates of the intersections M_3D_1 and M_4D_1 and e) the equation of the line perpendicular to D_1 going through the ellipse centre, f) in case F, the equations of the line parallel to D_1 and tangent to the ellipse at point T_0, and of the lines perpendicular to D_1 and tangent to the ellipse at points T_1 and T_2. In case E, the image length was equal to M_1M_2 or to $M_1{-}M_3D_1$ (or $M_2{-}M_4D_1$); this latter was used if the shortest diagonal line, M_1M_3 (or M_2M_4), was shorter than M_1M_2. In case F, the image length was equal to the sum of (i) the longest length among $M{-}T_2D_1$ (when T_2 was in the slice), $M{-}M_1$ and $M{-}M_4D_1$, and (ii) the longest length among $M{-}T_1D_1$ (when T_1 was in the slice), $M{-}M_2$ and $M{-}M_3D_1$. Image lengths shorter than L_S were neglected.

CHAPTER 4

Estimating the number and diameter distribution of opaque objects from their images through transparent thick slices: application to analysis of synaptic vesicles

Abstract

Estimation of the numbers and diameter distributions of opaque circular, cylindrical, or spherical objects dispersed in a transparent matrix from images obtained by slices perpendicular to a diameter is an important problem in many fields. In many microscopy studies, the slices are thicker than the diameters of the objects of interest. Often, the main question for statistical analysis is whether the distribution of object diameters is normal, near normal, or asymmetrical. Here a first method is proposed for the case of an approximately or perfectly normal diameter distribution. It distinguishes the images of the objects with centres within the slice from those of the objects with centres outside the slice. As the image of an object centred outside the slice is equivalent to one obtained by a slice of zero thickness, the estimation of number and diameter distribution can be assessed using a recent method valuable in this case if the diameter distribution is symmetrical. Then, based on this first method, a general method is proposed for any distribution by treating the distribution as a set of juxtaposed normal distributions. These methods were successfully tested and used to study a published data set of tissue slices containing synaptic vesicles. The number of vesicles and the diameter distribution were assessed. The frequency of the vesicle diameters in the range 38–50 nm was found to be lower than expected from a normal distribution.

1. Introduction

Modern methods of microscopy are often used to estimate the number and diameter distribution of opaque objects dispersed in a transparent matrix. These parameters are estimated by slicing through the matrix to infer numbers and morphological parameters from the images of the objects or object fragments projected onto a plane. Ideally, slice thickness is adjusted according to the size of the studied objects, the matrix nature, slicing method, and observation method. When the slices are thinner, the probability of observing individual overlapping objects is decreased. Furthermore, if the matrix is not quite transparent, the transparency of the slices is improved. However, the proportion of objects that are cut by the slices is increased. Therefore, two extreme cases can be distinguished: when the slices are thinner than the smallest objects and when the slices are thicker than the largest diameter objects.

In many cases, the main aim is to determine whether the object diameter distribution is normal or not quite normal. Indeed, deviations from normality may have functional significance. The problem is to estimate the parameters of a normal diameter distribution that yields an image size distribution as close as possible to the observed image size distribution. **Fig. 4.1** shows the image length distributions for two

populations of circles with symmetrical diameter distributions. Image length distributions from thick slices (25 nm) differ from distributions from slices of thickness nil for both populations (10 nm and 15 nm in diameter) and in all cases, the distribution deviates from normality. In many others cases, the true object diameter distribution is not normal, with possibly several peaks.

In cases where the slices are thinner than the object diameters, methods have been proposed to estimate the numbers and diameter distributions of circles, spheres, or cylinders from images obtained when the distribution is approximately or perfectly normal (see Chapter 1). A unique case is obtained when the slice thickness is nil, as when a matrix is cut into two parts by a razor. In this case, the images are the circle or sphere sections visible on the cut surfaces of the matrix. Then a method has been proposed for any distribution (see Chapter 2) that treats the distribution as a set of juxtaposed normal distributions.

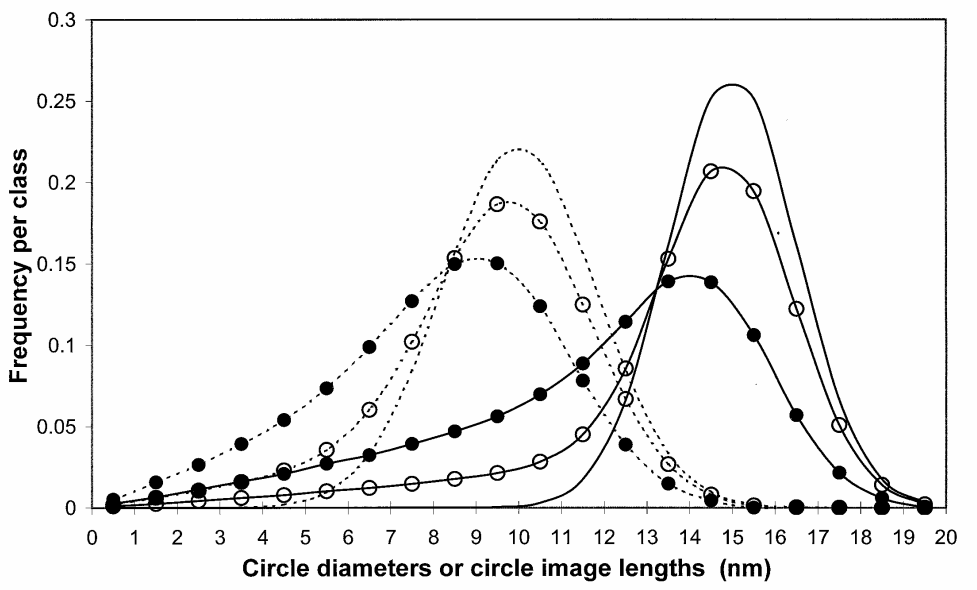

Fig. 4.1. Examples of image length distributions (lines with circles) obtained by slices 25 nm thick (empty circles) or of thickness nil (full circles) that cut circles with a normal diameter distribution.

The mean and coefficient of variation of diameter were 10 nm and 0.2 (dotted lines) or 15 nm and 0.1 (full lines). Data are marked at the centres of the classes 1 nm large. In case of slices 25 nm thick, the images are calculated based on the analysis presented here.

In cases where the slices are thicker than the largest object diameters ("thick slices" should be used only in this case), the problem is more complex because both entire objects and object fragments are present in the slices. Methods have been proposed by Feuerverger et al. (2000) and Kim et al. (2000), who also provided references to earlier methods. They applied their methods to synaptic vesicles to assess the mean diameter. However, these methods are based on mathematical principles unfamiliar to most biologists (e.g. the Volterra integral equation).

For this case of thick slices, a method is proposed here. It is applicable when the distribution is approximately or perfectly normal. It uses relations previously established for slices of thickness nil. Based on this new method, a general method for any distribution is then proposed. After validation with

two examples, the proposed methods are used to analyze synaptic vesicle distributions studied by Feuerverger et al (2000).

2. Theory: analysis and relations developed

The cases of circular, cylindrical, and spherical objects are considered. The cases for cylindrical and spherical objects are extensions of the case for circles, however, so the analysis of circular objects in a matrix will be presented first.

Consider a slice of thickness T through a transparent matrix containing circles that are in any plane P perpendicular to the slice and that are opaque relative to the matrix (**Fig. 4.2**). The diameters are smaller than T. The images of the circles within the slice or cut by the slice are observed on a plane PI parallel to the slice. These images are line segments. The circles are assumed to be dispersed at random in the plane P, and sufficiently spaced so that several circle images do not overlap. It is also assumed that all the circle diameters are longer than the shortest visible image line segment length L_S (if smaller circles exist, they will be neglected in these estimations). Similar to the approaches of Feuerverger et al. (2000) and Kim et al (2000), the method considers two circle groups, those with centres within the slice and those centred outside the slice.

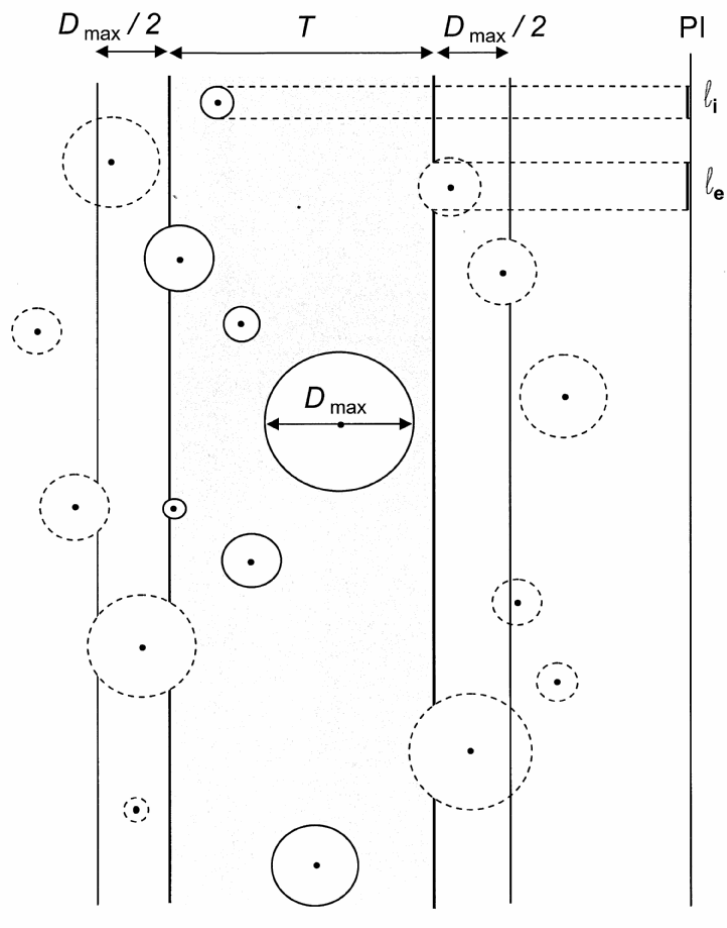

Fig. 4.2. Section of a transparent matrix with opaque circles through which a T thick slice perpendicular to the plane P is made.

The largest circle diameter is denoted D_{max}. The two D_{max} / 2 wide zones adjacent to the matrix are shown. The circles have centres either within the slice (circles with full lines) or outside (circles with dotted lines). When the two D_{max} / 2 wide parts are removed from the matrix, the image of a circle transposed onto a plane PI outside the slice (from left to right) has a length equal to the circle diameter if its centre is within the slice, or smaller if it is only partly in the slice. Two images corresponding to these two cases are shown on the plane PI.

Let n_T be the number of circles centred within the slice, and D_{max} be the largest circle diameter. The number of images m_T of these n_T circles is equal to n_T. As the lengths of the images of the circles are equal to their diameters, the mean and coefficient of variation of the image lengths are equal to the mean D_m and coefficient of variation cv_D of the diameter of the circles.

Consider the two regions of the matrix juxtaposed on each side of the slice of width D_{max} / 2 (**Fig. 4.2**). The total number of circles n_E that have centres in these regions is

$$n_E = n_T D_{max} / T . \quad (1)$$

Obviously, the diameter distribution of the n_E circles is the same as that of the n_T circles and thus the mean diameter is D_m and the coefficient of variation of diameter is cv_D. Among these n_E circles, only those partially in the slice produce images, with image lengths equal to the chord lengths of the circle segments visible on the two sides of the slice (**Fig. 4.2**). On each side of the slice, the number of images of circles with centres external to the slice of thickness T is half the number of images produced by a slice with thickness nil that would cut a matrix region D_{max} large. As the two sides of the slice T yield images, the number of images produced by the n_E circles is equal to the number of images that the two regions would give if they were juxtaposed and sectioned by a slice having a thickness nil.

If L_S is not too great relative to the diameters and if the diameter distribution is approximately or perfectly symmetrical, the number of images m_E is given by

$$m_E \approx n_E c_{1, Dlm} D_m / (D_{max} + t) \quad (2)$$

(See Chapter 1), where $c_{1, Dlm}$ is a coefficient equal to cos[asin(L_S / D_{lm})] as the slice thickness t is equal to 0, D_{lm} – note the difference with D_m – being the diameter of a fictive circle that would give, if it was cut by a great number of slices equally spaced by a small distance, images with mean length equal to the mean length l_{mE} of the m_E images of the n_E circles. In this D_{lm}-diameter circle cut by a slice of thickness nil, there exist relations between the ratio L_S / l_{mE}, the ratio l_S / D_{lm}, and the ratio l_{mE} / D_{lm}. The ratio l_{mE} / D_{lm} increases with the ratio L_S / l_{mE}. For example, if L_S / l_{mE} = 0, l_{mE} / D_{lm} equals 0.785; if L_S / l_{mE} = 1, l_{mE} / D_{lm} equals 1; if L_S = 28 and l_{mE} = 39.76 (values chosen for future reference), L_S / l_{mE} equals 0.704 and l_{mE} / D_{lm} equals 0.886.

The total number of images $\mathcal{M}$ is

$$\mathcal{M} = n_T + m_E \quad (3)$$

and the mean length λ_m of the $\mathcal{M}$ images is

$$\lambda_m = (n_T D_m + m_E l_{mE}) / (n_T + m_E). \quad (4)$$

From Eqs. (1) and (2), it follows that

$$\lambda_m \approx D_m (T + c_{1, Dlm} l_{mE}) / (T + c_{1, Dlm} D_m). \quad (5)$$

It is easy to show that the coefficient of variation ($cv_{lengths}$) of the lengths of the $\mathcal{M}$ images depend on the numbers of images (n_T and m_E), the means (D_m and l_{mE}), and coefficients of variation ($cv_{lengths, T}$ and $cv_{lengths, E}$) of the image lengths of the two circle subpopulations - in the slice and outside the slice - according to the equation

$$cv_{lengths}^2 = [n_T D_m^2 (cv_{lengths, T}^2 + 1) + m_E l_{mE}^2 (cv_{lengths, E}^2 + 1)] / (\mathcal{M} \lambda_m^2) - 1. \quad (6)$$

In this equation, $cv_{lengths, T}^2$ is equal to cv_D^2. As the diameter distribution is approximately symmetrical $cv_{lengths, E}^2$ is

$$cv_{lengths, E}^2 \approx [3(cv_{L,Dlm}^2 + 1)(cv_D^2 + 1) - 2 (cv_{L,Dlm}^2 + 1)] / (cv_D^2 + 1)^2 - 1 \quad (7)$$

(see Chapter 1). In Eq. (7), $cv_{L,Dlm}$ is the coefficient of variation of the lengths of the images of the D_{lm}-diameter circle. In the case of slices of thickness nil, $cv_{L,Dlm}$ decreases as L_S / l_{mE} increases (See Chapter

1). For example, if $L_S / l_{mE} = 0$, $cv_{L,Dlm}$ equals 0.284; if $L_S / l_{mE} = 1$, $cv_{L,Dlm}$ equals 0; if $L_S / l_{mE} = 0.704$ (as previously indicated), $cv_{L,Dlm}$ equals 0.122.

The previous relations are also valid if the circles are on different planes parallel to P. They are also valid for spheres dispersed in the matrix because an image of a sphere cut by a slice is a circle on the plane PI with a diameter equal to the length of the image of the equatorial circle of the sphere in a plane P given by the slice. Moreover, these relations are valid as well for cylinders dispersed in the matrix and perpendicular to the plane P because a cylinder section perpendicular to the cylinder axis is a circle.

3. Proposed methods

Based on these relations, the following methods are proposed to assess the object diameter distribution.

3.1. Method for approximately or perfectly normal distributions

The unknown value of l_{mE} is obviously greater than L_S but smaller than or equal to λ_m because the lengths of the images of the n_T objects are equal to the object diameters, while the lengths of the images of the n_E objects are smaller than or equal to the object diameters. Therefore, the following calculations are repeated with all the values of l_{mE} between λ_m and L_S that differ by a quantity $(\lambda_m - L_S) / w$, w being sufficiently great for the desired precision.

Given l_{mE}, the ratio l_{mE} / D_{lm} is obtained by the iterative calculations given in Appendix A. The ratio L_S / D_{lm} and $c_{1, Dlm}$ are calculated according to Eqs. (2) and (4) in **Table 4.1**. Then, D_m, n_T, m_E, n_E, and $cv_{L,Dlm}$ are calculated according to Eqs. (5) to (11) in **Table 4.1** (derived from Eqs. (2) to (7)), and D_{max} is estimated by the greatest image length L_{max}. As cv_D is greater than or equal to zero, cv_D is obtained by successive approximations (Appendix B), starting with $cv_D = 0$ and increasing cv_D by increments until the value of $cv_{lengths}$, calculated by Eq. (6) with $cv_{lengths, T}$ equal to cv_D and with $cv_{lengths, E}$ replaced by its value obtained by Eq. (7), is equal to the observed value of $cv_{lengths}$.

The value of l_{mE} which yields the smallest difference between the calculated and observed frequencies of the images in the largest classes (i.e. those classes containing the largest sized images) is selected. The reason for this adjustment is that the diameter of the greatest images is equal to the diameter of the largest objects. To calculate the frequency of the largest images, the lower and upper limits of one hundred classes (a number chosen for practical reasons) of diameters are calculated, with the cumulative frequencies increasing successively by 0.01 between 0 and 1 according to the normal distribution defined by D_m and cv_D. In each class, the number of images of objects with centres in the slice, which is equal to the number of objects in the slice, is $n_T \times 0.01$. The number of images of objects with centres outside the slice is calculated as follows. The lengths of the simulated images of the circles with diameters equal to the class middle obtained by one hundred slices of thickness nil spaced by 0.01× the largest circle diameter (equal to the diameter of the largest image) are calculated as previously described (see Chapter 1). Briefly, for a circle of radius R and a given slice at a distance x from the circle centre, the image length is equal to $2 (R^2 - x^2)^{0.5}$ if $x < R$. If not, no image is obtained. If the image length is shorter than L_S, no image is considered. The numbers of images that fall in each of one hundred diameter classes are calculated as the image frequencies obtained from the hundred circles multiplied by the estimated number

($\mathcal{M}$ - n_T) of images outside the slice. Finally, for each diameter class, the calculated numbers of images given by all the objects (with centres in or outside the slice of thickness T) are added and the frequency of the images in each diameter class is calculated. These calculations are detailed in the file "diameters-thickslices.xls" which is online on the website http://www.diameters-slices.org.

Table 4.1. *Parameters successively estimated by the method proposed for normal diameter distribution and their values obtained for the data set of synaptic vesicles from Feuerverger et al (2000) with L_S = 28 nm and adjustment to the (three) or four highest frequency classes.*

Parameters		Number of Eqs.	Estimated values
(L_S / l_{mE}) =	L_S / l_{mE}	1	0.704 (0.790)
(l_{mE} / D_{lm}) =	See calculations in Annex A		0.886 (0.913)
L_S / D_{lm} =	$(L_S / l_{mE})\ (l_{mE} / D_{lm})$	2	0.624 (0.721)
b =	$\text{asin}(L_S / D_{lm})$	3	
$c_{1, Dlm}$ =	$\cos b$	4	
D_m =	$T \lambda_m / [T - c_{1, Dlm} (\lambda_m - l_{mE})]$	5	41.63 (43.31) nm
n_T =	$T \mathcal{M} / (T + c_{1, Dlm} D_m)$	6	646 (661)
m_E =	$\mathcal{M} - n_T$	7	280 (265)
n_E =	$m_E D_{max} / (c_{1, Dlm} D_m)$	8	574 (588)
$c_{2, Dlm}$ =	$3.1416 - 2 b + \sin(2 b)$	9	
$c_{3, Dlm}$ =	$(3 - \cos^2 b) \cos b$	10	
$cv_{L, Dlm}$ =	$(16 c_{1, Dlm} c_{3, Dlm} / (3 c_{2, Dlm}^2) - 1)^{0.5}$	11	0.122 (0.089)
cv_D =	See calculations in Annex B		0.145 (0.127)

3.2. General method for any distribution

The method is largely based on the approach previously used in the case of thin slices (See Chapter 2). It considers the object population to be an assembly of several juxtaposed normal populations. Several (at least two) image macro-classes composed of several (at least two) image classes are distinguished. When the image length distribution presents several peaks of frequencies, these macro-classes are distinguished based on the minimum frequencies in the image length distribution (the higher limit of a macro-class being the lower limit of a class composed of greater images with a locally minimal frequency). First, the classes with the largest images are grouped in a first composite class named "macro-class 1". The mean and coefficient of variation of the diameters of the objects that produce the images in macro-class 1 are estimated from the mean and coefficient of variation of the lengths of these images as previously described for a population with a symmetrical diameter distribution, setting the value of L_S as equal to the lower limit of this macro-class. The general method then considers a smaller macro-class (i.e. composed of classes of smaller images). After subtraction of the images given by the objects of macro-class 1, calculated assuming that the distribution of diameter is normal, the mean and coefficient of variation of the diameters of the objects that produce the remaining images are estimated from the mean and coefficient of variation of the lengths of these images, with the value of L_S now set to the lower limit of

this macro-class. Macro-classes of smaller images are successively considered to estimate the entire distribution from the numbers of images remaining in these macro-classes after subtraction of the images of the circles that are in the greater image size macro-classes.

Note that the value of L_S of the smallest size macro-class has to be raised if the numbers of images remaining in the smaller size classes vary alternately from positive to negative after subtraction of the estimated numbers of images produced by the objects in the greater size classes. These variations indicate that the random component of the estimated numbers of images in these classes and in the greater classes is too high. These calculations are detailed in the previously cited file "diameters-thickslices.xls".

4. Material and methods used for validation and application of the proposed methods

4.1. Validation of the method for perfectly or approximately symmetrical diameter distributions

Method validity was tested with five virtual populations of one hundred circles with approximately or perfectly symmetrical diameter distributions as described previously (See Chapter 1). The numbers (m_T and m_E), mean (λ_m), and coefficient of variation ($cv_{lengths}$) of the lengths of the images obtained from one hundred T thick slices equally spaced and perpendicular to a plane on which one of the five circle populations was included were calculated for different values of T and L_S (**Table 4.2**). Then, from these calculated values and from T, L_S, and L_{max} (equal to the greatest circle diameter), the values of D_m and cv_D were estimated by the proposed method and compared to the true values.

4.2. Validation of the method for any distribution

Validity was tested with 159 images of a mixed population of 225 euro coins consisting of 38% one-centime-euro coins 16.19 mm in diameter, 44% two-centimes-euro coins 18.73 mm in diameter, and 18% five-centimes-euro coins 21.22 mm in diameter, with cv_D values very close to 0. The mean diameter and coefficient of variation of the total population were 18.21 mm and 0.100. There were 5 photos, 204 mm × 297 mm, similar to that shown in **Fig. 4.3a**, each of 45 coins. The images were obtained by slices 21.72 mm thick (**Fig. 4.3a**). The image lengths were different (**Fig. 4.3b**) from those previously observed with slices 5 mm thick (See Chapter 2). The longest and shortest images measured were 21.22 mm and 2.12 mm. As the image length distribution of the mixed coin population was quite asymmetrical with several peaks, the method for any distribution was applied. For that, twenty sub-classes were defined, each 21.22/20 mm large.

4.3. Application to data of synaptic vesicles from Feuerverger et al. (2000)

These authors estimated the size distribution of synaptic vesicles in nerve terminals from 933 images obtained by slices 75 nm thick. From their data, which were expressed as the lengths of the vesicle image radii, the length of the smallest image (its diameter) was 23.2 nm, the mean image length (λ_m) was 40.78 nm, and the measured longest image (L_{max}) was 66.7 nm. By reading their Figure 3 for each image radius class (10–12, 12–14, ... 32–34 nm), the numbers of images (1, 6, 77, 177, 208, 188, 151, 92, 25, 5, 2, and

Table 4.2. *Mean (D_m) and coefficient of variation (cv_D) of diameter estimated by the proposed method in five cases where the diameter distribution is either perfectly normal (distributions 1 and 2) or perfectly symmetrical (distribution 3) or only very roughly symmetrical (distributions 4 and 5) for different slice thicknesses (T) and lower image detection limits (L_S).*

The greatest diameters were 12.6, 14.9, 14.9, 12.3, and 15.8 units, similar to that of T, L_S and D_m, in distributions 1 to 5, respectively. (in distribution 5, D_m and cv_D were also calculated for T equal to 15 as the greatest diameter was only slightly greater than 15). Note that T, L_S and D_m are expressed in a same unit (i.e. nm, µm …).

		Distributions									
		1		2		3		4		5	
		D_m	cv_D	D_m	cv_D	D_m	cv_D	D_m	cv_D	D_m	cv_D
Real values:		10.00	0.099	10.00	0.189	10.01	0.185	10.02	0.171	10.03	0.243
Estimated values											
T	L_S										
15	0	10.2	0.073	10.4	0.155	10.4	0.161	10.6	0.081	10.9	0.178
15	3	10.2	0.080	10.3	0.165	10.3	0.167	10.6	0.099	10.9	0.183
15	5	10.1	0.085	10.2	0.170	10.2	0.172	10.6	0.101	10.9	0.188
20	0	10.2	0.075	10.3	0.167	10.2	0.170	10.7	0.019	10.8	0.179
20	3	10.1	0.086	10.2	0.170	10.2	0.171	10.5	0.103	10.7	0.187
20	5	10.1	0.089	10.2	0.174	10.1	0.176	10.5	0.105	10.2	0.206
25	0	10.1	0.079	10.2	0.170	10.2	0.172	10.4	0.100	10.6	0.190
25	3	10.1	0.085	10.2	0.174	10.1	0.177	10.4	0.105	10.6	0.190
25	5	10.1	0.090	10.1	0.177	10.1	0.180	10.4	0.108	10.6	0.196
50	0	10.0	0.091	10.1	0.179	10.1	0.181	10.3	0.111	10.4	0.199
50	3	10.0	0.093	10.1	0.182	10.0	0.184	10.3	0.111	10.4	0.199
50	5	10.0	0.095	10.0	0.184	10.0	0.186	10.2	0.147	10.3	0.224
500	0	10.0	0.099	10.0	0.189	10.0	0.191	10.1	0.117	10.2	0.210
500	3	10.0	0.100	10.0	0.190	10.0	0.189	10.0	0.165	10.1	0.237
500	5	10.0	0.100	10.0	0.190	10.0	0.186	10.0	0.169	10.0	0.241

1) in each image length class (20–24, 24–28, ... 64–68 nm) were determined. The values λ_m and $cv_{lengths}$ calculated from these data were 40.39 nm and 0.161 (λ_m was slightly lower than that given by the authors – 40.78 nm - presumably because they calculated it directly from the individual images).

The methods proposed for thick slices could be applied because all the images and thus probably all the diameters were smaller than 75 nm. The distribution was first assumed to be approximately normal. There were only small numbers of images in the two shortest image classes, one image 23.2 nm long in the 20–24 nm class and 6 images in the 24–28 nm class. These accounted for less than 1% of all images, so L_S was set to 28 nm. The values of λ_m and $cv_{lengths}$ were re-calculated to exclude these seven small images while retaining the value given by the authors as a base (40.78 nm); λ_m was equal to [(40.78 × 933) – 23.2 – (6 × 26)] / (933 – 7) = 40.895 nm and $cv_{lengths}$ was equal to 0.159. The calculations were repeated with one hundred values of l_{mE} between λ_m and L_S in steps of (λ_m - L_S) / 100. A value of l_{mE} was selected that gave the smallest positive difference between the sums of the estimated and observed numbers of images in the 56–60, 60–64, and 64–68 nm classes. As there were very few images (8) in these three classes, this sample could be suspect and therefore the calculations were also repeated with the four largest classes (52–56, 56–60, 60–64, and 64–68 nm).

In a second step, the distribution was not assumed to be approximately or perfectly normal and the method proposed for any distribution was applied. Five macro-classes (28–36, 36–44, 44–52, 52–60, and 60–68 nm) were defined, each with two classes 4 nm large. The value of l_{mE} that gave the smallest positive difference between the estimated and observed numbers of images in the largest size class of each macro-class was selected.

5. Results

5.1 Validation of the method proposed for perfectly or approximately symmetrical distributions

The estimates were very close to the true values when T was much greater than the greatest object diameter (**Table 4.2**). When T was only just greater than the greatest object diameter, the estimates of D_m were overestimated, but by less of 4% in the perfectly normal distributions (1 and 2 in **Table 4.2**) or perfectly symmetrical (3) distribution, and by less 9% in distributions 4 and 5 that are only very roughly symmetrical (Fisher's coefficients of asymmetry of -0.77 and 0.61). The estimates of cv_D were underestimated by up to 53% in distribution 4 and 27% in the others distributions. These deviations were slightly lower when L_S was higher.

5.2. Validation of the general method for any distribution

Based on the distribution of the image lengths of the coins (**Fig. 4.3c**), three macro-classes were distinguished: 21.22–19.10, 19.10–16.98, and 16.98–10.61 nm, with 2, 2, and 6 sub-classes, respectively. The lower limit of the smallest macro-class (10.61–16.98 mm) was set to 10.61 nm because the numbers of images remaining in the classes smaller than 10.61 mm alternated from positive to negative after subtraction of the numbers of images estimated from circles of larger classes. Therefore, the estimates were obtained from 151 greatest images.

The method identified three sub-populations of coins (**Fig. 4.3c**) consisting of 44%, 42%, and 14% (true values: 38%, 44%, and 18%) with mean diameters of 15.56, 18.74, and 20.77 mm (true values: 16.19, 18.73, and 21.22 mm) and coefficients of variation of 0.057, 0.001, and 0.001, respectively. The mean diameter and coefficient of variation of the total population were 17.65 mm and 0.115 (true values: 18.21 mm and 0.100). The estimates of n_T and m_E were 103 and 51, i.e. 33% of the images were from coins with centres outside the slices.

5.3. Application to the synaptic vesicle data from Feuerverger et al. (2000)

When the distribution was assumed to be approximately normal and when the calculations were based on the image frequencies in the three largest size classes, the estimates of D_m and cv_D were 43.31 nm and 0.127. **Table 4.1** details the values successively estimated and the estimates of n_T, n_E, and m_E. The frequencies of the smaller images predicted by the normal diameter distribution defined by these values of D_m and cv_D were lower than the frequencies measured (**Fig. 4.4a**). On the contrary, the frequencies of the larger images were higher. When calculations were based on the four largest size classes (**Fig. 4.4b** and **Table 4.1**), the estimates of D_m and cv_D were 41.63 nm and 0.145. Although the frequencies of the smallest images were close to the true values, the frequencies of the smaller images were still

underestimated, while the frequencies of the larger images were still overestimated. Similar values of D_m and cv_D (41.94 nm and 0.144) and the same figure as shown in **Fig. 4.4b** were obtained when the calculation was based on the five largest classes.

When the method was applied assuming the distribution to be a set of juxtaposed populations with normal diameter distributions, D_m and cv_D were 41.29 nm and 0.150, and the estimated diameter distribution was reassessed (**Fig. 4.4c**). The numbers n_T, n_E, and m_E were equal to 632, 561 and 284, giving 916 images. The image length distribution calculated from the estimated diameter distribution corresponded almost exactly to the observed distribution (**Fig. 4.4c**). The estimated diameter distribution had fewer vesicles in the range 38–50 nm than predicted from the normal distribution defined by D_m = 41.29 nm and cv_D = 0.150.

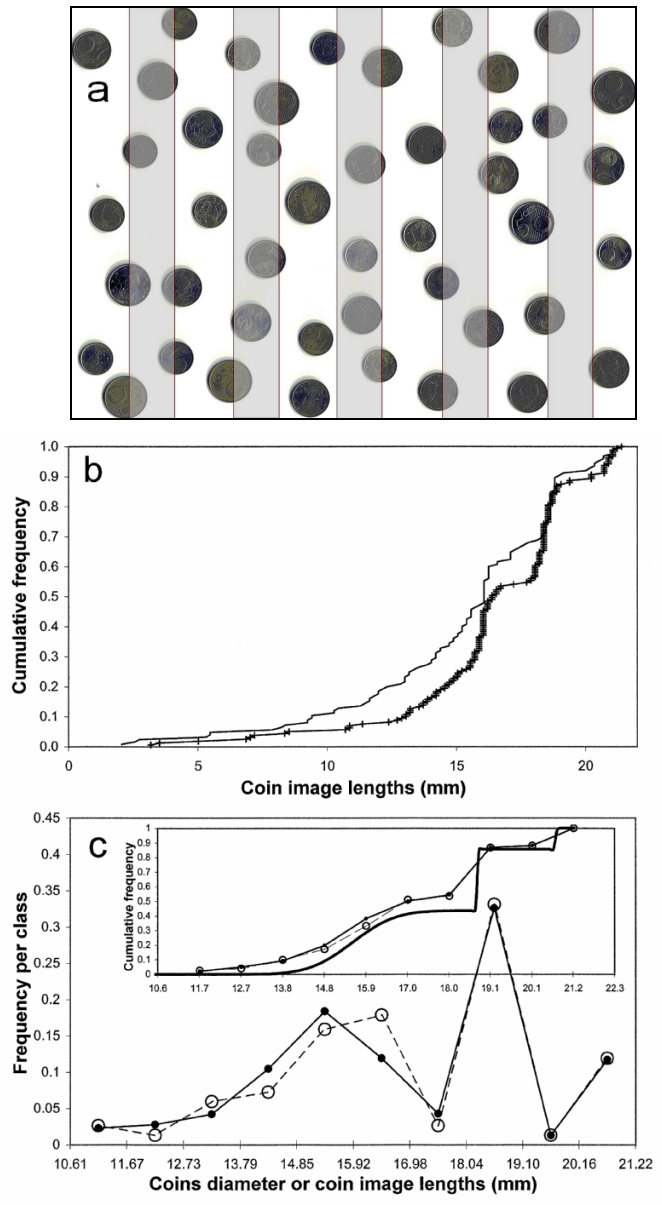

Fig. 4.3. Applying the proposed methods to the estimation of the diameter distribution of a mixture of one-, two- and five–euro coins (**a**) by thick slices (21.72 mm) perpendicular to the piece plane which delimit strips (grey surfaces 21.72 mm × 204 mm) through the plane remainder (white surfaces).

The lengths of the theoretical images were measured by Image J according to the indications in **Fig. 4.2** (but in some cases where it was possible to see that the images of two coins overlapped, they were assumed not to overlap). The distribution of the 159 image lengths (thin line with cruces in **b**) was different from that (line) obtained previously (see Chapter 2) with slices 5 mm thick (only 125 images were obtained). Figure **c** shows the distribution of the measured image lengths (dotted line with empty circles), the estimated coin diameter distribution (thick line in the inset) and the image length distribution calculated from the estimated coin diameter distribution (thin line with small points). Frequency per class is shown by a point or circle at the class middle.

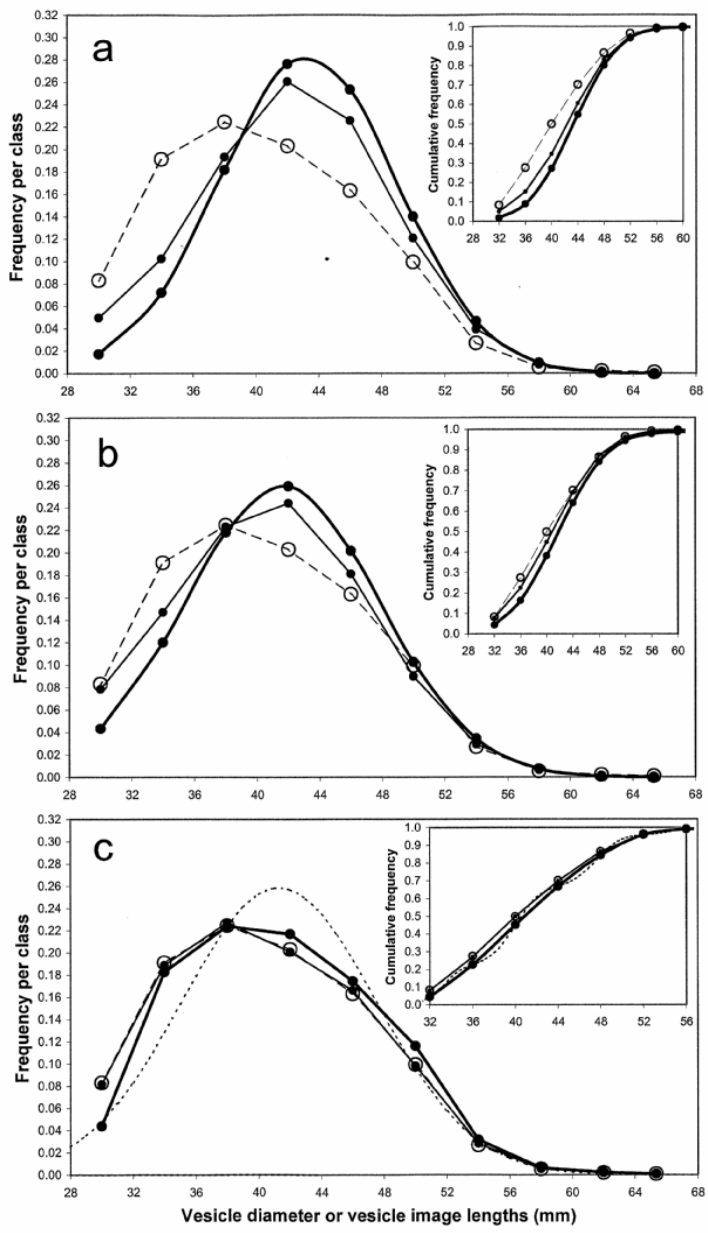

Fig. 4.4. Applying the proposed methods for estimation of the diameter distribution of synaptic vesicle in the data set from Feuerverger et al. (2000) assuming the diameter distribution to be normal (**a**, **b**) or asymmetrical (**c**). The image detection limit (L_S) is 28 nm.

The adjustment is based on the three (**a**) or four (**b**) highest frequency classes. In case (**c**), five image macro-classes were defined. Each figure shows the estimated vesicle diameter distribution (thick line with big points), the distribution of the measured vesicle image lengths (dotted line with empty circles), and the distribution of the vesicle image lengths calculated from the estimated vesicle diameter distribution (thin line with small points). In (**c**), the curve of the normal distribution calculated with the estimated values of D_m (41.29 nm) and cv_D (0.150) is shown (dotted line). Frequencies per class are shown by a point or circle at the class middle. The cumulative frequency is shown in the smaller insets. The curves of the estimated normal diameter distribution are smooth.

6. Discussion and Conclusion

The method proposed for approximately or perfectly normal distributions provided estimates of D_m and cv_D that were very close to the true values when the slices were very thick relative to the greatest diameter. This result is logical as the proportion of the images from circles with centres within the slice was high in this case and therefore the image length distribution was very close to the diameter distribution. When the slices were just thicker than the largest object diameters, D_m was only slightly overestimated while cv_D was underestimated, especially in distribution 4 that was only approximately symmetrical.

This method was used for the data set of synaptic vesicles assuming the diameter distribution to be sufficiently close to normal for useful estimations. As the smallest and largest classes contain few images (with an enhanced probability of sampling error) the estimates obtained with L_S equal to 28 nm and the four or five highest frequency classes were probably the best. In these cases, the estimated value of D_m (41.63 nm) was only slightly lower than the value (42.54 nm) estimated by Feuerverger et al (2000) with their "isotonized" method. The comparison between the observed and estimated distributions of the image lengths indicated that the observed proportion of images in the range 40 to 50 nm was lower than expected from a normal distribution while the observed proportion of the images in the range 30 to 40 nm was higher.

The test conducted with the different euro coins (a three peak distribution) strongly validated the method for any distribution, even if the coefficient of variation of diameter of 1 centime of euro coins was overestimated. Therefore, the method could be used for the data set of synaptic vesicles without prior assumptions regarding the symmetry of the diameter distribution. With this method, the image length distribution estimated from the estimated diameter distribution coincided almost exactly with the observed distribution. The estimated diameter distribution was thus very likely close to the true distribution. There were fewer vesicles in the diameter range 38–50 nm than expected by a normal distribution and the estimated value of D_m (41.29 nm) was lower than the estimates (41.7 and 41.63 nm) previously obtained by Feuerverger et al (2000) and by Kim et al. (2000). The method also indicated that the images were from 632 vesicles with centres within the slice and from 284 vesicles centred outside the slice, or about 31% of the images.

It is expected that this general method should also be applicable to estimate the equivalent diameter distribution of slightly distorted circular objects within thick slices using a method in preparation.

References

Bussières, P. 2013. File “diameters-thickslices.xls” on the website http://www.diameters-slices.org.

Feuerverger A., Menzinger M., Atwood H.L., Cooper R.L. 2000. Statistical for assessing the dimensions of synaptic vesicles in nerve terminals. *J. Neurosci. Meth.* 103, 181-190.

Kim S., Atwood H.L., Cooper R.L. 2000. Assessing accurate sizes of synaptic vesicles in nerve terminals. *Brain Res.* 877, 209-217.

Appendix A

Scheme for estimating the ratio l_{mE} / D_{lm} (named hereafter like the variable "l_{mE}_on_D_{lm}") from values of l_{mE} and L_S by successive approximations (the ratio L_S / D_{lm} is named like the variable "L_S_on_D_{lm}").

For $i = 0.001$ To 1 Step 0.001
    l_{mE}_on_$D_{lm} = i$
    L_S on $D_{lm} = (l_{mE}$_on_$D_{lm}) \; L_S / l_{mE}$
    $b = \text{asin} \; (L_S$_on_$D_{lm})$
    $c_{1,\,Dlm} = \cos b$
    $c_{2,\,Dlm} = 3.1416 - 2\,b + \sin (2\,b)$
    $l_{mE,\,est} = c_{2,\,Dlm} \; D_{lm} / (4 \; c_{1,\,Dlm})$
    If $l_{mE,\,est} < l_{mE}$ Then $i = 1$
Next i
Print l_{mE}_on_D_{lm}

Appendix B

Scheme for estimating cv_D from cv_{length}, $cv_{L,\,Dlm}$, n_T, m_E, $\mathcal{M}$, D_m (j is here programmed to vary only up 1000, a value assumed to be sufficiently high in most cases but liable to be changed).

For $j = 0.001$ To 1000 Step 0.001
    $cv_D = j$
    $k_1 = cv_D^{\,2} + 1$
    $k_2 = cv_{L,\,Dlm}^{\,2} + 1$
    $cv_{length,\,E} = ((3 \; k_2 \; k_1 - 2 \; k_2) / k_1^{\,2} - 1)^{\,0.5}$
    $k_3 = cv_{length,\,E}^{\,2} + 1$
    $cv_{length,\,estim} = ((n_T \; D_m^{\,2} \; k_1 + m_E \; l_{mE}^{\,2} \; k_3) / (\mathcal{M} \; \lambda_m^{\,2}) - 1)^{0.5}$
    If $cv_{length,\,estim}^{\,2} > cv_{length}^{\,2}$ Then $j = 1000$
Next j
Print cv_D

CHAPTER 5

Cases of opaque or transparent objects in an opaque matrix visible only on section planes

In this very short chapter, some points are clarified for the cases of opaque objects and transparent objects in an opaque matrix visible only on section planes.

As described in the previous chapters, the images of transparent objects included in a opaque matrix (case E) or opaque objects included in a transparent matrix (case F) are obtained by a radiation through slices. The image size depends on the smallest (case E) or greatest (case F) dimension of object section in the slice thickness which delimits the direct light path through the slice.

Thus, when opaque objects are in an opaque matrix, no image can be obtained according to these models E and F. However, in some cases, planar sections of opaque objects can be distinguished from the opaque matrix section on a section plane made through the matrix, for example because the planar object sections on the section plane have not the same colour when the section plane is lighted. Such planar object sections have same sizes as the object images which would be obtained in cases E and F if the slice thickness was equal to zero. Therefore, the methods proposed in the chapters 1, 2 and 3 are applicable to these planar object sections. Evidently, a matrix section plane can be a face of slice made through the matrix.

Also according to model E, no image of transparent objects included in an opaque matrix can be obtained from section planes made through the matrix (assumed to be very thick) or from slices thicker than the greatest object diameter. However, in some cases, it is possible that planar object sections can be distinguished from the opaque matrix section on a plane which sections the matrix, for example because the planar object sections on the section plane have not the same aspect because of traces made only on the matrix by the cutting tool when the objects are gas bubbles. Such planar object sections have same sizes as the object images which would be obtained in cases E and F if the slice thickness was equal to zero. Therefore, the methods proposed in the chapters 1, 2 and 3 are also applicable to these planar object sections. Also, a matrix section plane can be a face of slice made through the matrix, but unlike the previous case this slice has to be thicker than the greatest diameter.

In the case of opaque objects, only the object sections observed on one of the two faces of the slice can be considered if the slice is less thick than the suspected greater object size. When the slice is thicker, in the two cases of opaque and transparent objects, the object sections can be observed on the two faces, but the slice thickness has evidently to be put equal to zero in the various calculations.

CONCLUSIONS, LIMITS AND PERSPECTIVES

The new proposed method provides valuable estimations of the number of objects included in a matrix and their size distribution from the images obtained by slices made through the matrix when the slice thickness is smaller than the smallest diameter, in cases E and F, or greater than the greatest diameter in case F (in case E, there is no image)

Some important precautions have to be considered. In two cases E and F, objects smaller than the image detection limit may evidently exist and do not give image. The estimated distribution concerns thus only the objects greater than the image detection limit. Moreover, in case E, as objects smaller than the slice thickness cannot give images (even if the image detection limit is very small), the estimated diameter distribution concerns evidently only the objects greater than the slice thickness. Therefore, the slice thickness in case E must be, if possible, smaller than the smaller diameter which has to be considered.

When the slice thickness is suspected to be between the smallest and the greatest diameter, the proposed method can however be applied in case F putting the image detection limit equal to the slice thickness and neglecting all the images smaller than this limit. Evidently, the estimated distribution will be only relative to the objects greater the image detection limit.

The size of the greatest images provides an underestimated value – depending on the slice thickness in case E – of the greatest diameter. This value can be useful to choice the method which has to be used (case of slice less thick than the smallest diameter or thicker than the greatest diameter, or intermediate, or section plane through the matrix).

The present results give thus methods useful for many cases. However, a lot of researches need still to be made for cases frequently observed in natural or made-up conditions. In particular, the following cases should be examined:

- only approximately circular objects with any equivalent diameter distribution,
- only approximately spherical objects. It is logical to suspect that the proposed method for only approximately circular planar objects, especially valuable for ellipses, are valuable for objects like ellipsoids of revolution because any image obtained from a slice which cuts an ellipsoid of revolution with axes a and b is an ellipse whose the greatest axis is an image of an ellipse with axes a and b,
- only approximately circular or spherical objects and thick slices.

The author hopes to provide in the future some findings about these cases on the website http://www.diameters-slices.org.

A version of this book in paperback (with Figures 1.6 and 2.3 in greyscales) is printed by The American Book Center, Amsterdam, Netherland.
This book can be ordered on the website www.abc.nl for express printing, even in a single copy, by a print-on-demand process.
February 2013

Dépôt légal à la Bibliothèque Nationale de France.
Février 2013

It is often important to estimate the number and size distribution of objects dispersed in a matrix from their images obtained by slices made through the matrix.

This book proposes new methods for objects which are approximately or perfectly spherical or with surfaces or sections which are approximately or perfectly circular and which are perpendicular to the slices.

The case of slices of thickness less than the smallest diameter is firstly considered. A new approach is proposed in the first chapter for the case of perfectly circular or spherical objects whose diameter distribution is symmetrical and normal. It is valid for both opaque objects in a transparent matrix and transparent objects in an opaque matrix and even with a detection limit of images. This new approach is then used for dealing with any distributions (second chapter) or only approximately circular shapes (third chapter). Then, it is involved for the case of slices thicker than the largest diameter (fourth chapter). Finally, it is indicated also when only section planes are observed (fifth chapter).

ISBN 978 - 2 - 9544261 - 0 - 5